UNIVERSITÀ DEGLI STUDI DI TRIESTE

UNIVERSITÀ DEGLI STUDI DI UDINE

DOTTORATO DI RICERCA INTERATENEO IN INGEGNERIA CIVILE-AMBIENTALE E ARCHITETTURA
Curriculum: Ingegneria Civile
Settore Scientifico Disciplinare: ICAR/09
XXXIII Ciclo

INNOVATIVE SEISMIC PROTECTION OF EXISTING BUILDINGS BY MEANS OF DISSIPATIVE AND SHAPE MEMORY ALLOY BRACES

Ph.D. program Coordinator

Prof. Alberto Sdegno

Thesis Supervisor

Prof.ssa Margherita Pauletta

Thesis Co-Supervisor

Prof. Gaetano Russo

Ph.D. Candidate

Marco Miani

ANNO ACCADEMICO 2019/2020

Abstract

The characterization, conservation and securing of heritage buildings has become a very important issue in many countries, as it is in Italy, where a great number of existing constructions, also of historical-artistic importance, are seismically vulnerable.

Knowledge of the history, and geometric and mechanical characteristics are fundamental aspects to assess the state of a construction and to analyse possible interventions.

In the first part of this thesis, the techniques of survey and mechanical characterization of the materials are analysed, and the costs of carrying out the materials' tests to reach two different levels of knowledge on a case study building are calculated.

Then the thesis focuses on the use of energy supplementary dissipation systems for seismic protection of existing buildings. The effects of using systems of this type on two Reinforced Concrete (RC) existing buildings, in terms of force reduction, energy absorbed and torsional stiffness, are evaluated.

Moreover, analysis of Shape Memory Alloys (SMAs), smart materials capable to undergo large deformations and go back to the initial shape, is performed. Different types of SMAs are taken under consideration for possible applications in RC structures. The benefits that can be obtained by their use in an existing building are also evaluated.

Finally, the main aspects and benefits related to the transition from the current traditional design of buildings towards the BIM methodology and the use of BIM also in the field of existing constructions are discussed.

INDEX

1   INTRODUCTION

The seismic vulnerability of the Italian building heritage, and consequently the need for its safety, is a much discussed issue in recent decades. The recent earthquakes that hit Italy, and the economic and social impact they have caused, have once again highlighted the actual and high risk that characterizes Italian territory. Although on the one hand our territory is characterized by a high seismic risk, on the other hand the building heritage is very old and vulnerable to seismic action.

The vulnerability of the building heritage, linked to age and structural characteristics, can be identified as the main cause for which the damage produced by earthquakes in Italy is much greater that those occurring in other countries, such as Japan, subjected to earthquakes of equal or greater intensity.

Italy has a medium-high level of danger, due to the frequency and intensity of seismic phenomena, a very high vulnerability, due to the fragility of the building, infrastructural and industrial heritage, and a very high exposure, due to the population density and the presence of a historical, artistic and monumental heritage unique in the world. It is the combination of all this factors that produces in the entire Italian territory to a high seismic risk, in terms of victims, damage to building and direct and indirect costs expected following an earthquake.

A great number of reinforced concrete buildings in Italy was made referring to codes and technical standards today obsolete, not able to guarantee adequate levels of security. Furthermore, most of the reinforced concrete buildings were built between the 50s and the early 80s, during economic boom when a strong increase in the demand, and the consequent need to build quickly may have led to less attention in the design and construction of the building in all its aspects.

Multiple causes can be identified at the base of the large number of buildings potentially at risk on the Italian territory, among which it can be certainly mentioned the use of poor materials, the lack of attention to construction details, the transverse reinforcement lacking and, as mentioned, the design with old conception standards which considered only vertical loads, and not actions induced by earthquakes.

With reference to the data relating to the 15th census conducted by ISTAT in 2011 [1], Fig. 1 shows the residential buildings divided by year of construction and materials. From these data it emerges that about 57% of residential buildings were built before the 1970s, 36% were built between 1971 and 2000, and 7% were built after 2000. Since the first seismic code was introduced with the Law n. 64/74 [2], on the basis of this data it is possible to conclude that more than 60% of Italian existing buildings are exposed to seismic risk, being designed without a seismic code.

Bearing in mind that the philosophy of capacity design was introduced in the early years of the 21st century, about 93% of the residential buildings have a limited structural seismic safety.
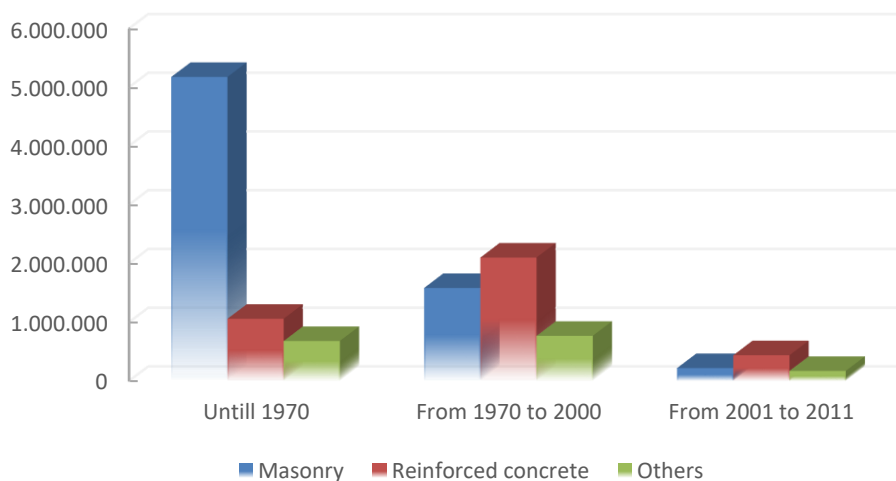
Fig. 1. Residential building for period of construction and materials.

The Italian National Council of Engineers (CNI) in a 2016 document [3], underlined that more than 21.5 million people live in areas of the country exposed to

very or quite high seismic risk (zone 1 and 2), and another 18 million live instead in territories classified as zone 3.

Understanding the vulnerability level of existing building heritage is therefore the initial phase for the definition of a seismic risk mitigation strategy through interventions improving the seismic behaviour of the buildings. A systematic approach to reduce seismic vulnerability is necessarily based on an initial analysis of the existing building, highlighting criticalities, vulnerable elements and structural deficiencies both globally and locally.

In this context, an in-depth knowledge of the building and materials and an accurate model of it are evidently necessary for a correct analysis of the building's deficiencies and an optimal choice of the type of intervention.

The management of existing buildings plays such an important role in the construction field and for the State economy that the Italian Building Code [4], later abbreviated as NTC, dedicates a specific chapter to the seismic assessment of existing structures.

In the past, often the knowledge data of the risk was not followed by the prevention one, and therefore the risk analysis was not followed by any intervention. This problem could have several reasons: the perception of the citizen of the risk is very high after a strong event, but swarms over time; another can be attributed to the cost of installing catting out reinforcement intervention or anti-seismic devices, which can also be substantial. A positive consideration is that in the last decade the sensitivity towards this risk has increased both among the population and at political level, so much that economic initiatives have been launched aimed at favouring a structural and seismic improvement of existing building heritage.

The study illustrated in this thesis is developed in 5 chapters:

- This chapter highlights the importance of the recovery of the existing building heritage and describes the situation in Italy about this issue.

- Chapter 2 describes the possible survey techniques for the acquisition of geometry of existing buildings and the destructive and non-destructive tests for the characterization of the materials of RC constructions. The contents of the Italian Building Code regarding existing buildings are analysed and the necessary investigations and tests and related costs to reach two of the three levels of knowledge provided by the Code are assessed.

  The methodology of Building Information Modelling (BIM) and the advantages that can be obtained from its use for the assessment, maintenance and retrofit of existing buildings are analysed.

- In Chapter 3, considering two RC existing buildings designed for gravity loads only, two different types of seismic retrofit interventions, one with Buckling-Restrained Axial Dampers (BRAD) devices and one with Viscous Fluid Dampers, are analysed in terms of dissipated energy, reduction of stresses and increase of torsional stiffness.

- Chapter 4 describes the special properties of Shape Memory Alloys and the advantages of their use on existing buildings. A seismic retrofit intervention through the use of SMA braces in an existing building is proposed and the obtained results are discussed. Also the possibility of using SMAs as reinforcement in the region of RC beams were plastic hinges occur is investigated.

2 SURVEY TECHNIQUES, MECHANICAL CHARACTERIZATION AND BIM FOR EXISTING BUILDINGS

As described in the previous chapter, the recovery of the existing building heritage will be an important topic in the next few decades in Italy. In order to assess the state of conservation of the building and plan any type of intervention, it is important to know the building in all its aspects, as its geometric and mechanical characteristics and any areas of degradation, in order to assess the state of conservation of the building. Because of the importance of this phase of preliminary analysis, in this chapter the techniques of geometric survey and the tests for the mechanical characterization of materials will be illustrated and analysed.

The final part of the chapter also illustrates the Building Information Modelling methodology, which can be developed starting from the results of this preliminary phase.

In the Italian Building Code the procedures for the evaluation and verification of existing buildings, which are different from those for new buildings, as well as types of interventions, are provided in a specific chapter, which is further and more specifically explained in instructional code Circolare 21 January 2019 [5].

Knowledge of the existing building is the first important step to start an assessment of its condition and to start designing, if necessary, the best retrofit solution. For this reason it is important to find out all the documentation concerning the building that can help to know its history, how it was built, the material used and the code in force in the years of construction. Architectural and structural drawings and reports of the original project, problems occurred during the construction,

information regarding modifications or interventions, natural events that affected the construction are all fundamental elements that must be taken into account in order to know the current state of the building.

Defined a first idea of the building configuration, identified the position of possible valuable elements, identified areas and/or elements that may present critical issues, it is possible to program and define the characteristic of the survey.

The survey moment is important to verify that all data and information acquired from the different documentation are true and that the building described in the documentation have the same characteristics of the built one. Different dimensions of the elements, different position and diameter of the reinforcement bars, different material use are just some examples of the differences that can be found. There could also be the possibility that architectural or structural changes have been made during the construction phase, but that the drawings have not been updated with these changes. In the same way there is the possibility that some changes the building has undergone over the years are not reflected in the available documents. For all these reasons the survey is so important to know the real status of the building.

In the survey phase it is important to check:

- the position and the geometry of the elements as columns, walls, beams and the typology and orientation of the floors;

- the connections between the elements;

- the position of the reinforcements;

- the layers of the walls;

- cracks and/or deterioration of areas or elements.

For the purpose of the structural analysis of existing buildings it is important to know what are the geometry of the elements and the mechanical characteristics of the

materials. In the following paragraphs the main methodology to define these characteristics are explained.

2.1 Geometric survey

Goal of the geometric survey is the description of the position, shape and dimension of the different elements. It is sufficient a sample examination if the as-built drawings are available, otherwise a thorough survey is required to obtain all the necessary geometric information. In the latter case it is also important to draw the plan of the different level of the building.

The choice of the survey method is mainly linked to the objective of the survey and to the extension and conformation of the building.

2.1.1 Direct and topographical survey

Direct survey is performed using simple tools such as the tape measure or the laser distance meter to obtain the dimension of the elements and their distance, the plumb line or the bubble level to check the verticality (Fig. 2 (a)), and the callipers for precision measurements as the diameter of the bars.

Survey planning is an important aspect for obtaining the meaningful data. To minimize errors it is useful to make redundant measurements and take them progressively, from the same point, which is assumed to be known, with respect to performing partial measurements.

To speed up the survey operation, especially in the case the building is very large topographical survey can be performed by using, the total station (Fig. 2 (b)). This tool allows to obtain distances, by measuring the time of flight of the signal, and angles in a more precise way than the direct survey. Also in this case is important to plan the survey, make redundant measurements and, to reduce the propagation of errors, it is good to note some points to be considered known and use them as base

for the survey. Topography survey is recommended mainly in the case of regular buildings and flat surfaces.

<table>
<tr><td align="center">(a)</td><td align="center">(b)</td></tr>
</table>
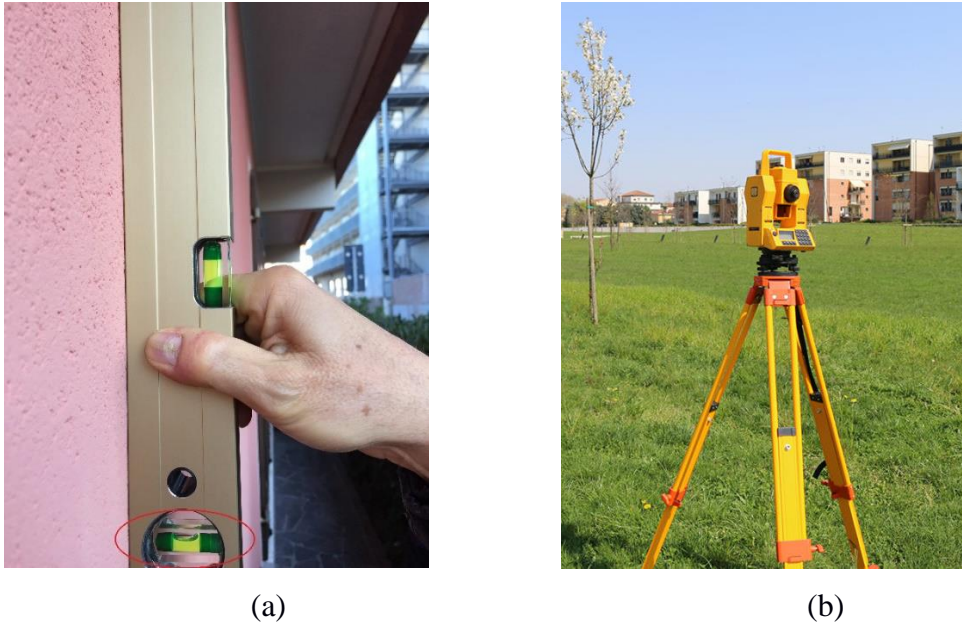
Fig. 2. (**a**) Verticality check of the wall and (**b**) total station.

2.1.2   Photogrammetry

Photogrammetry is a survey technique that allows to obtain metric data of objects (shape and position) through the acquisition and analysis of frames [6]. Using appropriate algorithms, the goal is to obtain the 3D structure of the building.

Starting from a certain number of images, which must have overlaps, through algorithms is possible to identify matching between points of different images and, after performing frame orientation, using specific software it is possible to reconstruct the shape and size of the object, as shown in Fig. 3.

From this operation various results can be obtained, including mesh of the object and orthophoto, that is the result of an orthogonal projection. From orthophotos it is possible to take measurements, that properly scaled, coincide with the real dimension of the object.

Images can be take manually using a camera or, for the external parts of the building using a drone. In this second way it is also possible to reconstruct even portions of the building that are difficult to access or irregular.

Fig. 3. Photogrammetric reconstruction [6].

2.1.3 Laser scanning

This is an active survey technique that allows to determine the shape and position of an object by measuring a large number of points of the surface, through a sequence of variously oriented laser pulses [6]. Laser scanning gives a point cloud, and, for each point, it is possible to know the coordinates.

Thanks to the controlled movement along the two main axes (rotary and oscillatory) at very high frequency, the surrounding space the laser scanner is detect. It is possible to scan both internal and external part of the building. In most of the cases more than one scan is required. For this reason it is important to plan how many scans are necessary and where do them. To obtain a continuous 3D model, once all the scans have been carried out, it is necessary to register all the point clouds in a single point cloud and georeference it. In Fig. 4 it is possible to observe a points cloud obtained from the laser scanning of a bridge deck.

Laser scanner can be useful when there are arches, vaults and not flat surface, that can be detected more easily than using the techniques described in the previous paragraphs.

Fig. 4. Bridge's scan [6].

2.2   Survey of construction techniques

The goal of the survey of constriction techniques is to describe the materials used, their position and how the elements were made. Another important aspect that must be investigated is the connection between the elements, whether structural or non-structural, and any connection with other buildings. It is important to define type and quality of the constraint.

A preliminary historical analysis of the construction techniques commonly used in the building period and area helps in both the analysis of the building during the survey and the definition of type and quantity of tests to be performed on the materials.

In the presence of damage or cracks, that may show the stratigraphy of the masonry, or exposed reinforcing bars, it could be necessary just a visible survey to

define the type and the technique of construction, otherwise more in-depth investigations are necessary.

2.2.1 Endoscopy

The endoscopy test is classified as non-destructive or weakly destructive test. It is usually used on masonry and provides knowledge about the morphology, stratigraphy, typology, conservation and depth of the materials crossed, but it can be used also on other structural or no-structural elements (Fig. 5). Its use is also useful for the evaluation of the presence of possible voids or cavities.

In the most recent versions, the endoscope consist of a camera, with a diameter of less than 1 cm, connected via cable to a device that allows images of the camera to be viewed.

The first step to perform on endoscopy test is to remove the surface plaster, and then make a small hole, of about 2/3 cm, with a drill or a diamond head micro core drilling machine, in the element to be analysed. After cleaning the hole, the endoscope is introduced up to the length necessary to collect all the information. Usually there is a light at the top of the cable to illuminate the inside of the hole, so it is possible also take pictures. The cable can be rigid or flexible, where the last solution is the best as it allows inspections even of non-straight path.

The knowledge of the state and stratigraphy of different elements can be useful not only for a structural and seismic analysis, but also for an energy analysis.

In the case of survey with horizontal perforation, like in the case in Fig. 5, the endoscopic test costs between € 100 and € 200, while in the case of vertical perforation, as in the case it is necessary to have information on the stratigraphy of the floor of a building, the cost increases to about € 350. On the other hand, professional endoscope has a cost that starts from € 500 and goes up to a few thousand euros, depending on the length of the cable and the quality of the camera.

Fig. 5. Endoscopy for the evaluation of the stratigraphy.

2.2.2 Thermography

With the thermography test it is possible to detect, point by point, the surface temperature of a building or one of its elements. This is a non-destructive test and allows you to carry out investigation on the building without interrupting or disturbing any activity in progress.

The thermography imaging camera, visible in Fig. 6, detects the intensity of the electromagnetic radiation emitted by the object in the infrared. It is then possible to correlate the temperature to this intensity through the Stefan-Boltzmann law.

This test can be of active type, if a thermal variation is deliberately caused, or passive type, if it is done at natural temperatures. In the first case the test allows to locate also the hidden elements, while, in the second case, it allows to analyse only the superficial parts of the building.

In order to obtain most accurate measurement possible, the correct calibration of the instrument is fundamental and it is obtained by setting the emissivity factor (ε)

and the reflection factor (ρ) of the considered surface. The ε value can be determined using tables or, in situ, measuring the surface temperature with the camera and a contact thermometer and varying the emissivity value until the same value of temperature is obtained with both methods. This value is influenced by the surface type and the presence of dirt, such dust or frost, which must therefore be removed.

For outdoor test, solar radiation must be taken into account. For this reason the best situation is when the sky is overcast. It is also important to have stable conditions throughout the test.

The result of the thermography test is a thermographic image, like the one show in Fig. 7, to which each intensity of radiation, and therefore each temperature, is associated with a colour raging from blue, for low temperature, to red, for high temperature. From the temperature discontinuity it is possible to identify a variation of material, thermal bridges, voids and any hidden system. Therefore, no mechanical characteristic of the materials is obtained from this test, but the test can be used to support the building characterization phase.

The cost of a thermography is between € 80 and € 500, depending on the extension of the surface, while the cost of the instrument start from € 300 up to €10˙000.

Fig. 6. Thermal imaging camera.
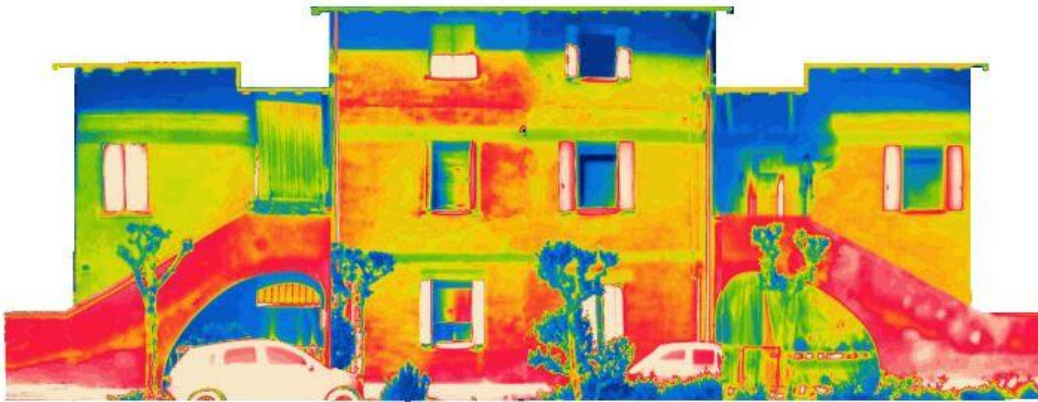
Fig. 7. Thermography results of a building site in Torviscosa.

2.2.3   Covermeter

The covermeter test is a non-destructive test, through which it is possible to detect the presence, direction and diameter of steel reinforcement inside reinforced concrete elements.

The device works on the principle of the magnetic induction, exploiting the magnetic properties of the reinforcing bars. The magnetic field generated by a scope causes an eddy current in the bars. A sensor measures the induced magnetic field and its variation, being able to identify the position and diameter of the bars. The reference code for this test is BS 1881:204/1988.

It is necessary to approach the instrument, highlighted in the red ellipse of Fig. 8 (a), to the surface of the element, and then move it in along two orthogonal direction to detect the position of the bars in these directions. It is possible to mark the position of the bars on the surface of the element or, using the most modern tools, to display the arrangement of the reinforcement on a monitor, as shown in Fig. 8 (b). The test must be performed by an experienced operator, able to correctly analyse the results provided by the instrument.

In addition to the position and diameter of the reinforcement, it is also possible to estimate the concrete cover and identify the pitch of transverse reinforcements. It is also possible to detect other metal object as pipes.

It is possible to measure diameters between $\phi5$ and $\phi60$ and the maximum depth of investigation is between 5 and 15 cm, according to the instrument. The measurement accuracy is about 1-2 mm.

The covermeter test is important because allows to detect the portions of the concrete elements where it is possible to carry out concrete core drills and perform sclerometric and pull-out tests because there are not bars present.

The cost of the test can be determined per single element or square meter, and it is between € 20 and € 70. The instrument's cost varies instead between € 100, for the simpler ones, up to about € 3˙000.

(a)   (b)
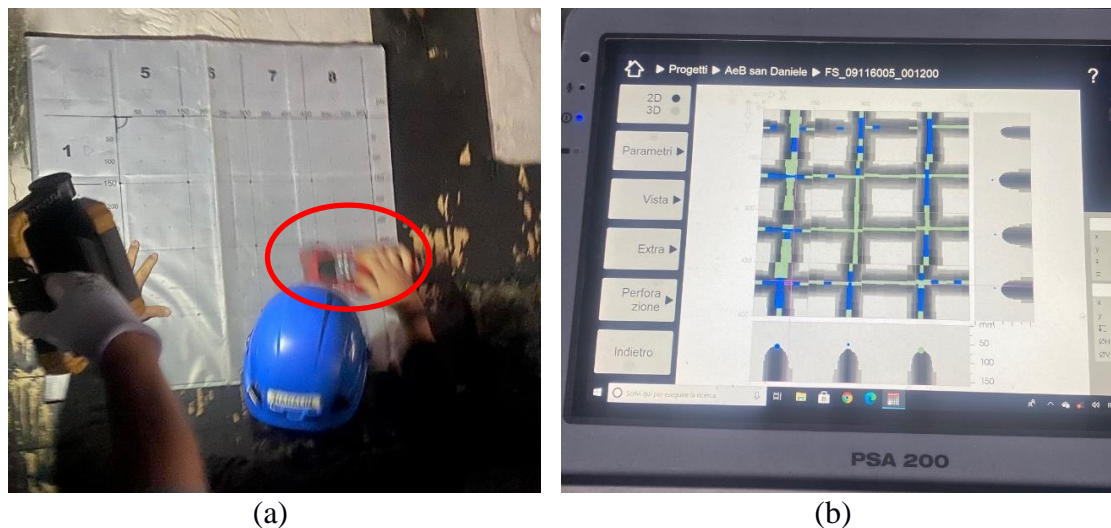
Fig. 8. (**a**) Instrument on the surface to test and (**b**) arrangement of reinforcement.

2.2.4 Georadar

The Ground Penetrating Radar (GPR), or georadar, is a tool (Fig. 9 (a)) that allows to acquire information on construction techniques, structural elements, reinforcement and defects in materials. It can be used also to find anthropogenic structures under the ground. It's a non-destructive test and it is used especially on

ground and floor when there are large area to investigate and allows to obtain a continuous description of the soil.

For the exploration of the subsoil the GPR makes use of electromagnetic waves with a frequency between a few tens of Mhz and a few Ghz, sent into the ground by means of a transmitting antenna. A receiving antenna collects the signals reflected by the objects present in the subsoil. Electromagnetic waves propagate in different ways depending in the dielectric constants of the materials and, in the presence of discontinuity, the waves are partially reflected and picked up by the receiver of the GPR. The result is a representation of the vertical section of the subsoil (radargram). By processing the collected data with particular programs that combine the data of the vertical section and that cut the investigated area with an horizontal plane placed at a certain depth, called slice, it is possible to identify any anomalies in this plane (Fig. 9 (b)). By varying the depth of this plane, it is possible to visualize the presence of anomalies on the areas located at different depths.

Among the natural factors that could influence the results of the GPR test, an extremely important role is played by the geological nature of the soil and the immediate subsoil. Ground dielectric constant and electrical conductivity are involved: the former in determining the propagation speed of the electromagnetic wave, the latter in determining the depth that can be investigated. The greater is the dielectric constant, the lower is the speed. The greater the physical contrast of materials and different their characteristic, the easier it is to identify their presence. As for the investigable depth, this depends on how quickly the wave degrades due to the absorption of electromagnetic energy by the ground. In dry sandy soil, energy absorption is lower than in damp clayey soils.

In the final image acquired by the radar it is possible to observe, with different colours, the different reflection or anomalies in the response, as shown in Fig. 9 (b).

The interpretation of this image is not always easy to perform, and for this reason it is necessary to rely on technicians with proven experience and ability.

The cost of this test is between € 2 and € 4 per sqm.

<table>
<tr><td>(a)</td><td>(b)</td></tr>
</table>
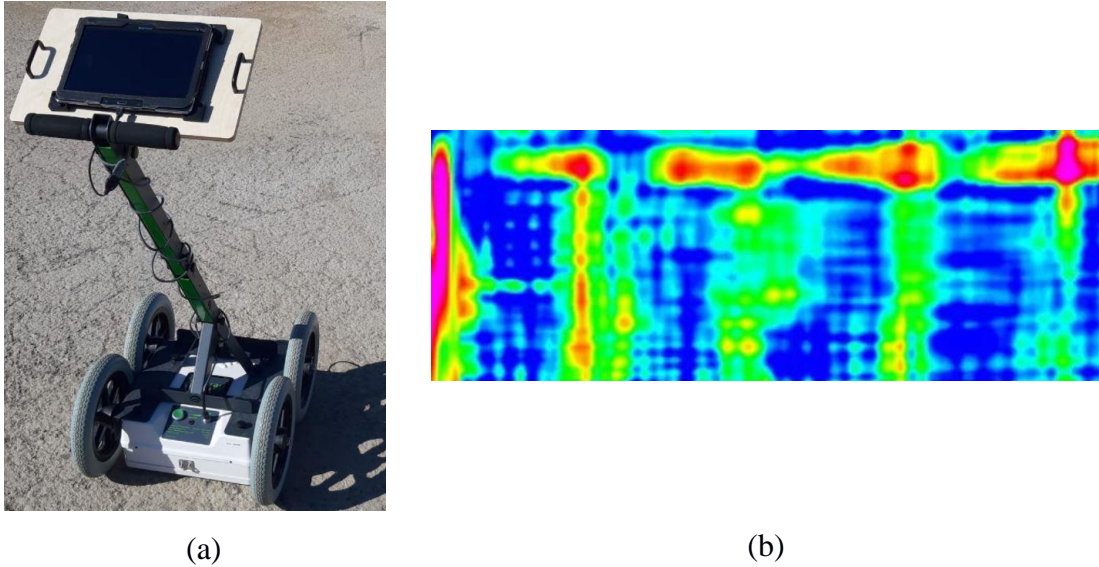
Fig. 9. (**a**) Ground Penetrating Radar and (**b**) slice results.

2.3 Non-destructive tests for mechanical characterization

In the following paragraphs non-destructive tests for mechanical characterization are presented. For the purpose of knowledge mechanical behaviour of existing buildings, Italian code [5] does not allow the execution of only non-destructive tests, but these can be performed in combination with destructive tests to reduce the number of the latter and, therefore, reduce the negative effects on the building.

To evaluate the characteristics of concrete it is also possible to refer to the guidelines of C.S.LL.PP. [7].

2.3.1 Sonic and ultrasonic test

The sonic or ultrasonic test can be use both on concrete and masonry and allows to estimate the quality of the material, its homogeneity or the presence of cavities, in a non-destructive way. The instrument used for this test is shown in Fig. 10. In the

sonic test the wave's frequency is between 16 Hz and 20 kHz [8], while for the ultrasonic test the frequency is between 20 kHz and 150 kHz.

The ultrasound test is characterized by very high wave's frequencies that allow to detect even very small defects and to obtain a meticulous investigation, but, since the emission energy of the waves is low, the signal path is limited and it is possible to investigate restricted areas. On the contrary the sonic test are characterized by the use of high energy emission sources and low frequency, which, by compensating the energy absorption of the investigated material, allow to detect longer paths. Sonic test are therefore preferred in case it is necessary to investigate elements characterized by strong heterogeneity and are able to cross even less compact walls.

The methods of carrying out the test are defined by the UNI EN 12504-4:2005.

Fig. 10. Sonic and ultrasonic instrumentation.

The test measures the speed of propagation of elastic waves, *V*, determined as ratio of the distance between a transmitter and a receiver, *L*, and the time taken to travel it, *t*:

$$V = \frac{L}{t} \tag{1}$$

A transmitter, placed in contact with a face of the element, emits a series of waves that pass through the element and are recorder by one or more receivers. On

the masonry, usually the wave is not generated by a transducer, but by a blow with a small hammer. In fact, waves generated by the hammer have a lower frequency and can pass also through a not very compact masonry.

Transmitter and receiver must be placed in contact with a clean face, and, as shown in Fig. 11, in function of their position it is possible to distinguish:

a) *direct or transparency measurement*, when transmitter (T) and receiver (R) are on the two opposite sides of the element at the same height. This is the best situation and it allows to evaluate the properties throughout the thickness;

b) *semi-direct measurement*, when T and R are on orthogonal faces, or on two opposite sides of the elements but not at the same height. The measurement is less accurate and the wave path is more difficult to determine;

c) *non-direct measurement*, when T and R are on the same side. It is used when just a single face of the element is available, but it is not easy to define the effective distance between T and R, because wave's path is uncertain.
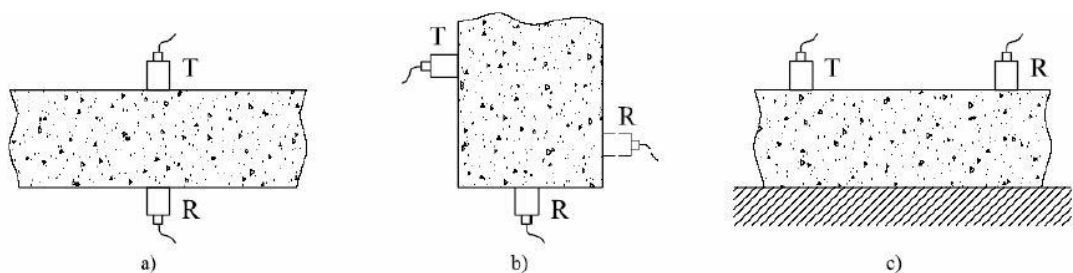

Fig. 11. Possible positions of the transmitter (T) and the receiver (R) [9].

For direct measurements, the correct positioning of T and R is important to evaluate the actual length of the path and consequently the speed.

19

If there are cracks or discontinuities, the wave's speed decreases as it is slower in correspondence with the vacuum. For Fermat principle, the wave follows the path at higher speed, i.e. in the material with higher density. For this reason cracks and voids cause an elongation of the path taken by the wave respect to the effective distance between transmitter and receiver. Furthermore, the presence of cracks and voids causes refraction and reflection of waves in the element and leads to an attenuation of the signal due to the absorption of the energy.

In this way, from the analysis of speed and attenuation of the waves, it is possible to locate cracks and voids.

In concrete elements the measurements can be distorted by the presence of surface micro-cracks. Due to this and by considering the presence of reinforcements and humidity, it is necessary to evaluate the right position where to perform the tests. In fact, the presence of reinforcement along wave's path, for example, can lead to an increase in speed and therefore consider a concrete with better characteristics.

For concrete elements, waves' speed greater than 4˙500 m/s corresponds to an excellent quality concrete, while for speed lower that 3˙000 m/s the concrete quality is poor.

As indicate in [7] it is possible to identify a correlation between the compressive strength and the speed of the elastic wave according to the following increasing exponential relationship:

$$R_c = Ae^{BV} \qquad (2)$$

where coefficient *A* and *B* must be calibrated with destructive test on appropriate specimen.

On masonry, waves' speed cannot be directly related to its property, as strength, due to the absence of the hypothesis of homogeneity and isotropy, but it is able to

provide qualitative data. To have an order of magnitude wave's speed less than 1˙000 m/s identifies heavily damaged walls with many internal voids, while speed greater than 2˙000 m/s identifies good masonry [8].

Sonic test can be use also to evaluate the characteristics of the masonry after consolidation interventions, such mortar injections.

Both for concrete and masonry elements, with sonic test it is possible to define the dynamic elastic modulus, E_d, through this equation:

$$E_d = V^2 \rho (1 + v) \frac{(1 - 2v)}{(1 - v)} \tag{3}$$

where ρ is the material's density and v is Poisson's modulus.

By increasing the frequency it is possible to identify gradually smaller defects. In fact the wavelength, λ, is related to the transmission speed and the frequency, f, according to the following relationship:

$$\lambda = \frac{V}{f} \tag{4}$$

and fixed V, an increase in f corresponds to a decrease in λ, but at the same time the detectable thickness decreases.

For these reason on concrete element frequencies between 40 kHz and 60 kHz are those used for the most common applications, while higher frequencies, between 60 kHz and 200 kHz are used for small distance (less than 50 cm) and lower frequencies, between 10 kHz and 40 kHz are used for large dimension, up to 10 m. On masonry, input frequency is about 3.5 kHz.

Sonic tests are often used in combination with rebound hammer test to achieve more reliable results.

One sonic and ultrasonic test costs around € 70.

2.3.2   Rebound hammer test

The rebound hammer test is a non-destructive test, which allows to estimate the compression strength of concrete or mortar. Its execution is regulated by the UNI EN 12504-2.

The tool used to performed the test (Fig. 12), also called Schmidt's hammer, contains a standardized mass connected to a spring, which reaches a predetermined energy pushing the tip of the instrument against the surface of the element. It is used to measure the superficial hardness, connected to the elastic energy absorbed by the material during the impact, which is then correlated, through empirical relationships, to stiffness and strength.

Fig. 12. Rebound hammer test.

The mass hits the surface of the material and the rebound height is measured. Since the kinetic energy of the mass is standardized, the rebound height depends by the energy dissipated under the impact.

The result of the single test is the rebound index, I_r, that is the measure, expressed in terms of percentage, of the height of the rebound with respect to the distance between the starting point of the mass and the impact surface. A number of tests have to be performed on the area of interest to consider then the average values of the measured rebound index values.

It is important that each of these measurements be performed in distinct points, a few centimetres away. In fact, every test causes superficial micro-cracks, that can distort subsequent measurements performed in the same point.

The presence of reinforcement or detached and damage concrete in the point of test could influence the measurement. For this reason it is essential to pick out the most suitable area to carry out the test, also using covermeter to identify the position of reinforcement.

Another aspect that must be taken into consideration is the carbonation depth: I_r have to be decreased using a coefficient equal to 0.95, if the carbonation depth is between 50-60 mm, and equal to 0.9, for greater depths.

As indicated in [10], for each investigated area it is necessary to perform about 10 measurements. The final result is expressed in terms of the average rebound index for each area and, if 20% of the measures are greater or lower than the value obtained adding or subtracting six to the average rebound index, the whole series of measurements must be discarded.

The rebound index is related to concrete's strength by empirical curves, as shown in Fig. 13.

Reliability of the results obtained with this method is poor for various reasons:

- as previously described this test involves just the superficial part of concrete, and this result cannot be representative of interior concrete;

- not very rigid and resistant concrete absorb more energy in the impact than the stiffer and more resistant ones, providing a minor rebound index value. Since it is possible for two concretes with different composition have the same strength but different stiffness, it is possible obtained different rebound index even if they have the same resistance. On the other way around, it is

possible for two concrete with different strength have the same rebound index, if the stiffness of the less resistant is greater than that of the most resistant.

For these reasons, in order to obtain more significant resistance values, it is advisable to combine the results of rebound hammer tests with the results of sonic tests.
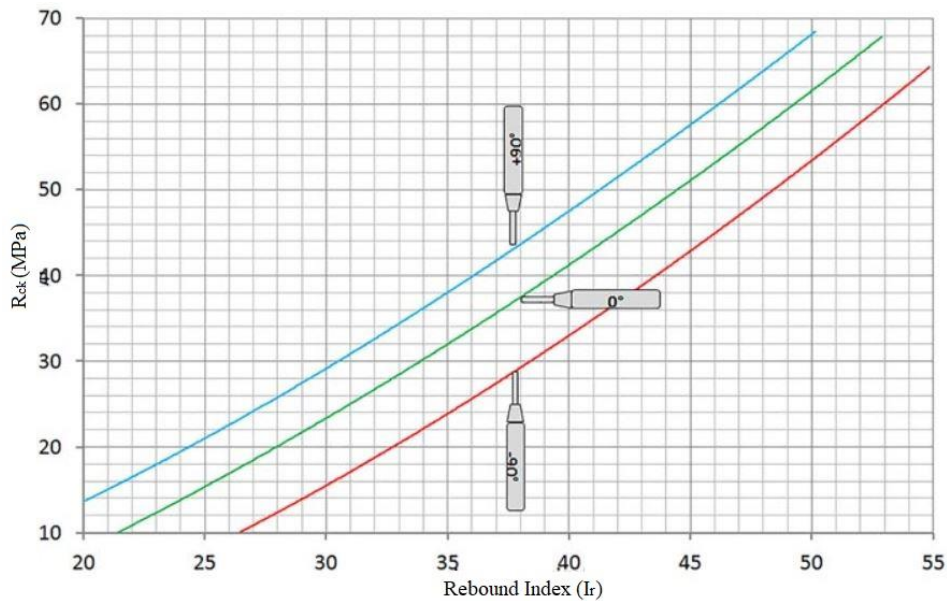
Fig. 13. Correlation graph between the rebound index (Ir) and the estimate of the characteristic compressive strength of the concrete (Rck).

2.3.3 Sonic and Rebound (SonReb test)

The combined use of the two tests described in §2.3.1 and §2.3.2, called the SONREB method (SONic + REbound), allows to reduce the errors committed by using them individually. In fact experimental results have shown that if on one side the moisture content increases the ultrasonic speed of waves and decrease the rebound index, on the other side as the age of concrete increases, the rebound index increases and wave's speed decreases.

The correlation between concrete strength, rebound index and ultrasonic speed is generally expressed using the following formula:

$$R_c = a \cdot I_r^b \cdot V^c \tag{5}$$

where *a, b, c* are coefficient used to correlate the results of the individual tests, I_r is the rebound index and *V* the ultrasonic speed.

Coefficient values are influenced by concrete's characteristics and composition. The calibration of the three coefficients, by means of statistical regression that minimizes differences, have to be done on the basis of the results of compression tests to be performed on samples taken in the same area in which the non-destructive tests are performed. Then it is possible to use the formula in the other places where destructive test are not carried out.

Different authors ([11]-[13]) have determined coefficient's values carrying out destructive tests on samples taken in the same areas where non-destructive tests were performed: for example Di Leo [13] defines *a*, *b* and *c* coefficients respectively equal to $1.0 \cdot 10^{-9}$, 1.058 and 2.446. By introducing the defined coefficients in (5) the different authors have obtained a series of curves in a *V- I_r* plane, each representative of a different value of strength, as shown in Fig. 14 where the graph obtained by [11] is reported. Entering the diagram with a *V* value on the x-axis and a I_r value on the y-axis, it is possible to obtain R_c (in Fig. 14 expressed with f_c).
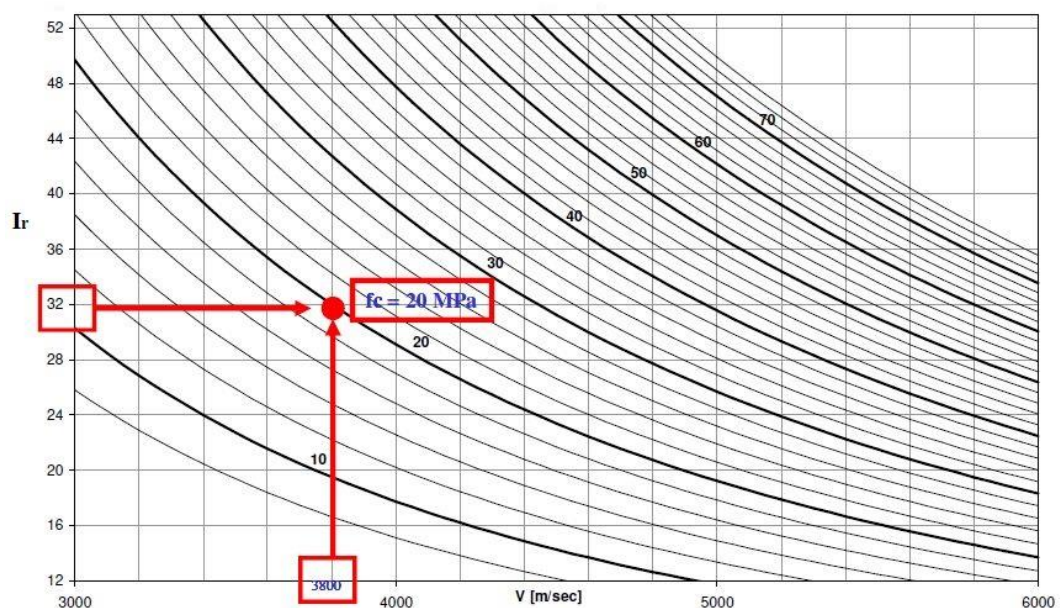
Fig. 14. Correlation graph to estimate R_c obtained by [11]

2.3.4 Pull-out test

The pull-out test is a semi-destructive test, based on the measurement of the force required to extract a standardized metallic insert from concrete. The force is applied by a hydraulic jack connected to the insert and a reaction ring which contrasts with the surface of the concrete, as shown in Fig. 15 (a).

To carry out the test, a suitable area is chosen, away from reinforcement and edges. In each area three extraction are made: a hole orthogonal to the surface is drilled, the metallic insert is inserted and its head expands giving to the hole section a T shape. The jack is connected with the metallic insert and a constant increasing load is applied (0.5 kN/s), until the extraction force is detected (Fig. 15 (b)). At the end of the three extractions, the value of the extraction forces are averaged. The single value must not deviate more than 20% from the average one.

<center>(a)   (b)</center>
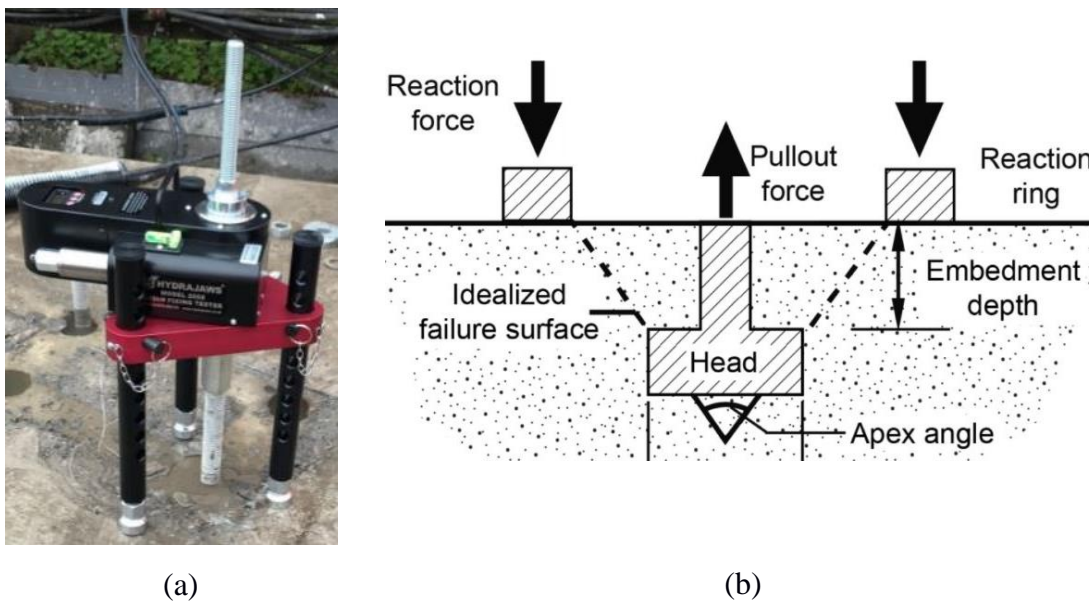
Fig. 15. (**a**) Instrumentation and (**b**) scheme test.

The correlation between the extraction force F, obtained from the force measured at the jack, and the cubic resistance R_c is generally defined by a linear relationship:

$$R_c = A + B \cdot F \tag{6}$$

where A and B are coefficient calibrated by destructive compression test.

2.4 Laboratory test on specimen extracted on site

In the laboratory different tests can be performed on the specimens extracted on site based on the number of specimens available and the information to be obtained. The number of tests to be performed and in particular their position must be carefully designed to avoid causing damage to the building or compromise its static equilibrium. Another aspect to take into consideration is the functional and aesthetic conservation of the building, especially when it belongs to the cultural and protected heritage.

Italian code [5], according to the level of knowledge of the building to achieve, provides for a different number of destructive tests, which in any case must be carried out. Furthermore, the characteristics of the materials determined with the destructive tests in the laboratory are useful for calibrating the correlations coefficients of non-destructive tests, as described previously.

2.4.1 Specimen extraction

The procedures for the extraction, processing of the extracted specimens and the subsequent compression test methods are described in UNI EN 12504-1, UNI EN 12390-2 and UNI EN 12390-3.

In Fig. 16 it is possible to observe a core barrel used to cut out the cylindrical specimens in the concrete element, while in Fig. 17 it is possible to see a piece of the specimen obtained before its complete extraction.

Compliance with the requirements of UNI EN 12504, from extraction to preparation of the specimens before tests, allows the reproducibility and repeatability of the results. On the contrary, results could be inconsistent and insignificant.

Fig. 16. Core barrel.

The following factors should be taken into account for designing number and location of the cores:

- the diameter of specimen should be between 75 and 150 mm and at least three times the maximum diameter of the aggregates;

- specimen must not contain reinforcement which would lead to evaluation errors in subsequent test;

- results of specimens with imperfections, such as microcracks and voids, should not be taken into consideration or at least be evaluated very carefully;

Fig. 17. Part of the specimen cut.

- the ratio height/diameter should be equal to 1, if we want to compare results with R_c, or equal to 2 if we want compare results with f_c. In any case this ratio should not be lower and greater than this value.

Each specimen must be accompanied by a sampling report that contains the identification code of the number of sample, the area and the date of extraction, the orientation of the core drilling with respect to the casting and the description of any irregularities.

2.4.2 Carbonation depth analyses

The carbon dioxide present in the air penetrate into naturally porous concrete elements, causing carbonation that develops from the surface of the element towards the inside. If the carbonation depth is greater than the concrete cover, the reinforcing bars are attackable by humidity or chlorides, with the risk of corrosion and consequent reduction of the reactive sections.

Indications for the execution of this test are contained in UNI 9944. This test can be performed in situ, on lesions or coring holes, or on specimen and consist in spraying a solution of alcohol and phenolphthalein on the area or specimen to investigate.

The non-carbonated concrete reacts with phenolphthalein turning purple. In this way, depth of carbonation is therefore measurable as the length of the cylindrical specimen which, starting from the external surface reaches the border of the coloured band.

In Fig. 18 it is possible to see the result of this test on the specimen extracted in Fig. 17. It can be noted that some centimetres at the right of the specimen, highlighted with the blue line, do not turn purple. Therefore the phenomenon of carbonation is present in this part of the specimen, while the remaining part, highlighted with yellow line, turn purple, meaning that this part is non-carbonated.

Fig. 18. Result obtained by spraying phenolphthalein on the specimen cut in Fig. 17.

2.4.3 Compressive strength test

The compression test has the purpose of determining the compressive strength of concrete specimens. As mentioned codes to follow for the execution of this test are UNI EN 12504-1, UNI EN 12390, that provide particular warnings for a correct extraction of specimens, recommending geometric limits and operational measures, all in order to avoid running insignificant results.

The specimen must be positioned in the testing machine so that the action is centered; the load is applied gradually, without shocks, with a gradient between 0.2 MPa/s and 1 MPa/s, until the specimen breaks (Fig. 19).

The strength determined with the specimens extracted by coring is generally lower than the one determined with the specimens taken during concrete casting. This is mainly due to the effect of the deterioration on the specimens caused by the coring. The Guidelines for the evaluation of concrete in place [7], in order to reliably estimate concrete strength, recognize these deterioration effects through the introduction of a multiplicative coefficient F_d, called the disturbance factor. This coefficient is equal to 1.10 for specimens' strength equal to 10 MPa and decreases

with the increase of the strength. Multiplying the extracted specimen's strength by F_d, gives the strength of the elements.

Fig. 19. Compressive strength test on cylindrical specimen.

2.4.4   Tensile strength test

The tensile strength test is performed on prismatic specimens, calculating the tensile strength in the center section, according to UNI EN 12390-5.

The specimen must be stored in an environment with a relative humidity of 90% and a temperature of about 20° C up to the maximum of two hours before the test.

The testing machine must be equipped with a support surface with two rollers supporting the specimen arranged symmetrically with respect to the axis. The load can be applied with a single roller centered in the middle, or with two application points, dividing the specimen into three equal parts.

Before the test, the geometry and the correct support on the rollers are checked. The load is applied gradually until failure, noting the maximum load and the location of the break.

The tensile strength (f_{ct}) is obtained know the flexural strength (f_{cf}), which is calculated as ratio between bending moment in the centerline and resisting modulus of the section, $W = b \cdot h^2/6$. In the case of single roller it results $f_{cf} = 1.5 \cdot F \cdot L/(b \cdot h^2)$, while with two rollers it results $f_{cf} = F \cdot L/(b \cdot h^2)$, where F is the applied force, L is the distance between the supporting rollers, b and h are the base and height of the section of specimen.

The tensile strength is obtained by inverting the relationship with the flexural strength:

$$f_{cf} = 1.2 \cdot f_{ct} \tag{7}$$

2.4.5 Determination of the modulus of elasticity

The instrumentation for the determination of the modulus of elasticity is constituted by the same testing machine of the compressive test and strain gauges for the measurement of deformations.

Cyclically variable stresses, from 1/10 to 1/3 of the compressive strength, are applied, measuring the strains at the maximum and minimum stress and in three intermediate values.

The modulus of elasticity value is obtained from the average of the E_i value calculated as:

$$E_i = (\sigma_0 - \sigma_1)/(\varepsilon_0 - \varepsilon_1) \tag{8}$$

where σ_0 is the minimum stress and ε_0 is the corresponding deformation.

2.4.6 Tensile test on reinforcing bars

The test performed in the laboratory to determine the mechanical characteristics of reinforcements taken on site from a reinforced concrete element is the same as

performed for new reinforcing bars. This test, performed according to UNI EN 10002-1, has the purpose of determining the yield and rupture stresses of the bars.

A piece of bar of about 50 cm is taken in an area of minimum stress of the element following these steps (Fig. 20):

1. identification of the reinforcement bar using the covermeter;

2. demolition if the concrete cover until the bar to be taken is exposed;

3. welding to the existing bar of a new bar of equal or greater diameter;

4. cutting of the piece of bar necessary for the test;

5. restoration of the initial condition to avoid corrosion of the reinforcements.

The extracted piece of bar is taken in the lab and, after having marked its initial length, is subjected to direct traction increasing the load until it breaks.

The cost of this test is about € 300 per bars.

Fig. 20. Extraction of reinforcement bar.

2.5   Destructive test for mechanical characterization on site

2.5.1   Single and double flat jack test

The flat jack test is an experimental investigation on site on the stress state of the element and elastic modulus of the material. The test instrumentation consist of a saw, to perform the cut, the flat jacks, which can have a rectangular or semicircular shape with a thickness of about 1 mm, an electric or manual pomp, a deformometer, to measure displacements, and a data acquisition unit.

The single flat jack test allows to estimate the state of local tension present in masonry structures. Having chosen a portion of the masonry wall representative of the type to be analysed, the measurement bases are placed above and below the position chosen for the execution of the cut, as equidistant as possible to it. At least four measuring points, that are the vertical elements in Fig. 21, are recommended. The strain gauges, used to measure the deformations, are positioned on a length equal to 75-90% of the distance between the jacks.

After taking the initial reference measurement of the distances, the cut is then carried out, usually along the mortar joint trying not to disturb the surrounding masonry. The cuts must be parallel and must be between 1 and 1.5 the length of the jack. The cutting involves the cancellation of the stress state and the approach of the two part of masonry divided by the cut, measured by the instrumentation.

After cutting, cleaning and positioning the jack, the pressure is applied from zero in increments of about 10% of the expected pressure and the deformations are measured after each settling pause. At each step, pressure of the jacks and deformations are measured and their increase is controlled in order to stop the test when it suddenly decreases, in order not to damage the masonry.

Fig. 21. Double flat jack test on masonry.

The corresponding pressure read at the jack (P) is the local tension in the masonry (σ), less two multiplicative non-dimensional constant, both lower than one:

$$\sigma = P \cdot k_1 \cdot k_2 \tag{9}$$

where k_1 depends on the ratio between the jack's area and the cut's area, and k_2, depends on jack's shape and stiffness.

The investigation with a double flat jack (Fig. 21), used to compress the masonry volume between them, aims of determining the elastic modulus and the Poisson's ratio.

For each step it is possible to calculate the tangent elastic modulus (E_{ti}) with the following equation:

$$E_{ti} = \frac{\delta f_{mi}}{\delta \varepsilon_{mi}} \tag{10}$$

where δf_{mi} is the increase of the stress and $\delta \varepsilon_{mi}$ is the corresponding increase in deformation.

The Poisson's ratio for the same interval is calculated as:

$$\nu = \frac{\delta\varepsilon_h}{\delta\varepsilon_m} \qquad\qquad \textbf{(11)}$$

where $\delta\varepsilon_m$ is the increase in vertical deformation and $\delta\varepsilon_h$ is the corresponding increase in transversal deformation.

At the end of the tests the jacks are removed and the cuts are closed with an appropriate mortar that does not shrink.

2.5.2   Diagonal compression test on masonry

This is a destructive test which aims to determine the shear strength and the tangential modulus of elasticity of a masonry, as indicated by UNI EN 1052-4:2001. It consists in isolating a piece of the wall panel, with dimensions 120 cm x 120 cm, and stressing it with a diagonal compression stress up to rupture.

The diagonal stress impressed faithfully reconstructs the stress's state that the masonry undergoes following the seismic action. In order to transmit this diagonal action to the panel, a series of metal elements must be applied to the opposite vertices of the free diagonal, designed to transfer the stress (Fig. 22). In the upper corner there is a hydraulic jack that works between two metal profiles: the innermost one rests on the edge of the panel, while the outermost one is connected by steel bars to the contrasting metal element located in the opposite edge. Once the metal system is installed, the panel is instrumented with four displacement transducers, arranged along the diagonals of the panel, to measure the deformation under the load.

Fig. 22. Diagonal compression test.

The test are performed with a loading phase and a subsequent unloading phase. In each cycle the load is increased respect to the previous one. The load is increased until the panel breaks, so as to identify the ultimate shear strength (τ_s) and define the value of the tangential stiffness (G) as a function of the progress of the cracks.

2.6 Dynamic tests and structural monitoring

Dynamic tests consist in applying a sinusoidal action to the structure obtainable with a vibrodine with rotating masses, gradually varying the rotation frequency. In this way it is possible to determine the main parameters that characterize the dynamic behaviour of the structure, for example the natural frequency of oscillation or the viscous damping coefficient. These parameters can be recorded and evaluated also by using the vibrations produced by the circulation of vehicles.

Structural monitoring allows to continuously monitor the evolution of the deformation process, displacements that can occur in a building, seismic effects and vibration. It can be performed when a damaged or suspected situation, such as

cracking, has to be kept under control, to know if the observed phenomena, such as cracks, are exhausted or still in development.

The instrumentation could be composed, for example, by inclinometers, to detect rotations, or crackmeters, to evaluate vertical and horizontal displacements due to opening of cracks, and a central unit to collect data and transmit them to the PC for processing.

The monitoring can involve various phases of the study if the building, starting from the survey phase, aimed at identifying the critical points where to install the instrumentation, continue during any load tests until the safety assessment is completed.

2.7   Italian code on existing buildings

Both NTC [4] and the relative explanatory Code [5] define an existing building as the construction that, at the date of the safety assessment or the intervention project, has been completely built, i.e. when the static test certificate has been issued or the structures, bearing walls, floors and roof have been entirely built.

The explanatory code [5], in order to take into account the different degrees of knowledge of the building, uses the concept of knowledge level, which is related to the knowledge of the building geometry, structural organization, construction details and materials. On the basis of the knowledge level a confidence factor is defined, which modifies the strength of the materials.

The assessment of safety and the design of the interventions must take into account the construction methods of the time, design or construction defects, if the building has been subjected to exceptional actions and if it has undergone degradation or modifications.

The designer of the retrofit, according to the available documentation and the quality and number of the investigation carried out, must specify the geometric and structural characteristics of the building and the permanent load and the degree of in-depth analysis achieved in the project.

The safety assessment of an existing structure is a procedure aimed at determining the actions that the structure is able to sustain. This assessment must be done when:

- there is a possible reduction in strength or deformation capacity due to foundational problem, damage from exceptional actions or degradation of materials;

- there is a change in the use of the building or part of it;

- design errors are found;

- works involving structural parts are carried out.

The safety assessment is performed with reference to the Basic Design Earthquake (BDE, with a 10% probability of being exceeded over the reference time period for seismic action, V_R), except for constructions in class IV for which also the verification under the Serviceability Design Earthquake (SDE, with a 50% probability of being exceeded over V_R) have to be performed.

The Italian Code [4], requires that the safety assessment of on existing building, as far as possible, must be carried out like that required for a new building. For this reason the Code introduces two new parameters for a quick comparison between the action that can be tolerated by an existing structure and that required for a new one:

- ς_E, defined as the ratio between the maximum seismic action that the structure can bear in its current condition and the maximum seismic action that would be used in the design of a new building with the same

characteristics. The parameter of the seismic action used to calculate the ratio is the peak ground acceleration, a_g, multiplied by the coefficient *S*, which accounts of the subsoil category and topographical conditions $(a_g S)$.

- ς_V defined as the ratio between the maximum variable vertical overload that can bear a specific part of the building and the value of variable vertical overload that would be used for a new building.

Three different types of intervention are identified in [4] and specified in [5]:

- **Repair or local interventions**, which concern individual parts or elements of the structure. This category includes interventions that do not significantly alter the overall construction behaviour, as reinforcement or replacement of structural elements, reinforcement or creation of new connections between individual elements, or interventions to increase ductility of the elements. For this interventions only the assessment of the local safety levels is required;

- **Improvement interventions**, that include all the interventions than can cause changes in the structural behaviour by making changes in the stiffness, resistance or deformation capacity of elements. As prescribed by [4], for this type of intervention the safety assessment is mandatory and aimed at determining the maximum admissible actions.

  The value of ς_E can be lower than 1. A retrofit intervention can be defined as an improvement for constructions in class IV, which include buildings with public or strategically important function, and school buildings in class III, if ς_E is greater than 0.6. For constructions in class III and II an improvement is obtained if ς_E is increased by 0.1;

– **Upgrade interventions**, which aim to achieve the safety levels required for new buildings. This involves that, after the intervention, ς_E is equal to 1. In the case that the change of use of the building or part of it leads to increases in vertical loads in the foundation greater than 10%, ς_E can be equal to 0.8.

2.7.1   Reference model for analyses

The definition of the reference model that describes the behaviour of the building as truthfully as possible is one of the most complex phases in the analysis procedure. Adequate knowledge of the building is a fundamental requirement for understanding the structural behaviour and possible criticalities.

The phase of knowledge and analysis are closely connected. For example, the type of tests of the investigation plan and their location can be chosen from an analysis based on preliminary data relating to the geometric, construction and material characteristics.

NTC prescribes a historical analysis, a survey of the building, the characterization of the materials and defines appropriate confidence factors, to be understood as indices of the level of depth reached in the knowledge of the building.

2.7.1.1   Historical analysis

The first step is to carry out an analysis of the building history, aimed at understanding the construction phases, any transformations undergone, instability and degradation phenomena.

The analysis begins with the acquisition of all the original available documents of the building, such as drawings and projects reports of the first construction and subsequent interventions, surveys already carried out, tests. This phase is used to identify the time of the building, the code used for the design the construction techniques and, the original shape and any variation or interventions carried out.

This work therefore allows to interpret the current condition of the building as a consequence of a series of events that have followed one another.

2.7.1.2 Survey
Concrete and steel constructions

For reinforced concrete and steel constructions, the survey is aimed at defining geometry and construction details. In particular, the geometry of the structural elements must be described as accurately as possible, while details can be detected by samples and then the performed evaluation can be extended to the other elements, taking account of the code and the construction techniques of the time of building.

For the geometry it is important to define the structural organization, position and dimensions of the bearing elements and secondary elements, type and layout of the floors. The analysis of structural details should lead to obtain information on the longitudinal and transverse reinforcement, thickness of the concrete covers, joints and connections.

Both geometric aspects and construction details information can be obtain from drawings or technical reports, but it is always good to carry out also an on-site check. The amount of in situ investigations depends on the level of knowledge to be achieved. Three levels of knowledge are provided:

- **limited investigation**, carried out to evaluate the correspondence between the design drawings and the building under analysis;

- **extensive investigation**, made when drawings are incomplete;

- **exhaustive investigation**, carried out when an accurate level of knowledge is desired.

2.7.1.3 Mechanical characterization of materials
Concrete and steel constructions

The test to determine the mechanical characteristics of concrete and steel are those described in the previous paragraphs. Tests on materials, that can be distinguished in three levels, can be performed on a number of different elements, depending on the level of knowledge to be achieve:

- **limited test:** they foresee a limited number of tests to complete the information on the properties of the materials derived from the construction drawings, from original test certificates or from codes of the time;

- **extensive tests:** a greater number of tests are carried out in situ or on specimens to obtain information in the absence of construction drawings or original test certificates, or when the values obtained with the limited tests are lower than those on the documents;

- **exhaustive tests:** a greater number of tests are carried out in situ or on specimens in addition to the previous level investigations to obtained a particularly accurate knowledge of the building.

For concrete and steel constructions, in Tab. 1 and Tab. 2, taken from [5], the level (limited, extensive and exhaustive) of the investigations is linked to the quantity of construction details to be examined and number of tests for the evaluation of the mechanical characteristics of the materials.

Tab. 1 Guideline definition of the survey and test levels for reinforced concrete building.

Level of investigation	Detail's survey	Test on material
	For each primary element (beams, columns …)	
limited	Quantity and arrangement of the reinforcement checked for at least 15% of the elements	1 concrete specimen every 300 m^2 of floor, 1 reinforcement bar for each floor
extensive	Quantity and arrangement of the reinforcement checked for at least 35% of the elements	2 concrete specimen every 300 m^2 of floor, 2 reinforcement bars for each floor
exhaustive	Quantity and arrangement of the reinforcement checked for at least 50% of the elements	3 concrete specimen every 300 m^2 of floor, 3 reinforcement bars for each floor

Tab. 2 Guideline definition of the survey and test levels for steel building.

Level of investigation	Detail's investigation	Test on material
	For each primary element (beams, columns …)	
limited	Characteristics of connections checked for at least 15% of the elements	1 steel specimen every 300 m^2 of floor, 1 bolt for each floor
extensive	Characteristics of connections checked for at least 35% of the elements	2 steel specimens every 300 m^2 of floor, 2 bolts for each floor
exhaustive	Characteristics of connections checked for at least 50% of the elements	3 steel specimens every 300 m^2 of floor, 3 bolts for each floor

Some important aspects to take into consideration are:

a) in checking the achievement of the percentages of the elements investigated for the purpose of surveying construction details, any repetitive situation are taken into account, as equal geometry and role in the structural scheme, to be extended to a larger percentage of elements;

b) for the purposes of material testing it is allowed to replace some destructive tests, up to a maximum of 50%, with at least three times of non-destructive tests;

c) it is advisable to provide for the carrying out of a second supplementary test campaign in the event that the rests of the first test are highly non homogeneous.

2.7.2   Levels of knowledge and confidence factors

The valuer of confidence factors is closely linked to the level of depth of the tests and the knowledge of the building achieved.

The Italian Code defines three levels of knowledge (LC) for existing buildings, which, in order of increasing knowledge, are LC1, LC2 and LC3. The level of knowledge depends on the depth of knowledge of the structure's geometry, the construction details, the mechanical properties of the materials, and the connections between elements. For every level of knowledge, a corresponding Confidence Factor (FC), greater than one, is defined to reduce the values of the mechanical properties of the materials.

For concrete and steel construction the level of knowledge acquired on the basis of the surveys, investigation on structural details and tests on materials, determines the value of the confidence factors to be applied. For the value of this factors it is possible to refer at Tab. 3.

Tab. 3 Level of knowledge in function of information achieved and confidence factor for concrete and steel structure.

Level of knowledge	Geometry	Structural details	Material property	FC
LC1	From original drawings with a quick survey or complete survey	Simulated project and **limited investigation** in situ	Usual values for construction practice of the time and **limited test** in situ	1.35
LC2		Original incomplete drawings with **limited investigation** in situ; or **extensive investigation** in situ	From the original project or from original test certificate, with **limited tests** in situ; alternatively from **extensive tests** in situ.	1.20
LC3		Original complete drawings with **limited investigation** in situ; or **exhaustive investigation** in situ.	From the original project or from original test certificate, with **limited tests** in situ; alternatively from **exhaustive tests**.	1.00

The quantity and type of information required for each of the three levels are specified below.

LC1: this level is reached when the historical-critical analysis has been carried out, the geometry of the structure is known on the basis of the original drawings or a relief characterized by *limited investigations* in situ on the reinforcements and connections, and the mechanical characteristics of the materials derive from projects or other documents, validated by *limited tests* in situ. The corresponding confidence factor value is **FC=1.35**.

LC2: this level is reached when the historical-critical analysis has been carried out, the geometry of the structure is known on the basis of the original drawings or a relief, the construction details are known either from drawings and *limited investigations* in situ on the reinforcements and connections, or from *extensive investigations*, and mechanical characteristics of materials are known either from the

project or other documents, integrated with *limited tests* in situ, or from *extensive tests*. The corresponding confidence factor value is **FC=1.2**.

LC3: this level is reached when the historical-critical analysis has been carried out, the geometry of the structure is known on the basis of the original drawings or a relief, the construction details are known either from drawings and *limited investigations* in situ on the reinforcements and connections, or from *exhaustive investigations*, and mechanical characteristics of materials are known either from the project or other documents, integrated with *limited tests* in situ, or from *exhaustive tests*. The corresponding confidence factor value is **FC=1**.

The investigation plan must be appropriately calibrated according to the preliminary analysis and the level of knowledge to be achieved, orienting the in-depth analysis in the most appropriate areas in relation to the safety of the structure and the homogeneity of the expected results.

2.7.3   Verification of the structural elements

According to [4], for existing building all the structural members must be verified for two different types of mechanisms: ductile and brittle ones. As defined in the explanatory code [5], ductile members and mechanisms are beams, columns, and walls subjected to moment with or without axial force, while brittle mechanisms are those involving shear.

The first step of the structural analysis of an existing RC building is the identification of the average strengths of concrete and reinforcing steel. These strengths can be determined through destructive and non-destructive tests and, if available, from the building design data.

For verifications of ductile mechanisms, concrete and steel strengths are calculated by dividing the average strength by the confidence factor, FC. For verifications of brittle mechanisms, the strengths are calculated by dividing the

average strength by FC and also by the partial safety factor of the material (γ_m), which is equal to 1.5 for concrete and 1.15 for steel [4].

The ductile behaviour of beams, columns and walls is verified checking Equation (12):

$$M_{Rd} \geq M_{Ed} \tag{12}$$

where M_{Ed} is the acting moment and M_{Rd} the resisting (yield) moment.

Regarding the brittle mechanisms, the verification is performed by comparing shear force with shear strength of the members. Considering beams and columns, the shear force is calculated in two different ways. If acting moments at the end sections of the member are lower than the respective yield moments, the shear force is derived from the results of the Finite Element Model (FEM) analysis.

On the contrary, if the acting moments calculated from the analysis are greater than the yield moments, shear force is calculated by considering the beam subjected to the yield moments amplified by FC at the ends and to the gravitational loads of the seismic combination along the beam length.

The shear force V has to be compared to the shear strength, V_{Rd}, which for cyclic loads, such as seismic loads, is calculated using the following equation [5]. The equation considers not only the three contributions due to axial force, concrete, and steel, but also the interaction with the flexural rotation of the element as function of the plastic ductility demand, $\mu_{\Delta,pl}$:

$$V_{Rd} = \frac{1}{\gamma_{el}} \left[\frac{h-x}{2L_v} \min(N; 0.55 A_c f_c) \right.$$
$$\left. + \left(1 - 0.05\min\left(5; \mu_{\Delta,pl}\right)\right) \left[0.16\max(0.5; 100\rho_{tot})\left(1 - 0.16\min\left(5; \frac{L_v}{h}\right)\right)\sqrt{f_c}A_c + V_W \right] \right] \tag{13}$$

where γ_{el} is equal to 1.15, h is the depth of cross-section, x is the compression zone depth, N is the compressive axial force, L_V is the shear span obtained by

dividing the acting moment by the acting shear, A_c is the cross-section area, f_c is the concrete compressive strength, ρ_{tot} is the total longitudinal reinforcement ratio, and V_W is the contribution of transverse reinforcement to shear strength.

V_W is calculated as $V_W = \rho_{sx}b_w z f_{yw}$, where ρ_{sx} is the transverse reinforcement ratio, z is the internal level arm, f_{yw} is the stirrup yield strength. $\mu_{\Delta,pl}$ is the plastic part of ductility demand equal to $\mu_{\Delta,pl} = \mu_\Delta - 1$, where μ_Δ is calculated as the maximum chord rotation at the considered seismic action, θ_m, normalized to the chord rotation at yielding, θ_y.

The maximum chord rotation is assumed equal to equation (14):

$$\theta_m = \frac{1}{\gamma_{el}} \cdot 0.016 \cdot (0.3)^\nu \cdot \left[\frac{max(0.01; w')}{max(0.01; w)} \cdot f_c\right]^{0.225} \cdot \left(\frac{L_v}{h}\right)^{0.35} \cdot 25^{\left(\alpha \cdot \rho_{sx} \cdot \frac{f_{yw}}{f_c}\right)} \cdot (1.25^{100 \cdot \rho_d}) \quad (14)$$

where γ_{el} is equal to 1.5 for primary seismic elements and 1 for secondary seismic elements, ν is the normalized axial force with respect to the concrete area multiplied by the concrete strength, w and w' are the mechanical reinforcement ratio of the tension and compression longitudinal reinforcement, respectively, and ρ_d is the percentage of any diagonal reinforcements.

The confinement effectiveness factor, α, is given by the following equation:

$$\alpha = \left(1 - \frac{s_h}{2b_0}\right)\left(1 - \frac{s_h}{2h_0}\right)\left(1 - \frac{\sum b_i^2}{6h_0 b_0}\right) \quad (15)$$

where s_h is the distance between the stirrups in the critical area, b_0 and h_0 are the dimensions of the confined core, and b_i are the distances between the longitudinal bars held by tie rods or stirrups present on the perimeter.

The chord rotation at yielding is obtained using the following expression:

$$\theta_y = \varphi_y \frac{L_v}{3} + 0.0013\left(1 + 1.5\frac{h}{L_v}\right) + 0.13 \cdot \varphi_y \frac{d_b \cdot f_y}{\sqrt{f_c}} \quad (16)$$

where φ_y is the yield curvature of the section, d_b is the mean diameter of the tension reinforcement, f_y is the steel yield strength divided by FC, and f_c is the concrete strength divided by FC.

Equation (13) is used when $\mu_\Delta > 3$, while for $\mu_\Delta < 1$, the following equation is used, Equation (17):

$$V_{Rd} = max \left\{ \left[0.18 \cdot k \cdot \frac{(100 \cdot \rho_l \cdot f_{ck})^{\frac{1}{3}}}{\gamma_c} + 0.15 \cdot \sigma_{cp} \right] b_w \cdot d; (v_{min} + 0.15 \cdot \sigma_{cp})b_w \cdot d \right\} \quad \textbf{(17)}$$

For $1 \leq \mu_{\Delta,pl} \leq 3$, the shear strength is obtained by interpolating between the value given by Equation (13) and the value given by Equation (17) for $\mu_{\Delta,pl} = 3$.

2.8   Example of different level of knowledge

This section presents an example of characterization of an existing building from the point of view of the knowledge level. The analysis is carried out on block 3 of the building, the plan of which is shown in Fig. 23, from which is also possible to identify the name of columns and beams. The phases of the survey and the mechanical characterization tests of the materials are hypothesized in order to reach different levels of knowledge (LC), and therefore different Confidence factors (FC). The cost of such analyses is also calculated.

The same building will be analysed in more detail in the next chapter (§ 3.1) and a seismic retrofit will be hypothesized (Building A).
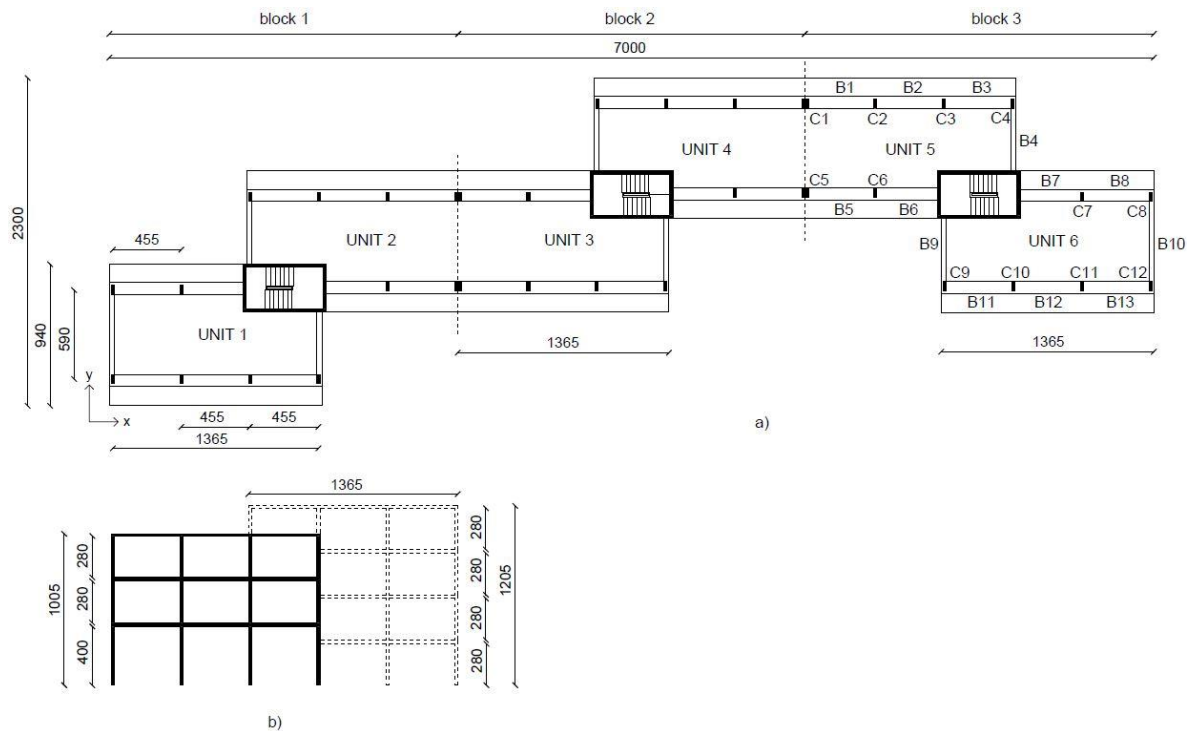
Fig. 23. Building analysed from the point of view of level of knowledge

2.8.1 Historical analysis and survey

The building is located in Udine, Italy, and was designed for gravity loads only. It is representative of many structures that were built in 1966, during the Italian national program of construction for worker housing.

Many documents about this construction were found: original drawings, technical reports, original material test certificates. From this documentation it was possible to understand that the building it was design just for gravity load, in addition to the materials used.

Building's vertical structures consist of columns, all with a section of 20×60 cm, with the larger side parallel to the y axis (Fig. 23 (a)), and walls only in correspondence with stairwells. All walls are 20 cm thick: the ones in X direction have length 520 cm and the ones in Y direction have length 315 cm.

Longitudinal reinforcement of central columns (columns like C2, C3 and C6 in Fig. 34 (a)) is made by 4Φ16 at corners along the entire height. The reinforcement of

external columns (columns like C1, C4 and C5) is composed of two layers per story, two layers each comprising 8Φ16 parallel to the two larger sides of the section in the lower three stories, and two layers of 6Φ16 in the top story where there are short columns that bear the roof. The transverse reinforcement of the columns consists of Φ6 every 10 cm.

Primary beams, oriented in X direction, have a section of 80×15 cm^2. Secondary beams, oriented parallel to the Y direction, are present only in the exterior sides of the building and have a section of 33×23.5 cm^2. All under-roof floors have beams parallel to the X direction, with a section of 80×15 cm^2, and beams parallel to the Y direction with a section of 20×15 cm^2. The longitudinal reinforcement of all beams is made by Φ16. The transverse reinforcement for beams in the X direction consists of Φ8 every 7 cm close to the beam ends and every 25 cm in the middle, while beams parallel to the Y direction are reinforced by Φ6 every 25 cm.

2.8.2   Procedures for carrying out the tests

The analysis is carried out on block 3, consisting of two units, unit 5 which consist of four floors and unit 6 which develops in height three floors.

The hypothesized destructive test are: tensile tests on reinforcing bars extracting from the building and concrete compression test on extracted cores. Non-destructive tests are: sonic test, cover meter test, rebound hammer test and carbonation depth analysis.

Cover meter test is planned to verify the positioning and diameter of the longitudinal bars, transverse reinforcement and the thickness of the concrete cover.

Extraction of reinforcing bars is planned in the areas of least stress of exterior columns; this test is not performed in the central columns because they have only four bars.

Regarding test on concrete, due to the little interaxle spacing of reinforcements of columns and beams in X direction, only micro-core drills are considered.

Both the sonic and the rebound hammer tests are performed to define the compressive strength of concrete.

The results of these non-destructive tests are used for the application of the SonReb method, which gives more precise results than just using sonic or rebound hammer tests results.

2.8.3 Typology, position and cost of tests

In this section the number of tests to be performed, their positioning and the total cost to obtain levels of knowledge LC2 and LC3 will be illustrated.

Block 3, which, as shown in Fig. 23 (a) consists of units 5 and 6, in this analysis is considered as a single building. To identify the number of tests to be performed, it is important to remember that each floor of each unit as an area of about 130 m^2 and that, as shown in Fig. 24, units 5 has four floors (continuous lines) and unit 6 has three floors (dotted lines).
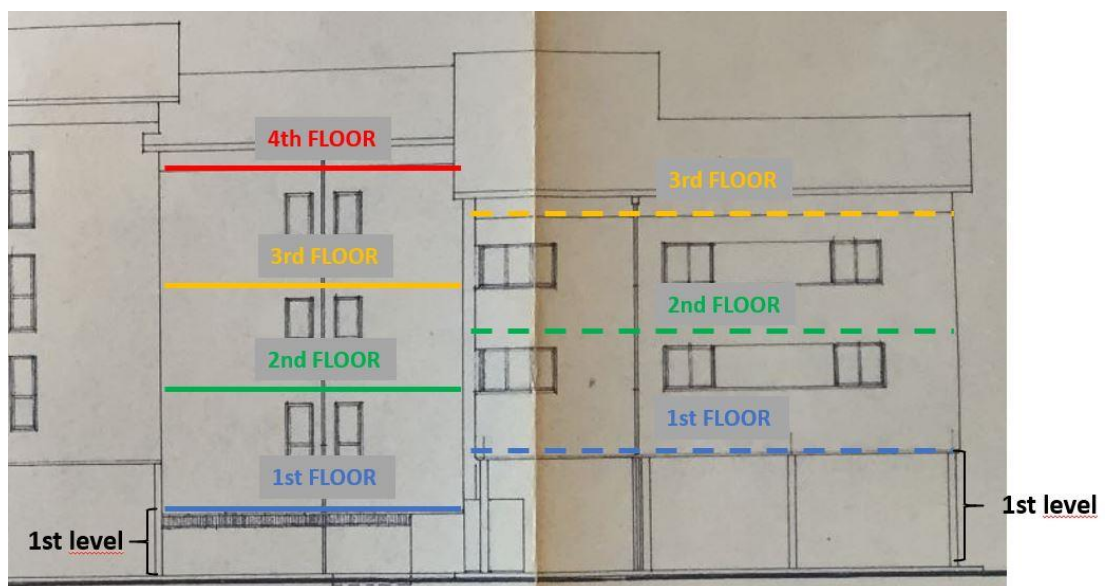

Fig. 24. Floor in unit 5 (continuous lines) and unit 6 (dotted lines)

For each of the two levels of knowledge three different hypothesis are carried out:

a) the first considering having architectural drawings, structural drawings and reports available and using destructive tests only for the mechanical characterization of the materials;

b) the second considering having the documents available and using both destructive and not-destructive tests for the mechanical characterization of materials;

c) the third considering not to having the documentation available and using both destructive and not-destructive tests for the mechanical characterization of materials.

Level of knowledge 2 (LC2)

a) documents available and destructive tests

With reference to Tab. 3 and Tab. 1, in case a), considering that the design documents are incomplete, it will be necessary to carry out **limited investigation** and **limited tests** in situ.

In unit 5 for each level 6 columns, 7 beams and 4 walls are present which multiplied by the four levels of the unit give:

$$6 \text{ columns } \cdot 4 \text{ levels} = 24 \text{ columns}$$

$$7 \text{ beams } \cdot 4 \text{ levels} = 28 \text{ beams}$$

$$4 \text{ walls } \cdot 4 \text{ levels} = 16 \text{ walls}$$

which added together give a total of 68 elements.

In unit 6 for each level 6 columns, 7 beams are present, which multiplied by the three levels of the unit give:

$$6 \text{ columns } \cdot 3 \text{ levels} = 18 \text{ columns}$$

$$7 \text{ beams } \cdot 3 \text{ levels} = 21 \text{ beams}$$

which added together give a total of 39 elements.

The total elements of block 3 are 68+39=107 elements.

To satisfy the request of the limited investigations, it is necessary to verify the quantity and arrangement of the reinforcement in 15% of the elements, i.e.:

$$107 \text{ elements } \cdot 0.15 = 16{,}05 \text{ elements}$$

Hence, it is necessary to investigate 17 elements.

To satisfy the request of limited tests in situ, since there are a maximum of 4 floors, each with an area of less than 300 m^2, it is sufficient to extract 4 samples of reinforcements and 4 concrete specimens, one for each floor, to be subject to compression test.

From Fig. 25 to Fig. 28 the position of the different tests for the different floors and levels relevant to analyse a) and b) is identified with symbols. Orange, blue and green filled symbols indicate destructive tests of hypothesis a), while blue and green symbols that have diagonal lines in light blue and light green respectively indicate destructive test that are not done in the analysis b) and which have been replaced by non-destructive tests done in analysis b), that are indicated with yellow and red filled symbols.
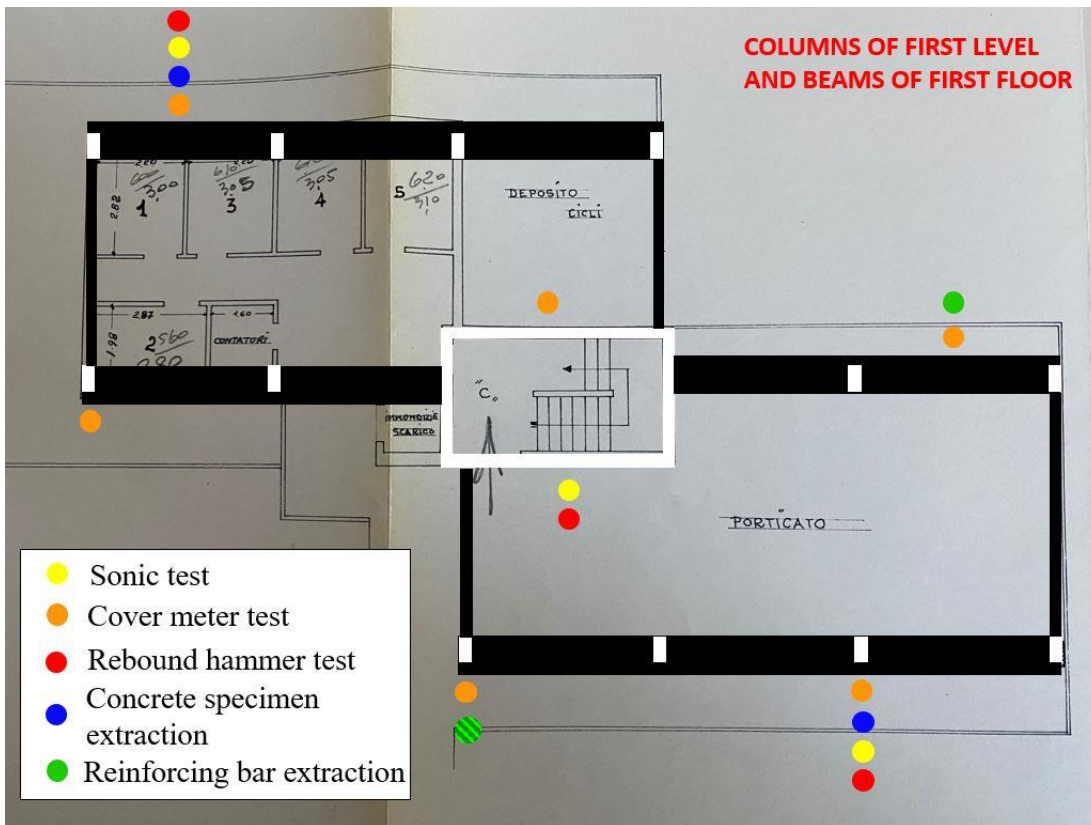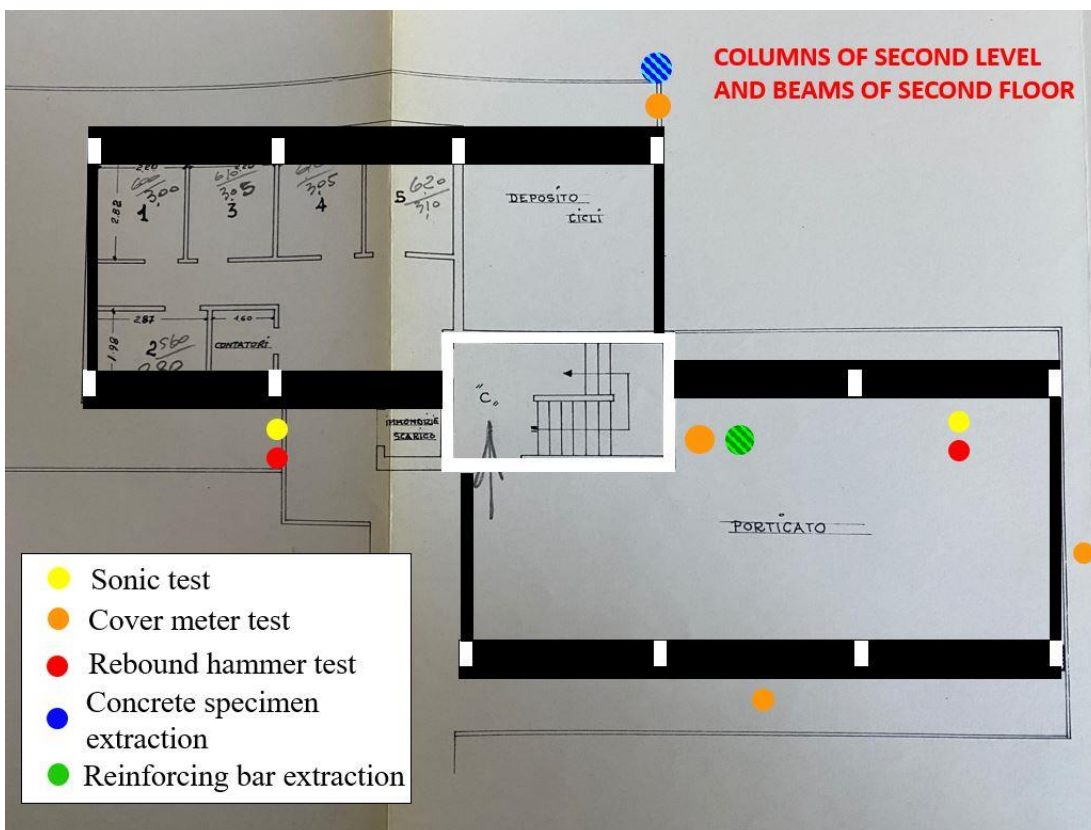
Fig. 25. Investigation and tests on level 1 and floor 1

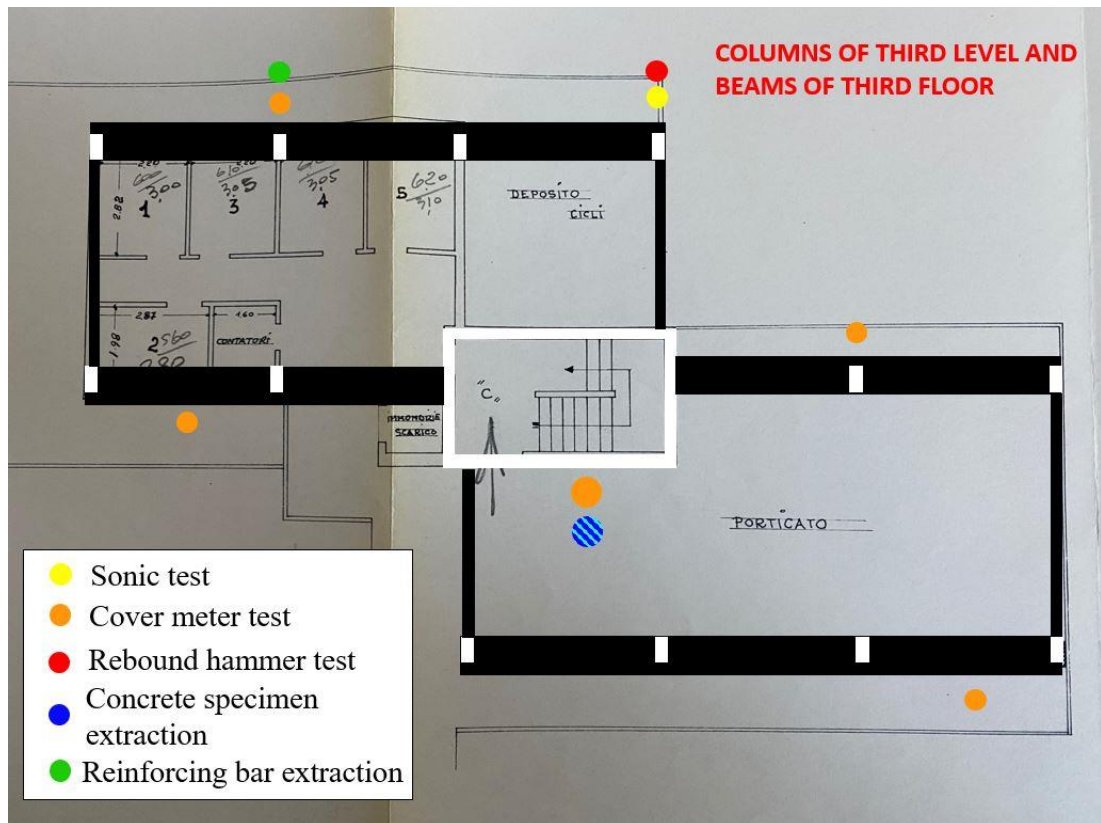**Fig. 26.** Investigation and tests on level 2 and floor 2

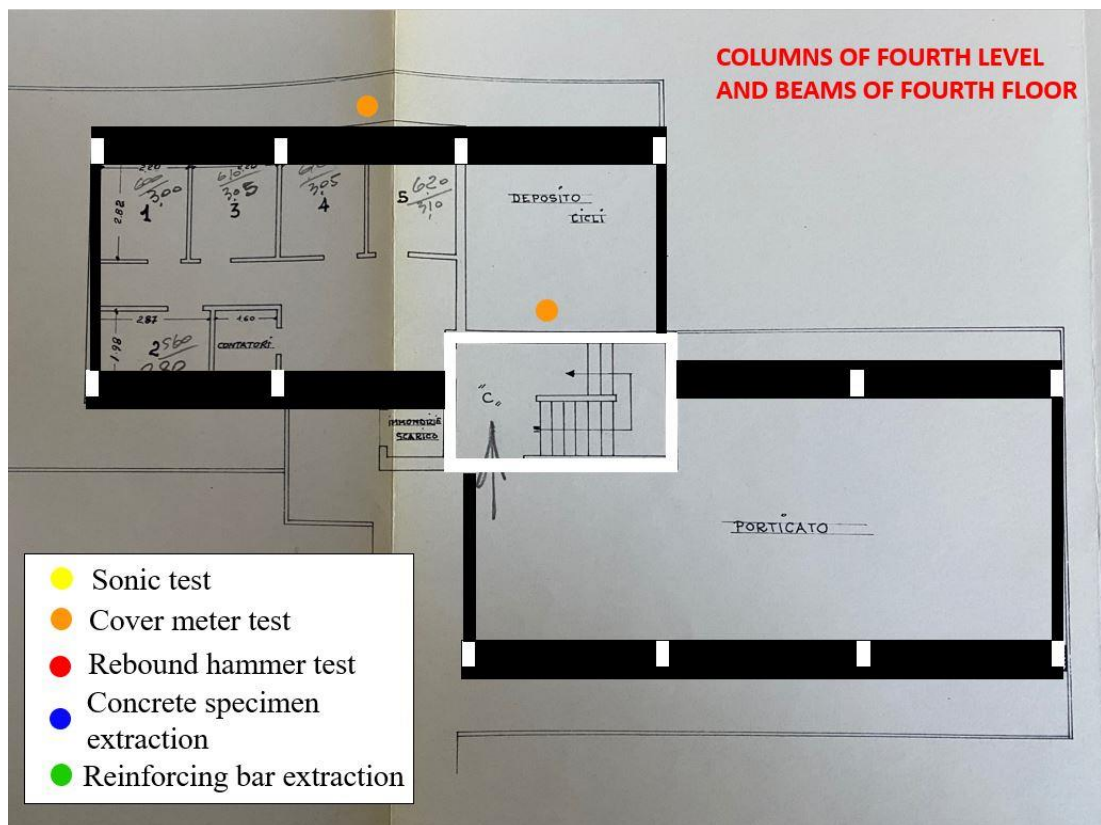**Fig. 27.** Investigation and tests on level 3 and floor 3

Fig. 28. Investigation and tests on level 4 and floor 4

Tab. 4 shows the total cost of the investigations and tests necessary to reach a level of knowledge equal to LC2 under the condition a).

Tab. 4 Total cost to reach LC2 using only destructive tests_case a).

Test	Unit price	Quantity	Total Price
Geometric verification	€ 10.00	10	€ 100,00
Cover meter test	€ 30.00	17	€ 510.00
Concrete specimen extraction and compression strength test	€ 275.00	4	€ 1˙100.00
Carbonatation test	€ 25.00	4	€ 100.00
Reinforcing bar extraction and tensile strength test	€ 205.00	4	€ 820.00
Foundation analysis	€ 350.00	2	€ 700.00
		TOTAL	€ 3˙330.00

b) documents available, both destructive and non-destructive tests

In case b) it is planned to use both destructive and non-destructive tests. According to [5], it is possible to replace some destructive tests, at most 50%, with a number of non-destructive test equal at least to the triple of the number of the substituted destructive tests.

To satisfy the request of limited tests in situ, it is possible to extract 4 samples of reinforcements, 2 concrete specimens and perform 6 SonReb tests.

Tab. 5 shows the total cost of the investigations and tests necessary to reach LC2 under the condition b).

Tab. 5 Total cost to reach LC2 using both destructive and non-destructive tests_case b).

Test	Unit price	Quantity	Total Price
Geometric verification	€ 10.00	10	€ 100.00
Cover meter test	€ 30.00	17	€ 510.00
Concrete specimen extraction and compression strength test	€ 275.00	2	€ 550.00
Carbonatation test	€ 25.00	2	€ 50.00
SonReb test	€ 65.00	6	€ 390.00
Reinforcing bar extraction and tensile strength test	€ 205.00	4	€ 820.00
Foundation analysis	€ 350.00	2	€ 700.00
		TOTAL	€ 3˙120.00

c) without documents available, both destructive and non-destructive tests

In case c), the second possibility given by [5] to reach LC2 is analysed, that is to carry out **extensive investigation and tests** in situ without having the documents available.

To satisfy the request of limited investigations, it is necessary to verify the quantity and arrangement of the reinforcement in 35% of the elements, i.e.:

$$107 \text{ elements} \cdot 0.35 = 37{,}45 \text{ elements}$$

Hence, it is necessary to investigate 38 elements.

Remembering that, according to [5] it is possible to replace at most 50% of destructive tests, with at least the triple of non-destructive tests, to satisfy the request of extensive tests in situ, it is necessary to extract 8 samples of reinforcement, 4 concrete specimens, to be subject to compression test, and to perform 12 SonReb tests.

Tab. 6 shows the total cost of the investigations and tests necessary to reach LC2 under the condition c).

Tab. 6 Total cost to reach LC2 with extensive investigation and tests in situ_case c).

Test	Unit price	Quantity	Total Price
Geometric verification	€ 10.00	10	€ 100.00
Cover meter test	€ 30.00	38	€ 1˙140.00
Concrete specimen extraction and compression strength test	€ 275.00	4	€ 1˙100.00
Carbonatation test	€ 25.00	4	€ 100.00
SonReb test	€ 65.00	12	€ 780.00
Reinforcing bar extraction and tensile strength test	€ 205.00	4	€ 820.00
Foundation analysis	€ 350.00	2	€ 700.00
		TOTAL	€ 4˙720.00

Level of knowledge 3 (LC3)

a) documents available and destructive tests

With reference to Tab. 3 an Tab. 1, to reach a level of knowledge LC3, considering that the design documents are incomplete, it will be necessary to carry out **limited investigation** in situ and **extensive tests** in situ.

As already seen for LC2, to satisfy the request of limited investigations, it is necessary to investigate 17 elements, while to satisfy extensive tests, only with destructive tests, it is necessary to extract 8 samples of reinforcements and 8 concrete specimens.

Tab. 7 shows the total cost of the investigations and tests necessary to reach LC3, for the analysis a).

Tab. 7 Total cost to reach LC3 using only destructive tests, with documentation available_case a).

Test	Unit price	Quantity	Total Price
Geometric verification	€ 10.00	10	€ 100.00
Cover meter test	€ 30.00	17	€ 510.00
Concrete specimen extraction and compression strength test	€ 275.00	8	€ 2˙200.00
Carbonatation test	€ 25.00	4	€ 100.00
Reinforcing bar extraction and tensile strength test	€ 205.00	8	€ 1˙640.00
Foundation analysis	€ 350.00	2	€ 700.00
		TOTAL	€ 5˙250.00

b) documents available, both destructive and non-destructive tests

Keeping the same number of investigation tests defined for reaching LC3 in analysis a), to satisfy the request of extensive tests in situ, it is possible to extract 8 samples of reinforcements, 4 concrete specimens and perform 12 SonReb tests.

Tab. 8 shows the total cost of the investigations and tests necessary to reach LC3 under the condition b).

Tab. 8 Total cost to reach LC3 using both destructive and non-destructive tests, with documentation available_case b).

Test	Unit price	Quantity	Total Price
Geometric verification	€ 10.00	10	€ 100.00
Cover meter test	€ 30.00	17	€ 510.00
Concrete specimen extraction and compression strength test	€ 275.00	4	€ 1˙100.00
Carbonatation test	€ 25.00	4	€ 100.00
SonReb test	€ 65.00	12	€ 816.00
Reinforcing bar extraction and tensile strength test	€ 205.00	8	€ 1˙640.00
Foundation analysis	€ 350.00	2	€ 700.00
		TOTAL	€ 4˙966.00

c) without documents available, both destructive and non-destructive tests

In case c), the second possibility given by [5] to reach LC3 is analysed, that is to carry out **exhaustive investigation and tests** in situ without having the documents available.

To satisfy the request of the limited investigations, it is necessary to verify the quantity and arrangement of the reinforcement in 50% of the elements, i.e.:

$$107 \text{ elements} \cdot 0.50 = 53.5 \text{ elements}$$

Hence, it is necessary to investigate 54 elements.

Remembering that, according to [5] it is possible to replace at most 50% of destructive tests, with at least the triple of non-destructive tests, to satisfy the request of extensive tests in situ, it is necessary to extract 12 samples of reinforcement, 6 concrete specimens, to be subject to compression test, and to perform 18 SonReb tests.

Tab. 9shows the total cost of the investigations and tests necessary to reach LC3 under the condition c).

Tab. 9 Total cost to reach LC3 with exhaustive investigation and tests in situ_case c).

Test	Unit price	Quantity	Total Price
Geometric verification	€ 10.00	10	€ 100.00
Cover meter test	€ 30.00	54	€ 1˙620.00
Concrete specimen extraction and compression strength test	€ 275.00	6	€ 1˙650.00
Carbonatation test	€ 25.00	4	€ 100.00
SonReb test	€ 65.00	18	€ 1˙170.00
Reinforcing bar extraction and tensile strength test	€ 205.00	12	€ 2.460.00
Foundation analysis	€ 350.00	2	€ 700.00
		TOTAL	€ 7˙800.00

Tab. 10 shows a summary picture of the costs to reach the two levels of knowledge following the three hypothesis made a), b), and c).

Tab. 10 Summary of the cost to reach different LC in different way.

Level of Knowledge (LC)	Documentation available	Test typology	Total Price
LC2	a) Incomplete documentation	Destructive tests	€ 3˙330.00
	b) Incomplete documentation	Destructive tests and non-destructive tests	€ 3˙120.00
	c) No documentation	Destructive tests and non-destructive tests	€ 4˙720.00
LC3	a) Complete documentation	Destructive tests	€ 5˙250.00
	b) Complete documentation	Destructive tests and non-destructive tests	€ 4˙966.00
	c) No documentation	Destructive tests and non-destructive tests	€ 7˙800.00

Analysing the costs calculated to reach LC2 level, it is observed that, if the project documents are available, even if incomplete, the use of only destructive tests or the use of both destructive and non-destructive test does not involve large price variations, with a saving in the second case (analysis b) of about 6%.

For analysis c), in which no documentation is available, using both destructive and non-destructive tests as made in hypothesis b), there is a cost increase of about 51% compared to analysis b), in which the documentation is available. This is due to the increase of investigations and tests required in the event that the documentation is not available.

Analysing the costs calculated to reach LC3 level with documentation available, as for LC2, the saving that occurs if both destructive and non-destructive tests are used compared to the use of only destructive tests is around 6%. From the

comparison between analysis b) and analysis c), where in both cases destructive and non-destructive tests are used, but in analysis c) the documents are not available, a price increase of about 57% in the analysis c) is found.

From these comparisons emerges the importance, also from an economic point of view, of the historical analysis and the possibility of having official documents of the analysed building.

On the other hand, it is observed that, by comparing the same types of analyse, reaching the highest level of knowledge (LC3) entails a higher initial cost that varies between 40% and 65% compared to that necessary to reach LC2. In particular, the largest cost difference is found if the documentation is not available, i.e. in the analysis c).

For this reason, it is necessary to preliminarily estimate, in economic terms, the benefit that the use of a lower confidence factor can bring.

2.9 BIM – Building Information Modelling

The knowledge of the geometric characteristics, through the use of the survey techniques as photogrammetry or laser scanning, and of the materials' properties, through the use of the tests described above, are the starting points for the application of the innovative Building Information Modelling (BIM) methodology also to existing buildings. Through BIM it is possible to create a 3D model of the analysed building that includes all the necessary information for its operation, maintenance and renovation.

2.9.1 Definition and benefit in the use of BIM methodology

As defined by Succar [14], Building Information Modelling is a set of technologies, processes and policies enabling multiple stakeholders to collaboratively

design, construct and operate an asset. The acronym BIM stands for both *Building Information Model* (product) and *Building Information Modelling* (process).

BIM is therefore not a specific thing or a specific software, but a methodology for design, construction and management of civil works that allows the integration, in a geometric model, of information related to different disciplinary sectors. The BIM process involves the work in all its phases, from design to construction and including maintenance and demolition, as show in Fig. 29.
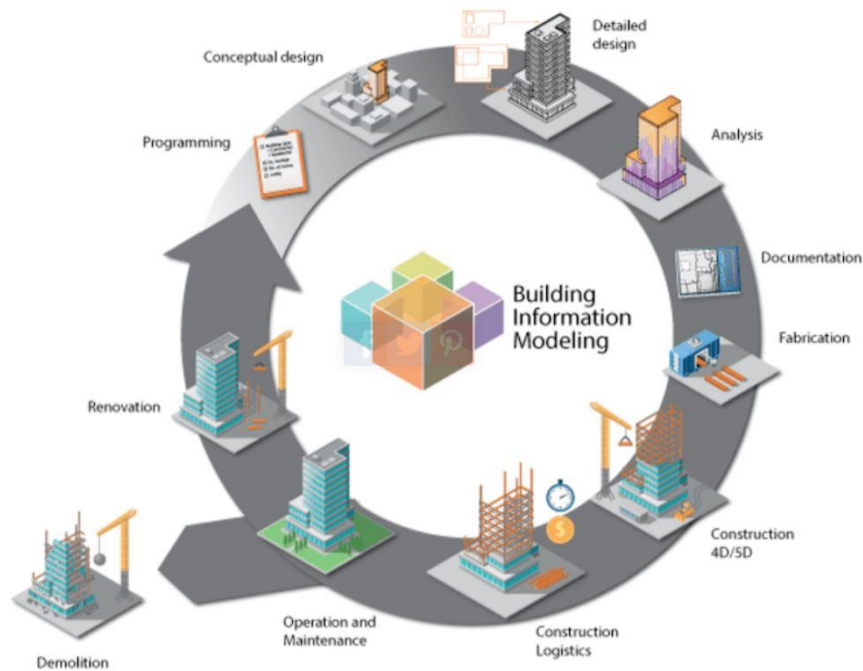
Fig. 29. BIM in all lifecycle.

As in the past, still today, in most cases, all the information of the various disciplines involved in the design phase is reported in numerous two-dimensional graphic tables, reports, technical diagrams and different documents.

As said, BIM is the acronym of *Building Information Modelling*, but this single words can be rearranged, as show in Fig. 30, to understand the true meaning of these methodology. In an initial phase, the different players involved in the design, depending on the discipline, work separately, preparing the model relating to their specialist subject. In a second phase all the specialistic models and the information

contained within then are merge into one single model, giving the final result, that is a virtual 3D twin of the asset (buildings, roads, gallery), through which it is possible to identify the positions of elements and systems, any interference among all the elements, and it can be traced back to who designed or supplied that element or material, its physical and mechanical characteristics, the history of its maintenance. From the model can be obtained geographical information, as dimension, position of the elements, and database information, as time, quality, cost, performance, who check the different design phases of a defined part of the project.

$$\textbf{B} \qquad \textbf{I} \qquad \textbf{M}$$

Building   Information   Modelling

$$\downarrow$$

$$\textbf{M} + \textbf{I} = \textbf{B}$$

Modelling   Information   Building
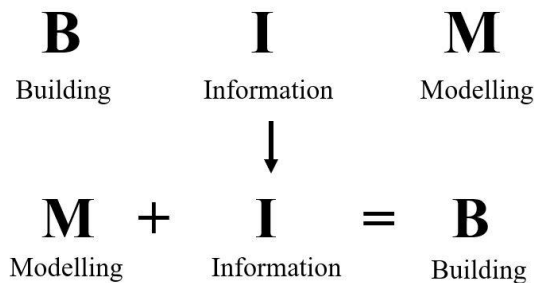
Fig. 30. Main part of BIM process: modelling and information.

The context in which the BIM methodology is developed is a Common Data Environment (CDE) in which is possible to find the 3D model of the building, which is only one of the parts of this methodology, the communications, documents, models updated to the last version, an indication of who did what and any problems encountered and to be solved.

The advantage of BIM is precisely the fact that the design decision are made at the beginning, taking into account the multiplicity of factor that influence the project and therefore fewer variations in the subsequent phases, which would lead to an increase in design costs. This concept is clearly illustrated in Fig. 31, where it is shown the MacLeamy curve, which relates the amount of work, in terms of time and cost, with the phases of the design process.

The blue line, n.1, determines the progress of the design choices during the project cycle. It is a decreasing curve as the choices are greater in the design phase,

especially in the preliminary phase. The red line, n.2, defines the cost of design changes. It is observed that the impact of design changes is much more expensive as the work progresses. The black line, n. 3, represents the standard workflow in a 2D process. It is noted that, in the current 2D design, there is a high effort in the executive design phase and in the preliminary construction phases. Therefore, in the current design, the resolution of design errors or problems in the construction phase not previously encountered occurs later in time, which causes a greater effort, cost and spend of time. With the BIM workflow, represent by the green line, n. 4, the design choices are anticipated, the identification of errors, interferences, design problems between the different disciplines move in the preliminary phase.
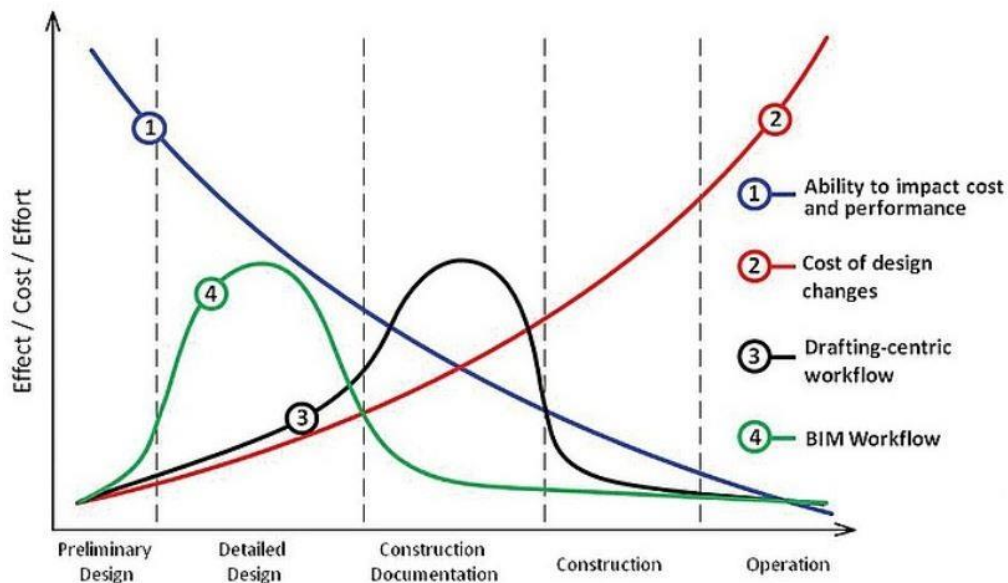
Fig. 31. MacLeamy curve [15].

One of the advantages of BIM is therefore to anticipate changes in the design phase compared to that in the construction phase, where the impacts are different. This translation of the curve towards the initial stages of design is, for example, allowed by the possibility of introducing in a single model all the elements that will form the asset, from the heating systems to the structural ones. In this way the information does not come from different tables but they are all collected in a single

model. The union of models of different disciplines in a single one, allows to identify clash between different elements.

BIM moves to a model based collaboration, to a logic based on a database, on a 3D model in which the information part is a fundamental aspect, to a sharing of information between the different disciplinary sectors by integrating the data. One of the BIM characteristics, once the rules are well defined, is that the models of the different disciplines can be created separately and then superimposed.

This interoperability between the various operators is ensured through the use of the Industry Foundation Classes (IFC) format, which is an open data format, not controlled by a single software developer.

2.9.2   DHBIM – Historic/Heritage Building Information Modelling

In the last years particular interest is focusing on the use of the BIM methodology on existing constructions, named Historic/Heritage Building Information Modelling (HBIM). Murphy et al. firstly defined HBIM in 2009 [16], that express the prospects of BIM in existing constructions. In many developed countries, such as Italy, the existing heritage is very extensive and it becomes essential to have technologically advanced tools for a proper conservation and management of it. The use phase is the longest phase of a building's life cycle and, for this reason, the use of advanced technologies to increase the efficiency of the facility management has become spreading in recent years. In this prospective Succar proposes a new interpretation of the acronym BIM that becomes Modelling Information – to manage and maintain – a Building, highlighting the great advantage that the use of BIM can bring within the maintenance of existing constructions.

The application of HBIM leads to the development of an inverse process, i.e. the model describes what is already built, and not what will be built, using parametric objects that represent architectural elements mapped onto laser scan or

photogrammetric survey data. Therefore, through the reconstruction of digital 3D models and, subsequently, the parameterisation of individual objects in the BIM environment, it is possible to associate physical-mechanical characteristics with each structural or architectural element and other imitated information [17]. This parametrization allow fast change of element's property, and control and automatic variation of the materials' quantity in case of modification.

Today, to obtain information about an existing building, it is necessary to analyse many documents, often even absent, which give a fragmented, incomplete and often inaccurate vision. Moreover, often several years after the end of the works, the building undergoes changes which are lost track for example because the drawings are not updated. This therefore leads to the inconsistency between the documentation and the actual state of the building. The implementation of the BIM methodology would instead allow to have a single data sharing environment, the CDE, to find all the information concerning the building, from the position of the systems, to the thermal characteristics of the envelope, to the maintenance carried out.

The use of BIM in the recovery and enhancement of the existing heritage is therefore a very important aspect, which would lead to an effective state of the art of the existing heritage in the area and would ensure easier availability of information and maintenance interventions. Consequently, a careful digital survey is necessary for the realization of this model, using tool such as laser scanners. The so-called SCAN to BIM process is defined in which the starting point is the point cloud and the end point is the BIM model.

2.9.3   Scan to BIM process

Beside geometrical characterization, existing building require further information   for the maintenance and conservation of the building itself, as past

intervention or details of the elements. Often historical construction are characterized by irregular geometries of its elements and non-constant section along their length, and, for a structural assessment, it is important to take into account the degradation of the materials properties.

If the information about the construction are not sufficient, techniques of data acquisition or survey are applied, that could be distinguished in non-contact techniques as photogrammetry and laser scanning and contact techniques as tape measurers. The choice of the type of survey technique, in addition to cost and ease of execution, is closely linked to the LOD of the elements of the model to be achieved. The most used techniques to take this data are laser scanning or photogrammetry. To acquire the geometric data of a building, often multiple scans with laser scanner, that has sufficient capability to provide dense point cloud and have to be merged into the same coordinate system, are required.

The major challenge of heritage BIM is the process of creating a parametric building information model from a point cloud, i.e. the modelling phase of HBIM that is the called scan-to-BIM [18]. This process has three main problems. The first one is that BIM software libraries do not contained complex element as ornaments. The second problem is that the process of automatic arrangement of the elements has not evolved and many errors are made, requiring a manual control and rearrangement of the elements in the model. In this way manual and semi-automated modelling techniques have dominated scan-to-BIM modelling procedures. The last main problem is that the point clouds only represent the external shape of an element, so the information regarding composition of assembly, construction procedures, internal layer's material are absent, and this property have to be found in documentation.

3 EFFECTS OF DISSIPATIVE SYSTEMS ON THE SEISMIC BEHAVIOUR OF IRREGULAR BUILDINGS – TWO CASE STUDIES

Having reached an adequate level of knowledge of the building history, the state of conservation and the geometric and mechanical characteristics, using the techniques described in the previous chapter, it is possible, if necessary, to proceed with the design of the building rehabilitation. Techniques for structural reinforcement and improvement of the seismic behaviour of the building as, for example, through the use of additional energy dissipation systems, can be used.

In this chapter, two case studies represented by RC residential buildings, both irregular in plan and along their heights, will be analysed. The buildings are both located in Udine, Italy, and were designed for gravity loads only. They are representative of many structures that were built during the Italian national program of construction for worker housing, which was launched in 1963 and managed by Management of Workers' Houses (GESCAL). Interventions by means of Buckling-Restrained Axial Dampers (BRADs) for one building and viscoelastic fluid dampers for the other are presented. To evaluate the seismic response of the as-built structures and retrofitted ones, Finite Element Models (FEMs) are implemented through the software SAP2000 (Computers and Structures, Inc., California, USA), and nonlinear dynamic analyses are performed.

The improvement of structural members' verifications due to the introduction of the dissipative systems is shown, by considering the number of members that satisfy the Building Code verifications before and after the retrofit interventions.

Moreover, it is shown that the introduction of the dissipative devices improves the torsional behaviour of the buildings, by increasing their torsional stiffness, and it can eliminate the problem of soft stories.

3.1   First case study – Building A

3.1.1   Description and characteristics of the building

The first case study, building A, highlighted in the red rectangle of Fig. 32 and shown in Fig. 33, is an RC residential building in Udine, Italy, designed and built between 1963 and 1966, in accordance with the provisions of the first Italian Building Code [19].
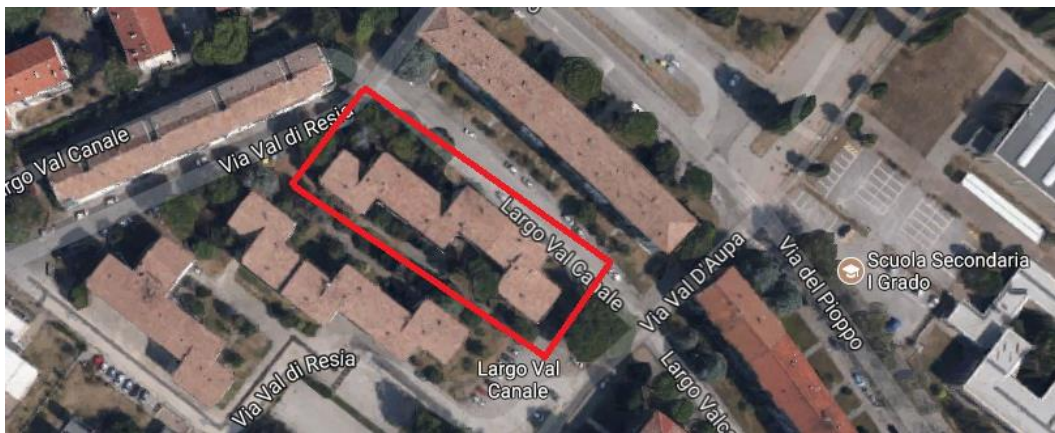
Fig. 32. Building's location.

Fig. 33. Building's photo.

To fully examine the building, following an archival research, all the graphic drawings of architectural and structural project were analysed, as well as the technical reports. Furthermore, in consideration of the years of construction, the construction techniques used in that period were also take into consideration.

This construction was built during the Italian program of worker housing, according to the code of the time that consider gravity load only.

Plan and elevation are shown in Fig. 34, while in Fig. 35 and Fig. 36 are shown respectively the original drawings of south-east and south-west elevation. The building is 70 m long and 23 m wide. Dotted lines in Fig. 34 (a) represent the presence of two technical joints, each made of elastomeric material and having a width of 4 cm. These two joints divide the building in three blocks. Each block is composed of two units, which are in opposite position with respect to the central stairwell.
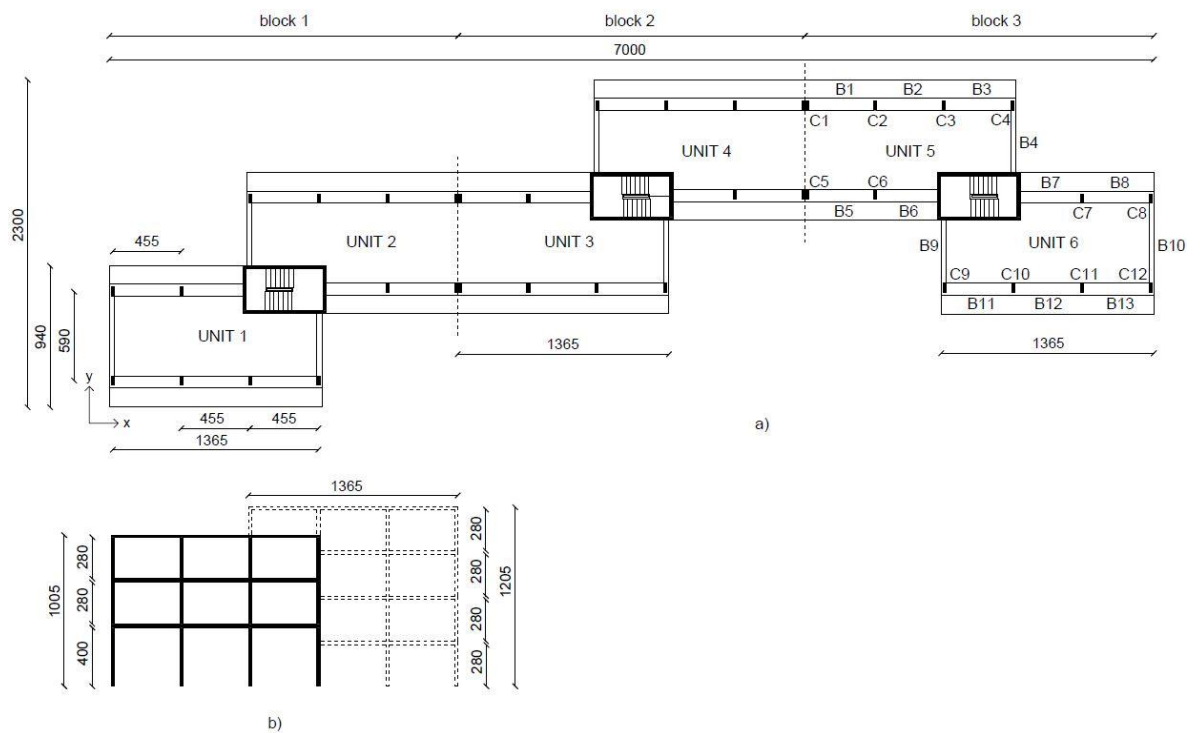
Fig. 34. Building A: (a) plan of the first floor and (b) elevation of block 1.
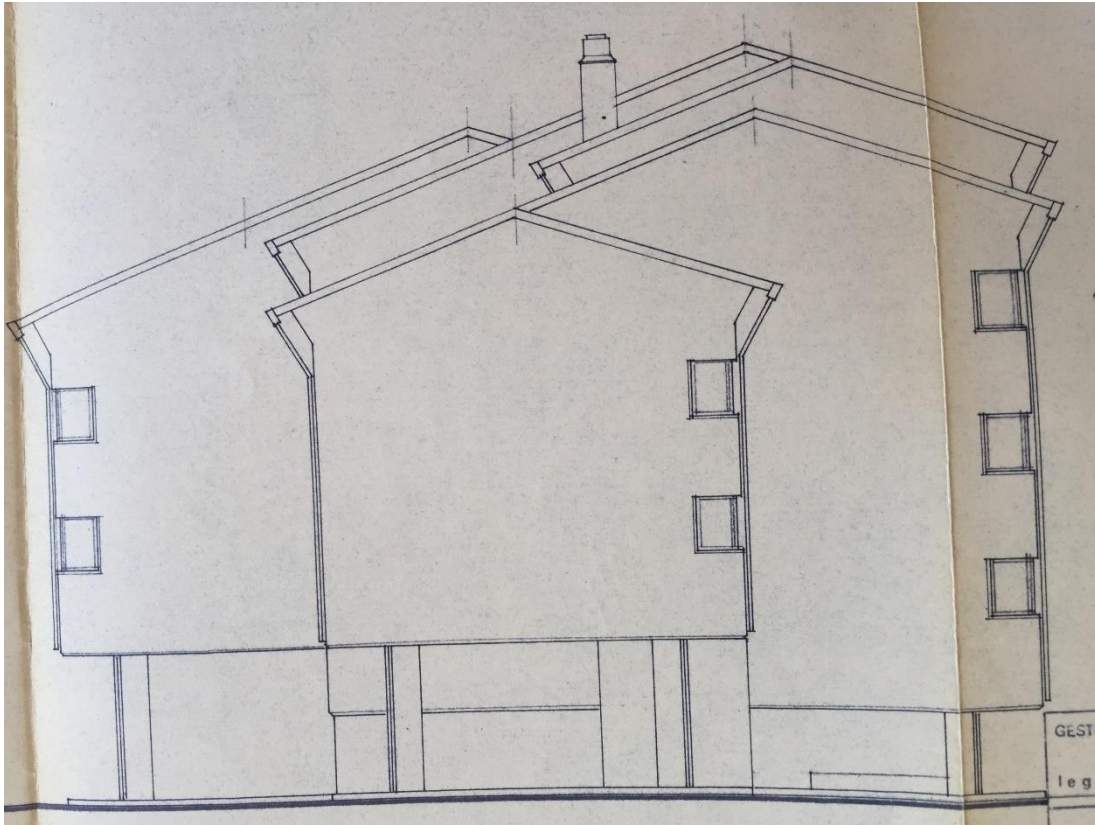
Fig. 35. South-East elevation in the original project.
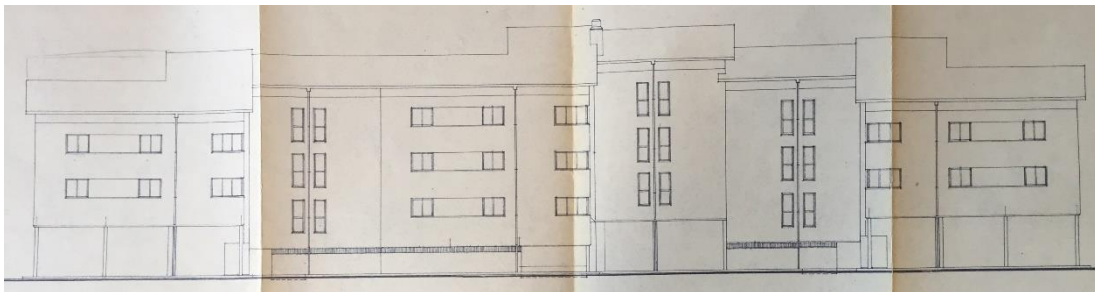
Fig. 36. South-West elevation in the original project.

Considering units 2 and 3, the maximum relative displacement in approach between them under seismic action occurs on the fourth floor and it is equal to 2.9 cm. Considering units 4 and 5, the maximum relative displacement in approach between them occurs on the fourth floor and it is equal to 3.2 cm.

In both cases the relative displacement of the two blocks is smaller than the width of the technical joint. Moreover, being that the joints are made of elastomeric material, their rigidity is assumed negligible. Hence, the blocks are not likely to

interact during the seismic motion. For this reason, the building can be divided into three independent blocks.

According to [4], each block is irregular both in plan and along the height. The irregularity in plan (Fig. 34 (a)) is due to the dispersed layout and the asymmetrical distribution of mass and stiffness with respect to two orthogonal directions of the block. The irregularity along the height (Fig. 34 (b)) is due to the different heights of the units and the staggered floors.

The two lateral housing units (no. 1 and 6) have three floors; the others have four floors. In all of the units the under-roof floor is impracticable, and the inter-story height of units is about 2.8 m, except for the first floor of units no. 1, 4, and 6, whose height is 4 m. On the ground floor of units no. 1, 4, and 6, the RC frame is not filled in by masonry walls, while the other three units have RC ground frames filled by masonry walls up to about 30 cm from the first floor. In this 30 cm there is a continuous strip window.

Building A's vertical structures consist of columns, all with a section of 20×60 cm, with the larger side parallel to the y axis (Fig. 34 (a)), and walls only in correspondence with stairwells. All walls are 20 cm thick: the ones in X direction have length 520 cm and the ones in Y direction have length 315 cm.

As shown Fig. 37, the longitudinal reinforcement of central columns (columns like C2, C3 and C6 in Fig. 34 (a)) is made by 4Φ16 at corners along the entire height. The reinforcement of external columns (columns like C1, C4 and C5) is composed of two layers per story, with layers comprising 8Φ16 parallel to the two larger sides of the section in the lower three stories, and two layers of 6Φ16 in the top story where there are short columns that bear the roof. The transverse reinforcement of the columns consists of Φ6 every 10 cm.
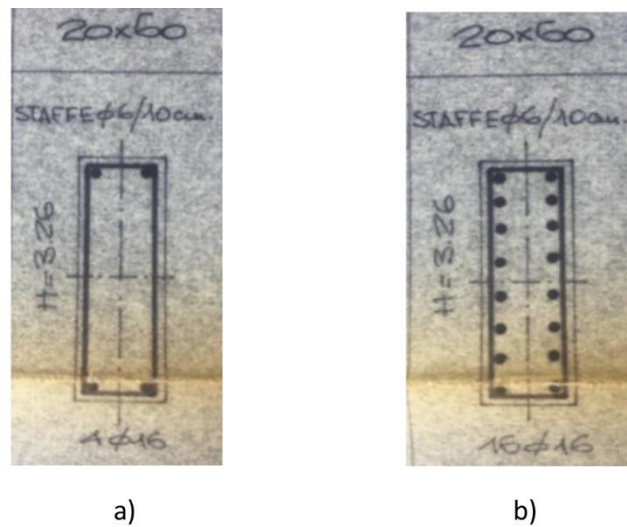
Fig. 37. Position of the reinforcements in the central (a) and external (b) columns.

Primary beams, oriented in X direction, have a section of 80×15 cm². Secondary beams, oriented parallel to the Y direction, are present only in the exterior sides of the building and have a section of 33×23.5 cm². All under-roof floors have beams parallel to the X direction, with a section of 80×15 cm², and beams parallel to the y direction with a section of 20×15 cm². The longitudinal reinforcement of all beams is made by $\Phi 16$. The transverse reinforcement for beams in the X direction consists of $\Phi 8$ every 7 cm close to the ends and every 25 cm in the middle, while beams parallel to the Y direction are reinforced by $\Phi 6$ every 25 cm.

Floors are made of precast RC joists, oriented parallel to the Y direction and having a depth of 20.5 cm and an interaxle spacing of 25 cm, completed with clay bricks and a cast-in-place concrete slab 3 cm thick. The under-roof floor is of the same type with the only difference being the joint depth, which is equal to 15.5 cm. In addition, the structure of the roof is similar, with a joint depth of 19.5 cm.

Foundations are composed of inverse T-shape RC beams, which connect the columns in the Y direction, and RC curbs in the X direction.

The characteristics of the materials are defined on the basis of available documentation. The concrete characteristic cylindrical compressive strength is equal

to 25 MPa. The concrete average strength can be calculated as $f_{cm}= 25+8 = 33$ MPa. Reinforcing bars are of Aq50 type, hence, according to [20], have a characteristic yield strength of 264.9 MPa. According to [5], the yield average strength of steel can be calculated as $f_{ym}= 264.9\times1.125 = 298$ MPa.

It was not possible to carry out tests on the building to define the mechanical characteristics of the materials, but, according to the hypotheses on the number, type and position of the tests illustrated in §2.8.3, it is believed that the tests to reach the level of knowledge LC2 would be easily performed. Furthermore, the economic impact that these test would have on the overall intervention is considered acceptable.

For this reason, for the considered case study, a level of knowledge LC2 is assumed, to which a confidence factor FC=1.2 corresponds [5]. Consequently, as described in §2.7.3 the concrete design compressive strength to be used for ductile mechanism verifications is:

$$f_{cd} = \frac{f_{cm}}{FC} = \frac{33}{1.2} = 27.5 \; MPa \tag{18}$$

and that for brittle mechanism verifications is:

$$f_{cd} = \frac{f_{cm}}{FC \cdot \gamma_c} = \frac{33}{1.2 \cdot 1.5} = 18.3 \; MPa \tag{19}$$

The steel design yield strength for ductile mechanism verifications is:

$$f_{yd} = \frac{f_{ym}}{FC} = \frac{298}{1.2} = 248.3 \; MPa \tag{20}$$

and that for brittle mechanism verifications is:

$$f_{yd} = \frac{f_{ym}}{FC} = \frac{298}{1.2 \cdot 1.5} = 215.9 \; MPa \tag{21}$$

3.1.2   Building's model

The building presented herein as case study is modelled using the commercial software for structural analysis SAP2000. As shown in Fig. 38 beams and columns are modelled through frame elements, while walls are modelled with thick shell elements to consider in-plane and out-of-plane behaviour.
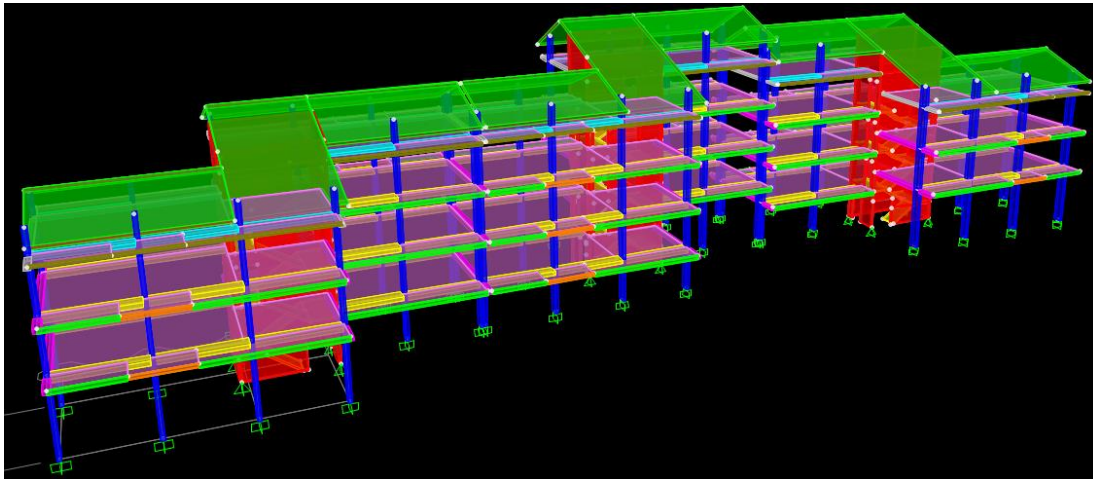

Fig. 38. Building A model in SAP 2000.

As prescribed in [4], cracking that arises in the structural members under the applied loads must be taken into account. This can be done by reducing the stiffness of the members. According to [4], the flexural and shear stiffnesses of cracked concrete members can be reduced by up to 50% of the stiffnesses of the corresponding non-cracked members. In this model the elastic modulus of the concrete is reduced by 50% for beams, while it is reduced by 30% for columns due to the presence of axial force on columns, which limits the depth of the cracks. For these reason, to take account of cracking, a reduced concrete elastic modulus equal to 22˙033 MPa for beams and 15˙738 MPa for columns is considered.

Floors of building A are 23.5 cm height and are made by a 3 cm thick upper RC slab and RC joists with height of 20.5 cm spaced of 25 cm. Between the joists, lightening elements made of traditional ceiling bricks are put. According to [4], a floor can be considered as rigid diaphragm only if the thickness of its slab is at least

4 cm. For this reason, the floors of the considered buildings are not modelled as rigid diaphragms, but as thick shells having the same thickness as that of the slab.

Gravity loads due to the floor weight are represented by a dead load of 4 kN/m^2 on habitable stories, 2.35 kN/m^2 on the under-roof story, and 2.70 kN/m^2 for the roof. The weight of the infill perimeter walls is considered assuming a linearly distributed load of 9.97 kN/m acting on the beams below. Live loads of 2 kN/m^2 are applied on all habitable stories, as well as 4 kN/m^2 on balconies and staircases, 0.5 kN/m^2 on under-roof floors, and 1.2 kN/m^2 on the horizontal projection of the roof, due to the snow.

Regarding the parameters of the seismic analysis, the nominal design life, V_N, representing the number of years in which the structure is to be used for its purposes, is assumed to be 50 years, which is typical for housing. The coefficient of use, C_U, related to the importance of the building, is assumed equal to 1, which is the value normally adopted for private buildings. The reference time period for seismic action, V_R, is obtained from $C_U \cdot V_N$, hence it is equal to 50 years. The topographic category is *T1* (flat surface), and the soil is B-type (coarse-grained soil).

To evaluate how much the FE model was representative of the actual building and reach an acceptable level of reliability, the forces obtained by the model were compared with those present in the design report. It was observed that the building was calculated using the method of admissible stresses and variable loads prescribed by the Code at that time are different from those prescribed by the current Code [4]. Hence, to make a comparison with the used FE model, a combination of actions, very similar to the one generally used for irreversible limit states of exercise (rare combination) was used.

The results obtained with the FE model have the same order of value and differ slightly from those present in the project tables.

The comparison made in this way made it possible to assess that the FE model is actually representative of the existing building.

In the Finite Element (FE) model, infill masonry walls are represented to take account of the stiffness and strength they give to the building. As regards the modelling of infill walls, the literature contains several schematizations with one or more compressive struts differently arranged (from [21] to [26]). This research work employs the schematization having an offset with respect to the top beam–column joint [22], as shown in Fig. 39 (a).

It is decide to model only the infill walls of the ground floor and not those of the upper floors, because the latter are less thick and have also many windows. The infill walls on the ground floor have an opening 30 cm high in the upper part, hence they are modelled as shown in Fig. 39.

(a)   (b)
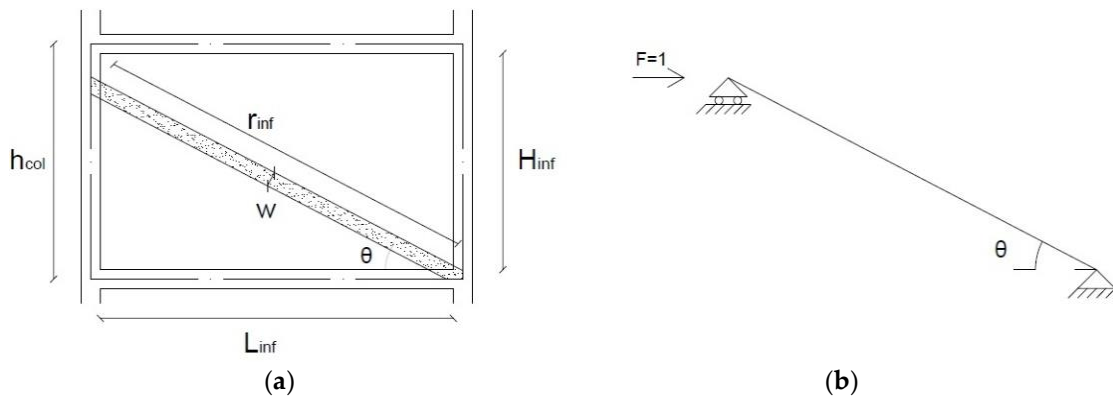
Fig. 39. Infill wall: (**a**) schematization and (**b**) static scheme to determine the equivalent stiffness of the infill walls.

The following equation proposed by Mainstone [27] is used to calculate the equivalent strut width, Equation (22):

$$w = 0.175 \cdot (\lambda \cdot h_{col})^{-0.4} \cdot r_{inf} \tag{22}$$

where r_{inf} is the strut length and λ is a dimensionless parameter that takes into account the effect of relative stiffness of the masonry panel to the frame, given by Equation (23):

$$\lambda = \sqrt[4]{\frac{E_w \cdot t_{inf} \cdot \sin(2\theta)}{4 \cdot E_f \cdot I_{col} \cdot h_{inf}}} \qquad (23)$$

with E_w the masonry elastic modulus, t_{inf} the thickness of the equivalent strut, θ the inclination angle of the strut with respect to the horizontal direction, h_{inf} the height of the masonry wall, and E_f and I_{col} the elastic modulus and the moment of inertia of the column, respectively. Angle θ is calculated as Equation (24):

$$\theta = \arctan\left(\frac{H_{inf}}{L_{inf}}\right) \qquad (24)$$

where H_{inf} and L_{inf} are the lengths of the strut vertical and horizontal projections, respectively.

Assuming a thickness of the masonry equal to 21 cm, from equation (22) the obtained equivalent struts width is obtained equal to 52 cm.

As mentioned, it is decided to represent the masonry with an equivalent diagonal strut resistant only to compression, since the masonry tensile strength is negligible. Precisely for this reason, in the FE model the masonry equivalent struts are modelled with the non-linear link (Nlink) element "gap", which is resisting to compression only. This Nlink consist of a spring, to which an equivalent stiffness is assigned, with an opening in series. The opening is closed when the masonry strut is subjected to compression, hence the Nlink works according to the equivalent stiffness assigned to the spring. While, when the strut is subjected to tensile action, the opening is open and the Nlink does not work.

Each masonry panel is modelled with two diagonal gaps arranged in a cross configuration, in order to consider the masonry's behaviour for an earthquake acting in both directions.

Fig. 40 show the definition of the Nlink "gap".

Fig. 40. Definition of Nlink "gap".

The axial stiffness k assigned to the Nlink is calculated by subjecting the diagonal strut to a unitary point load, as shown in Fig. 39 (b). The elastic modulus of the diagonal is assumed equal to 2˙700 MPa, as proposed by [5] for existing walls. Using the calculated displacement δ of the strut top joint, the axial stiffness is given by Equation (25):

$$k = \frac{F}{\delta \cdot \cos\theta} \tag{25}$$

A k value equal to 60˙000 kN/m is obtained that is assigned to the Nlinks.

The method of Fast Non-linear Analysis (FNA) is used to analyse the structure. This is a modal analysis method, implemented by SAP2000, designed to be used for structural systems which are primarily linear elastic, but which have a limited number of predefined nonlinear elements only. FNA is well-suited for time-history analysis, which is the analysis used in the two case studies, because of its computational efficient formulation. FNA formulation's efficiency is due to the separation of the non-linear-objects vector from the elastic stiffness matrix and the

damped equations of motions. At each time increment, forces within the non-linear-objects vector are resolved through an iterative process, while the uncoupled modal equations are solved exactly. This allows the formulation to rapidly converge to the equilibrium solution. Regarding the considered case studies, in the as-built structures the only non-linear members are the infill walls' equivalent struts, while in the retrofitted structures, the only non-linear members are the dissipative braces. Hence, FNA is a suitable analysis method for the case studies.

In the FNA, the modal damping does not depend on the structural stiffness, but only on the properties of the structural vibrational modes. Since the structural vibrational modes do not change during the FNA, the modal damping coefficients c_n associated to the n_{th} mode remain constant throughout the analysis, even when the structural stiffness changes. Thus, to define the modal damping it is sufficient to specify the damping ratios ξ_n for each mode.

For the case study, the modal damping has been defined by assigning a constant value of the modal damping ratio to all vibration modes. In particular, for the analysis of the existing building $\xi_n = 0.05$ has been assumed, while for the retrofitted structure $\xi_n = 0.02$ has been assumed.

To perform the FNA, firstly only permanent and variable gravitational loads are applied to the building's model by means of a ramp function. Starting from the deformed state of the structure due to these loads, a seismic load is applied, by means of accelerograms. The accelerograms are obtained from a SIMulation of earthQuaKE ground motion software (SIMQKE, prof. Piero Gelfi, Brescia, Italy). According to [4], the accelerogram compatibility with the design response spectrum occurs if the spectral ordinates of the elastic response spectrum obtained from the accelerogram are not 10% smaller than the corresponding ordinates of the design spectrum within

the greater interval between the 0.15 s–2 s and 0.15 s–2 T, where *T* is the fundamental period of the structure.

Fig. 41 illustrates the elastic response spectrum obtained from one of the accelerograms used in the analysis of building A, overlaid on the design elastic spectrum in the interval 0.15 s–4 s.
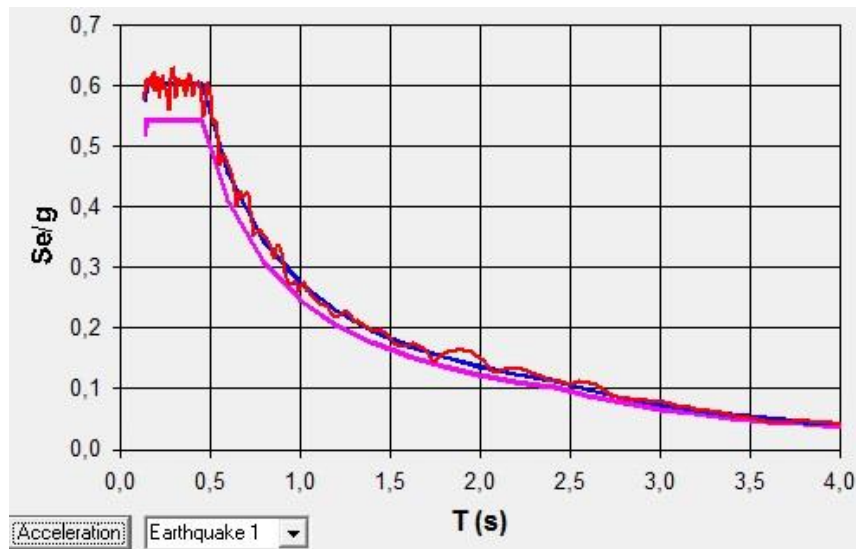

Fig. 41. Compatibility verification of one of the accelerograms used.

From Fig. 41 it can be seen that the red line, representing the spectral ordinates obtained from the accelerogram, is always above the violet one, representing the design spectrum with spectral ordinates reduced by 10%. Similar results are obtained for the other accelerograms used. It follows that the accelerogram is compatible with the design response spectrum defined by [4].

As prescribed by [5] for the case of non-dissipative structure, for the design spectrum it is possible to use a behaviour factor between 1 and 1.5. In this case study the value of 1 is assumed. Every accelerogram has a total duration of 30 s. Three groups made by two artificial accelerograms, one in the X and one in the Y direction, are considered to represent the seismic action, according to [4]. The most

unfavourable effects obtained from the three groups of accelerograms are used for the verifications the structures.

Since the three two-unit blocks of which the building is made are equivalent to each other, an analysis of only the block formed by units 5 and 6 is presented in the following.

3.1.3   Results of the Modal and FNA Analyses

The results of the modal analysis on block 3, made of unit 5 and unit 6, are summarized in Tab. 11, where the period of vibration of the main modes are reported together with the corresponding Modal Participating Mass Ratio (MPMR) in the three principal directions of the building. Tab. 11 shows that the fundamental period of the building is 0.67 and that modes 8 and 10 are mixed rotationally around the vertical axis z and translationally along Y axis. Mode 12 is translational along X.

Tab. 11 Modal parameters of building A.

Vibration Mode	Period (s)	Modal Participating Mass Ratios		
		Ux	Uy	Rz
1	0.67	0.00002	0.001	0.0017
8	0.59	0.0005	0.10	0.62
10	0.46	0.02	0.60	0.14
12	0.28	0.71	0.02	0.0007

As define in §2.7.3, equation (12) is used for ductile mechanisms of beams and columns, and Equation (13) or (17) for brittle verification. All the results for beams and columns are shown in Fig. 42-Fig. 45, where on the horizontal axis the names of the members are reported, with beams indicated by letter B and columns by C. The letter is followed by an ordinal number, which identifies the position of the member with respect to the building plan, as shown in Fig. 34.

In the diagrams, for every structural member, three or four differently coloured columns are drawn. These columns indicate the position of the member with respect

to the stories of the building, where the lightest coloured column corresponds to the lower level, while the gradually darker columns indicate higher and higher levels.

For the verification of ductile mechanisms, in Fig. 42 and Fig. 43 the ratio between demand and capacity is represented on the vertical axis. For the verification of brittle mechanisms, in Fig. 44 and Fig. 45 the ratio between acting shear force and the shear strength is reported. For both types of mechanisms, the verification is satisfied if the ratio is less than 1; otherwise it is not satisfied.
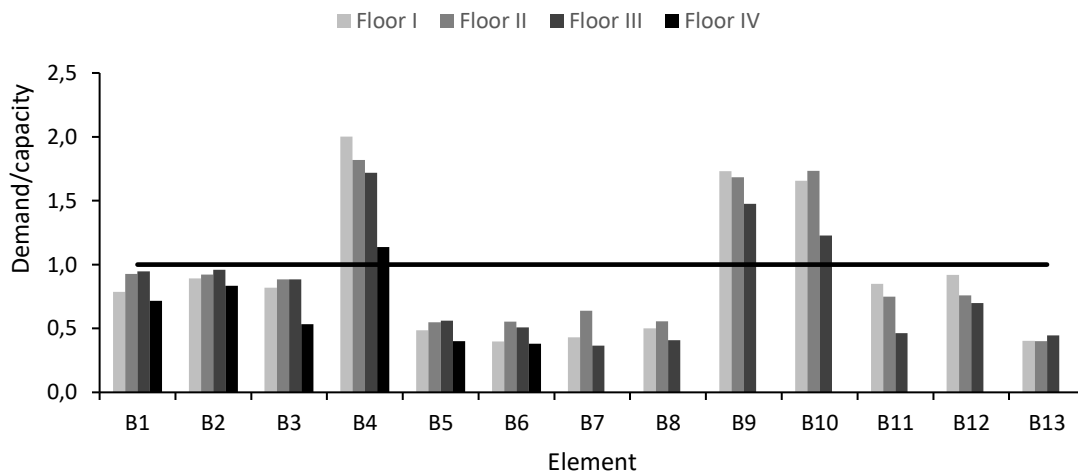
Fig. 42. Bending verifications of beams in as-built condition.
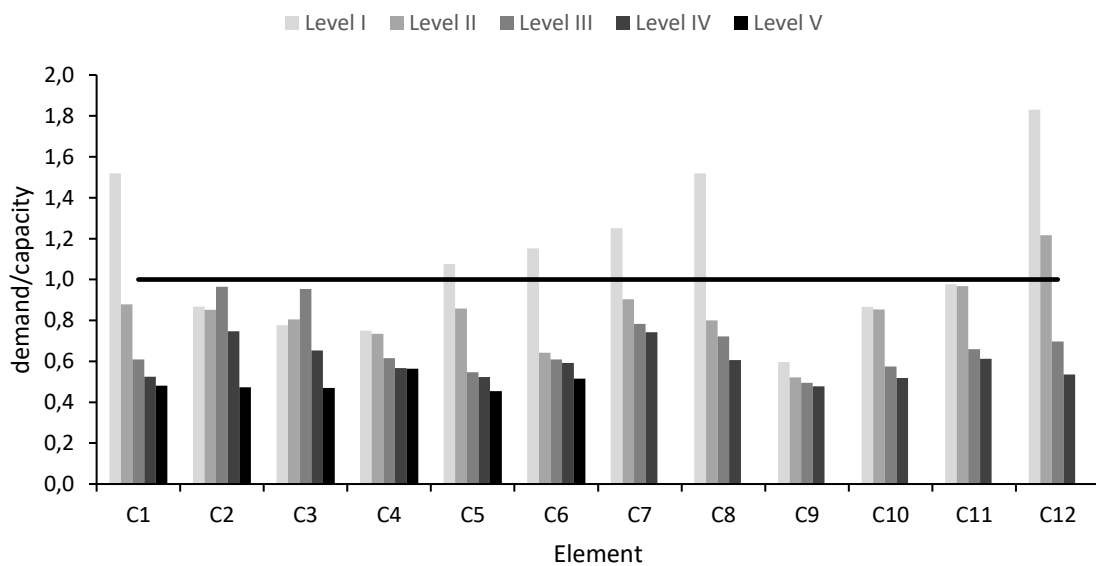
Fig. 43. Combined bending and compression verifications in as-built condition.
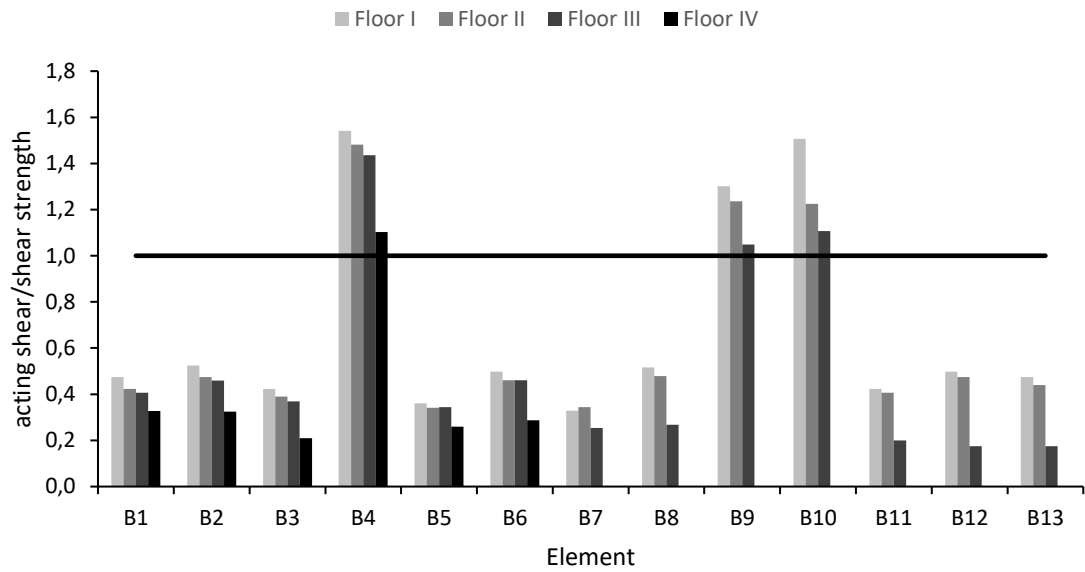
Fig. 44. Shear verifications of beams in as-built condition.
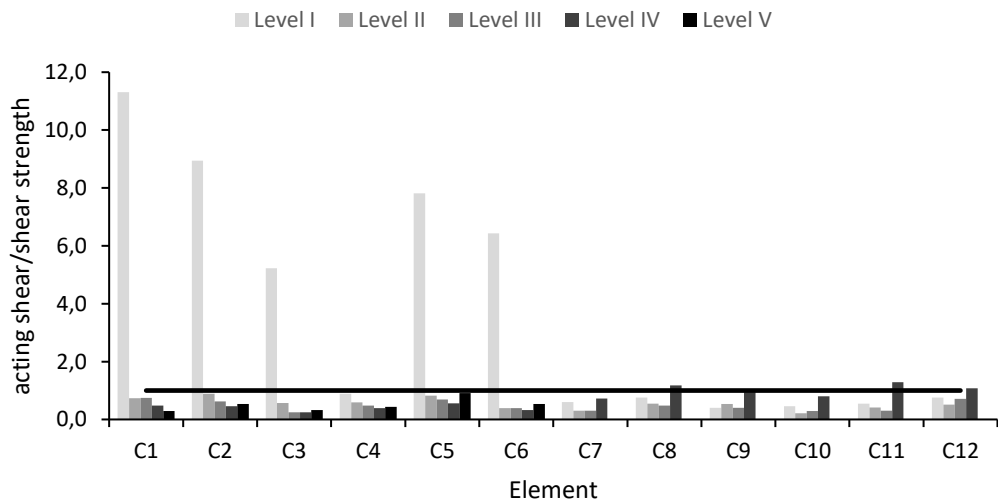
Fig. 45. Shear verifications of columns in as-built condition.

Fig. 42 shows that all beams in the x direction satisfy ductile mechanism verifications, since the ratio between demand and capacity is lower than 1 in all cases. Secondary beams, in the y direction, do not satisfy this verification, due to the small section and the low amount of steel reinforcement.

Fig. 43 shows that the columns that are more distant from the walls, namely C1, C5, C8 and C12, do not satisfy the ductile verification at the base. Additionally,

columns C6 and C7 do not satisfy the ductile verification at the base, because they have less longitudinal reinforcement.

Fig. 44 shows that the ratio between shear acting force and shear strength is lower than 1 for all beams in the X direction (B1–B3, B5–B8 and B11–B13), which have transverse reinforcement spacing equal to 25 cm in the middle and 7 cm at the beam ends. Conversely, the ratio is greater than 1 for the beams in the y direction (B4, B9 and B10), which have a constant spacing of 25 cm everywhere along the beam.

Fig. 45 shows that, in unit 6, the acting shear force exceeds the shear strength on the last level, where columns connect the top floor with the roof and have a short length, equal to 1.4 m. In unit 5 this occurs also on the first story, due to the presence, at this level, of infill walls with an opening of about 30 cm at the top. This configuration induces shear failure due to short column effect.

The joints of the building have no transverse reinforcement for shear resistance. For this reason, none of them satisfy the tensile verification for beam–column joints according to [5]. Furthermore, none of the interior joints satisfy the compressive verification, which is satisfied only for the exterior joints.

Regarding the walls, both ductile and brittle verifications are satisfied. On the basis of the previously described results, it can be said that the building may develop brittle non-dissipative failure mechanisms under seismic action. To improve its behaviour a retrofit intervention with the use of dissipative devices is proposed.

3.1.4   Retrofit Intervention with BRADs and Effects

A BRAD ([28]-[29]) is a non-linear anti-seismic device whose behaviour depends on displacement. The most common configuration of BRADs consists of an internal steel core encased in an external hollow steel profile, filled with concrete. A layer of low friction material is interposed between the steel core and concrete and

allows relative axial deformation between the inner core and the external steel profile. This slip surface allows the steel core to deform in the plastic field and, therefore, dissipate energy. Lateral confinement, conferred by the concrete layer and the external steel profile, prevents buckling of the steel core during the compression phase. In this way, it is possible to dissipate energy both during tension and compression phases.

BRADs are particularly suitable to be mounted on steel braces for seismic retrofit of steel and RC frame buildings, both new and existing. Their use leads to an improvement in the dissipative capacity of the building, concentrating the dissipation in the devices and, therefore, reducing the actions on the building structural members. The advantages of BRADs are evident from the large hysteresis loops, energy dissipation when loaded in both tension and compression, significant stiffness after yielding, and slight strength deterioration under cyclic loading, all of which contribute to a reduction in displacements and good energy dissipation capacity.

Within the passive energy dissipating systems, BRADs belong to the category of displacement-activated devices. This devices dissipate energy through the relative displacement occurring between their connected points. Because the building in the as-built configuration has inter-floor displacements of about 1.5 cm, it is decided to use BRADs devices for the retrofit intervention, since displacements of this order of magnitude allow BRADs to work properly and dissipate a satisfactorily energy amount. Moreover these displacements are compatible with the maximum displacements allowed for numerous BRADs available on the market.

In SAP2000, BRADs can be implemented by using the Nlink "*Plastic wen*", due to the fact that the hysteretic cycles obtained using this Nlink are similar to the ones obtained from experimental tests.

In the catalogue [29] from which the devices have been chosen, each BRAD type is identified by a code of the type N/M-b, where N is the number of the model. As this number increases, there is an increase in the elastic stiffness, the yielding strength and the ultimate strength of the device. The second number, M, represents the sum of the devices' allowed displacements in tension and compression and the letter "b" means BRAD. Elastic stiffness, yield strength, post yield stiffness ratio and yielding exponent are the parameters required to define the constitutive relationship of the devices.

The design of the BRAD devices is obtained by imposing the yielding of the device for an axial action intermediate between that at the SDE and that at the BDE. The idea is to impose that the dissipation begins after exceeding the SDE and enough before the BDE to contain lateral deformations and reduce stresses compared to the as built building.

The design strategy resides in minimizing the difference between the seismic input energy and the energy dissipated by the dampers, so that the seismic energy absorbed by the building is as low as possible. In this way the stresses on the building structural elements are reduced. The intervention and arrangement of the devices, in addition to reduce the stresses on structural elements, also aim to regularize the torsional behaviour of the building. The goal in the choice of BRADs' type and their disposition is to reduce as much as possible the number of ductile and brittle mechanisms, which may produce damage in the building.

BRAD choice and position inside the structure have been arranged by a trial and error method. Different in plan and in elevation dispositions, with different BRAD types, were analysed. It was observed that placing the devices as much as possible near the perimeter gave the best results. Moreover, it was observed that by using different devices with gradually lower stiffness along the elevation, large hysteretic

cycles were developed also by the devices in the highest floors. Many of the studied configurations gave good results, but the one proposed in the following (Fig. 46) gave the best results in terms of width of device hysteretic cycles and, consequently, in terms of energy dissipation.

In one of the analysed configurations, the same position of the devices, as the final one shown in Fig. 46, was maintained, but, instead of using devices with gradually lower stiffness along height, a single type of device, the one with the bigger stiffness, was used. In this case, the energy dissipated by the devices was found to be about 8% less than that of the final configuration, and the energy dissipated by the building through modal damping was greater than that dissipated by the devices. For these reasons it was decided to analyse other configurations.

Another configuration analysed consisted in using devices with gradually lower stiffness along the height, but different position in plan. In particular, with reference to Fig. 34, the devices were set between columns C1 and C2 in Unit 5 and between columns C11 and C12 in Unit 6. The devices were placed in proximity to those in the y direction. In this configuration, the energy dissipated by the devices is a little big greater, about 2%, than the one dissipated by the final configuration used. However, since there are windows in the corners of the building and to avoid two different devices being connected to the same column, it is decide to use the solution show in Fig. 46. As in can be seen in this figure, to realize the building retrofit, V-shaped steel braces on which BRADs are mounted are installed.
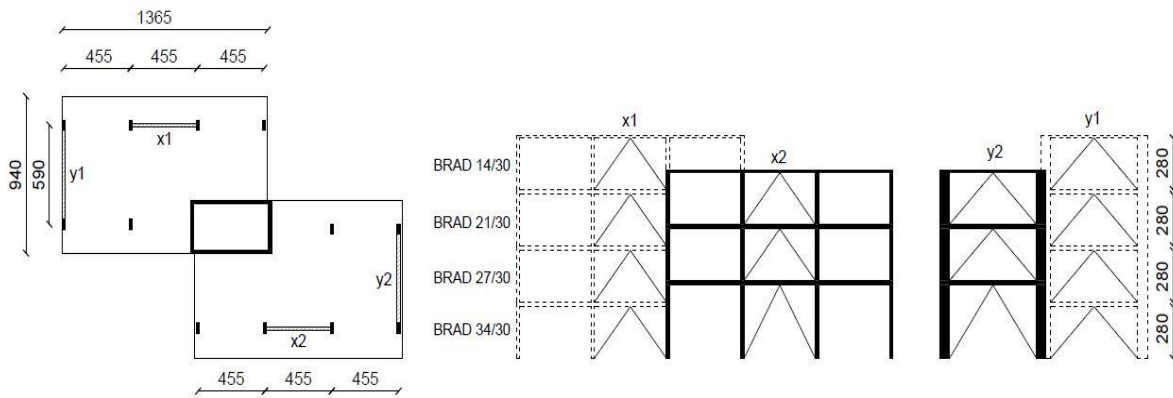
Fig. 46. Distribution of dissipative device in plan and elevation.

Considering that the distribution of the total shear force in buildings decreases with the height, and that the building has bays without infill walls on the first level, starting from this level, gradually less rigid devices are used. In particular, BRADs of 34/30-b type are installed on the first story, 27/30-b on the second, 21/30-b on the third and, only in unit 5, which has a fourth story, 14/30-b on the last level. The braces are inserted in both the two main directions of the building to globally increase its resistance. They are placed in the perimeter frames, to increase the torsional stiffness of the building.

For BRADs of 34/30-b type the elastic stiffness, the yielding strength, the post yield stiffness ratio and the yielding exponent are equal to 194˙000 kN/m, 301 kN, 0.01 and 1, respectively. The same properties are equal to 156˙000 kN/m, 239 kN, 0.01 and 1, respectively, for BRADs of 27/30-b type, to 115˙000 kN/m, 178 kN, 0.01 and 1, respectively, for BRADs of 21/30-b type, and to 79˙000 kN/m, 119 kN, 0.01 and 1, respectively, for BRADs of 14/30-b type.

After the introduction of the devices in the FE building model, the FNA is performed and the energy dissipated by the devices is evaluated. The graphs representing the energy patterns are plotted in Fig. 47.
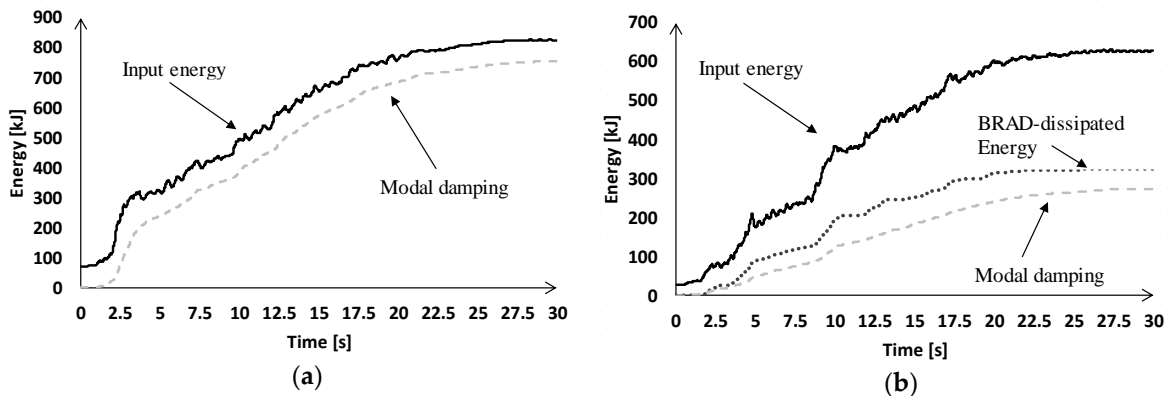
Fig. 47. Energy diagrams for building A in: (**a**) as-built configuration; (**b**) after retrofit.

In Fig. 47 (a), the graph relative to the energy dissipated by the as-built construction through modal damping is compared to the total input energy. It is observed that the great part of input energy is dissipated precisely by modal damping, while the remaining small amount is balanced by the kinetic and the elastic energy of the building, not represented in the diagram.

In Fig. 47 (b), the graph relative to the energy dissipated by the retrofitted building is shown. From this figure it can be seen that, at t = 30 s, i.e., at the end of the seismic event, more than half of the input energy is dissipated by BRAD devices. For the energy balance it follows that, at the same instant of time, the energy dissipated by the modal damping of the structure is lower than the half of the input energy. Thus, from the comparison between Fig. 47 (a) and Fig. 47 (b), it can be observed that the adoption of BRADs leads to a reduction in the energy absorbed by the building structural members, represented by the modal damping energy, and a consequent reduction or elimination of structural damage.

Great reliability of the energy dissipation system is required by the Italian Building Code [4], due to the important role the devices play during a seismic event. In particular, it is required that the devices not break or exhibit damage under the MCE. This is assured by checking the device peak displacement, which, as prescribed by [4], is obtained by the sum two values. The first one is the

displacement due to an earthquake with intensity greater than the one used for the BDE, for which the displacement due to the MCE is assumed. The second value is obtained considering the maximum between the residual displacement at the SDE and the displacement corresponding to axial force equal to zero, following the path starting from the point of maximum displacement at the SDE, reduced by 50%. The peak displacement obtained by the sum of these two values must be kept below the device's allowed displacement.

Fig. 48 shows the cyclic response of four devices, one for each type used, under the MCE, representing the most stressed ones.
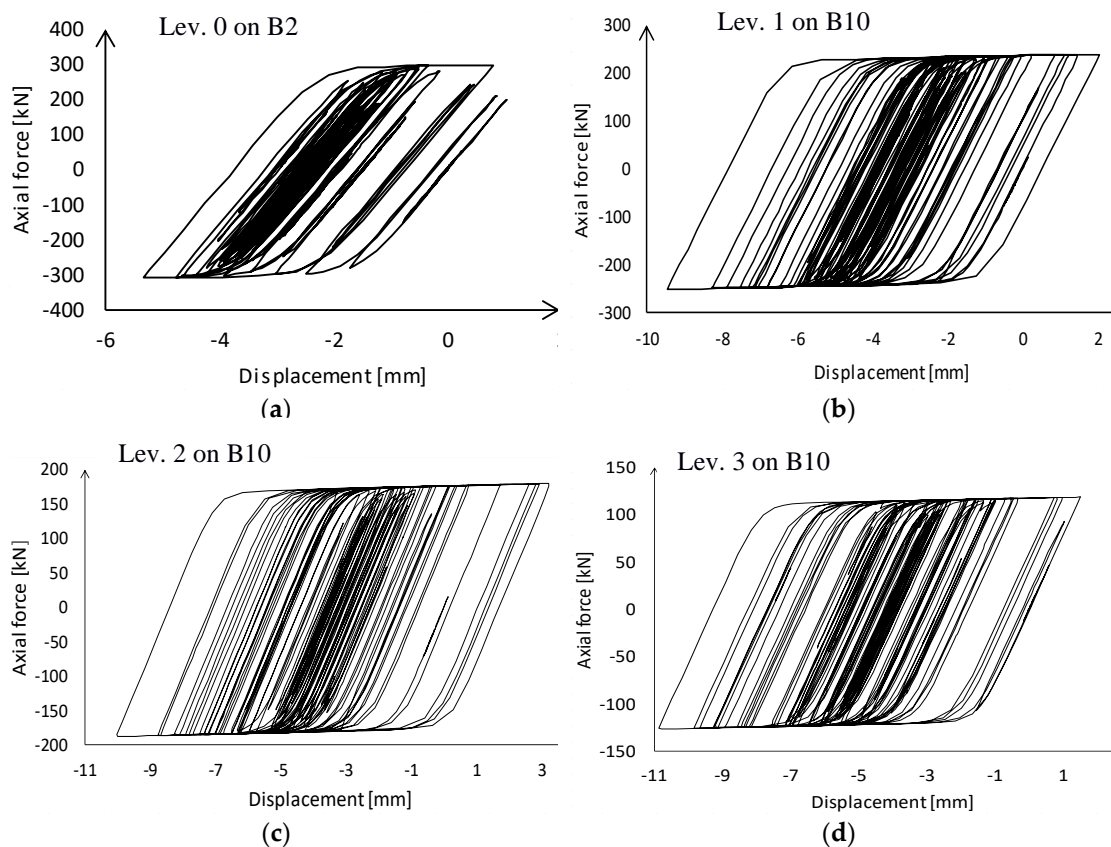
Fig. 48. Cyclic response of different Buckling-Restrained Axial Damper (BRAD) Types under an accelerogram of the Maximum Considered Earthquake (MCE): (**a**) 34/30-b; (**b**) 27/30-b; (**c**) 21/30-b; (**d**) 14/30-b.

From the diagrams in Fig. 48 it is possible to obtain the first value necessary to calculate the peak displacement. For the four devices, the second value is always

found to be the residual displacement at the SDE. The peak displacements, obtained as described, for BRAD 34/30-b, 27/30-b, 21/30-b and 14/30-b are, respectively, 3.1 mm, 8.7 mm, 10.7 mm and 11.1 mm. All of them are lower than the device's allowed displacement, that is 15 mm.

Having verified that the behaviour of the anti-seismic devices is compliant with the code [4], verifications of the structural members are performed. In the as-built configuration, secondary beams and some of the columns at the base do not satisfy ductile verifications. Hence the verifications of only these members of the retrofitted building are shown in Fig. 49.
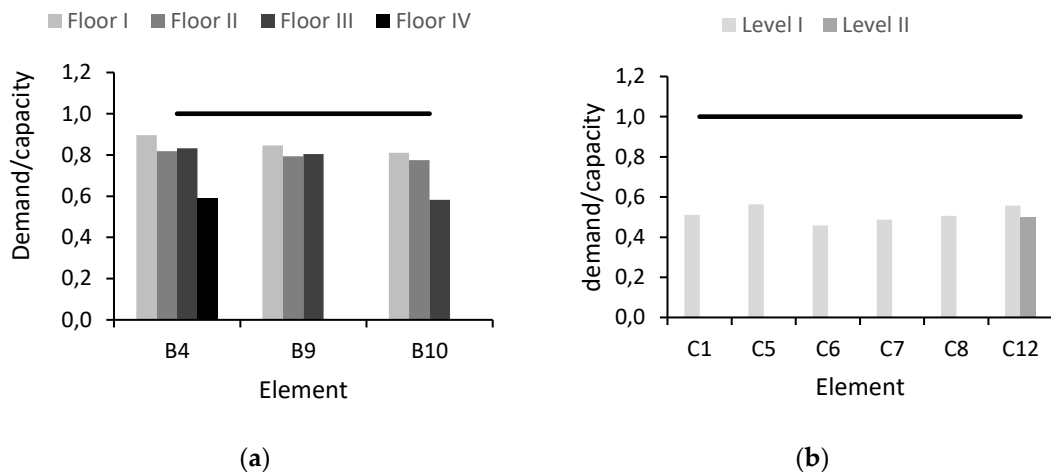
Fig. 49. Ductile verifications after retrofit of: (**a**) beams and (**b**) columns.

In this figure, the names of the members are reported in the horizontal axis, where beams are indicated with letter B and columns with C. From Fig. 49 it can be observed that, thanks to the retrofit intervention, the ratio demand/capacity is always lower than 1. For example, column C1, which does not satisfy the ductile verification in the as-built condition, after the retrofit intervention shows a reduction in the acting bending moment of about 66% (from 322.2 kN·m to 108.6 kN·m). On average, the reduction in the acting bending moment is of 49% for beams and 62% for columns.

The results of brittle verifications only, for members not verified before the introduction of BRADs, are shown in Fig. 50.
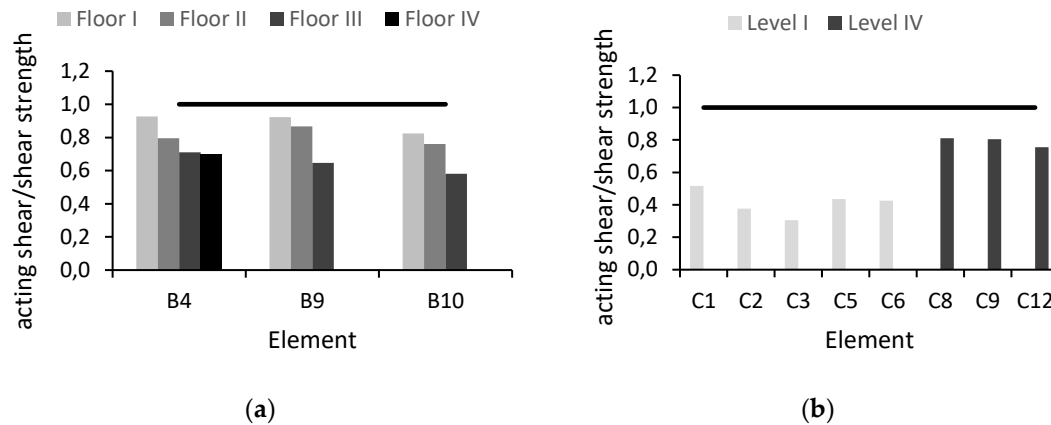
Fig. 50. Shear verifications after retrofit of: (**a**) beams and (**b**) columns.

From this figure it can be observed that, thanks to the retrofit intervention, the demand/capacity ratio is always lower than 1. For example, beam B4, which did not satisfy the shear verification in the as-built condition, after the retrofit intervention shows a reduction in the acting shear of about 57% (from 23.4 kN to 10.1 kN). On average, the reduction in the acting shear is of 55% for beams and 64% for columns. These results show the great benefits obtained from the use of the dissipative system.

Regarding verification of beam–column joints, many of them are still not verified even after retrofit. Hence, for improving their performance, local strengthening interventions are needed.

Regarding the walls, verifications are already satisfied in the as-built configuration, before the introduction of the dissipative devices.

3.1.5 Building Torsional Stiffness

Torsional stiffness of the building is an important parameter that has to be considered in the design of retrofit interventions. In fact, low torsional stiffness, together with irregularity in plan, may produce additional non-negligible displacements in the columns, especially in those that are placed along the building perimeter. To evaluate if the installation of dissipative braces is able to increase the building torsional stiffness, this parameter is calculated before and after the

introduction of BRADs. To calculate the torsional stiffness of the building, the torsional stiffness of each floor has to be determined, and the minimum among the determined stiffnesses has to be considered. The torsional stiffness of each floor is calculated by applying a torsional moment around the z-axis (perpendicular to the floor) and surveying its rotation.

To perform this calculation, since the considered building has slightly staggered floors (Fig. 34 (b)) a simplification is introduced by assigning the same diaphragm constraint to the pairs of floors that are closest to each other. Then the torsional moment M_{tor} around the Z-axis is applied to the center of mass of a diaphragm, while all other diaphragms are embedded. The rotation of the center of mass, γ, due to this torsional moment, is obtain from the FE model, and the torsional stiffness, k_{tor}, is calculated as Equation (26):

$$k_{tor} = \frac{M_{tor}}{\gamma} \tag{26}$$

To evaluate the improvement of the torsional stiffness of each building floor due to the presence of BRADs, k_{tor} is calculated in the same way on the FE model with dissipative devices. Relative results are reported in Tab. 12.

Tab. 12 Comparison of torsional stiffness and deformability of block 3 before and after retrofitting.

	Before Retrofitting				After Retrofitting				k_{tor}	r_s^2/l_s^2
Level	k_{tor}	k_f	r_s^2	r_s^2/l_s^2	k_{tor}	k_f	r_s^2	r_s^2/l_s^2	Variation	Variation
	(GN·m/rad)	(GN/m)	(m²/rad)		(GN·m/rad)	(GN/m)	(m²/rad)			
1	90.91	5.30	17.15	0.28	101.32	53.22	19.04	0.31	+ 11.5%	+ 11.0%
2	100.00	5.74	17.41	0.28	106.78	57.70	18.51	0.30	+ 6.8%	+ 6.3%
3	66.67	4.33	15.41	0.25	71.43	43.33	16.49	0.27	+ 7.1%	+ 7.0%

The introduction of the dissipative devices increases the building torsional stiffness, especially on the first level (ground floor), where an improvement of about 12% is obtained, while in the other two levels, the increase in torsional stiffness is about 7%.

To assess whether a structure is torsionally deformable, the Italian Building Code [4] prescribes the determination of the minimum of the ratios between r_s^2 and l_s^2, where $r_s^2 = k_{tor}/k_f$ is the ratio between k_{tor} and the flexural stiffness, k_f, of each floor, and l_s^2, in cases of a rectangular plan, is equal to $(L^2 + B^2)/1^2$, with L and B the dimensions of the floor in the plan. For building A, considering the floor coinciding with a diaphragm, $l_s^2 = 61.9$ m^2 for all diaphragms. Since l_s^2 is constant, to obtain the minimum ratio r_s^2/l_s^2, the minimum value of r_s has to be considered; hence, the maximum k_f has to be calculated.

To do this, a unitary point load, F, is applied, along one of the building's principal directions, to the center of rigidity of the considered diaphragm, while the other diaphragms are embedded. This results in a translational displacement, d, of the floor without torsional effect. The flexural stiffness, is then obtained from Equation (27):

$$k_f = \frac{F_y}{d} \tag{27}$$

The maximum flexural stiffness of the building is gained in the y direction. The corresponding results are shown in Table 2, where it can be seen that the ratios r_s^2/l_s^2 are higher than 1.0 for all levels. This is the limit above which a building can be considered not torsionally deformable according to [4]. For this reason, from the point of view of torsional deformability, the behaviour of building A before retrofitting cannot be regarded as satisfactory.

There is still a benefit brought by the use of BRADs, because, after retrofit, on the first level r_s^2/l_s^2 increases by about 11%, and on the other two levels it increases by more than 6%.

3.2 Second case study – Building B

3.2.1 Geometrical and Structural Characteristics of the Building

The second case study, building B (Fig. 51), is another residential building, situated in Udine, Italy, designed in 1966 in accordance with [19].

Fig. 51. Building B.

All the graphic drawings of architectural and structural project were analysed, as well as the technical reports. As for the previous building, from the documentation was possible to understand that this construction was built during the Italian program of worker housing, according to the code of the time that consider gravity load only.

Plan is shown in Fig. 52, while in Fig. 53 and Fig. 54 it is possible to see the original drawings of elevations.
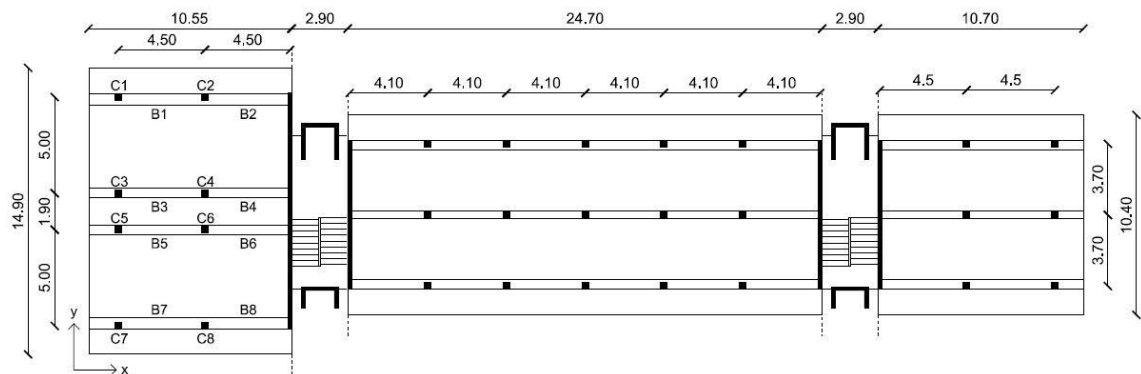
Fig. 52. Plan of the first floor of building B.
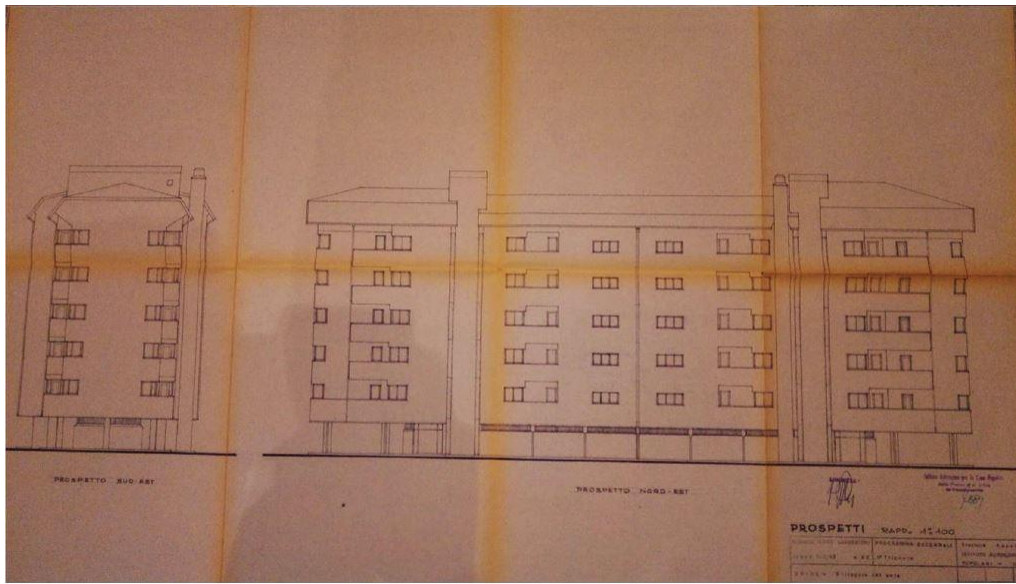
Fig. 53. Original North-East and South-East elevations.
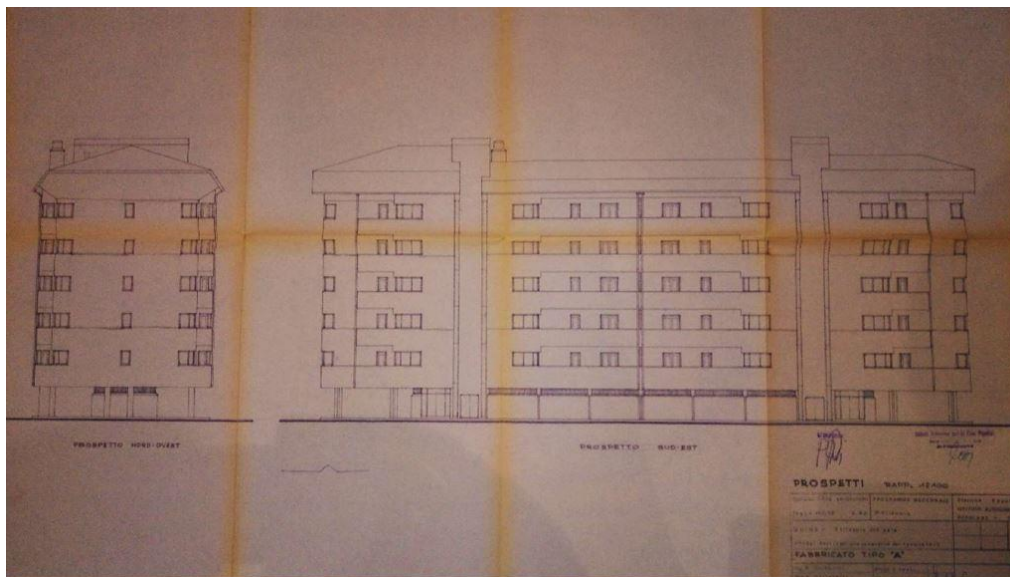
Fig. 54. Original North-West and South-East elevations.

It is a six-story building having a rectangular plan, with approximate dimensions of 50×10 m^2. The building can be divided into three main blocks plus two staircases, separated from each other by the seismic joints that are indicated by dotted lines in Fig. 52. The two lateral blocks have no infill walls on the ground floor, while in the central block there are masonry infill walls between the perimeter ground floor columns, with a continuous strip window at the top.

The bearing structure of the central block is made of two RC walls in the y direction, positioned at the ends of the block, and three RC frames in the X direction. Structural walls are 20 cm thick. Columns have a square section of 35×35 cm^2 on the ground floor, and 30×30 cm^2 on the upper floors. The longitudinal reinforcement of the column is made by $4\Phi16$, one for each corner, for all the levels.

In the two lateral blocks, the bearing structure is characterized by a single RC wall in the Y direction and, in the X direction, by three RC frames in the right-side block, and four RC frames in the left side one. As for the central block, columns have a square section of 35×35 cm^2 on the ground floor, and 30×30 cm^2 on the upper floors. The longitudinal reinforcement of columns C1, C3, C5 and C7 Fig. 52 on the ground and first floor consists of two layers, each made by $3\Phi20$ parallel to y direction. On the second floor, the longitudinal reinforcement of the same columns consists of $6\Phi16$, distributed in two layers, each layer made of three bars, parallel to y directions; on the other floors, the longitudinal bars are reduced to $4\Phi16$, one bar for each corner. The reinforcement of C2 and C8 on the ground floor consists of $8\Phi20$, three parallel to each side; in the same orientation, there are $8\Phi16$ on the first floor. On the second floor, longitudinal reinforcement consists of a total of $6\Phi16$, divided into two layers of three bars parallel to the longer side of the section. On the other floors, reinforcement consists of $4\Phi16$, one for each corner. The longitudinal reinforcement of columns C4 and C6 on the ground floor comprises $4\Phi20$, one for each corner; this is reduced to $4\Phi16$ on the other floors. The transverse reinforcement of the columns consists of $\Phi6$ every 17.5 cm.

In all the blocks, interior beams have a section of 50×23.5 cm^2, while perimeter beams have a section of 60×23.5 cm^2. There are no secondary beams in Y directions. On the under-roof floor, which is not practicable, beams have section of 40×15.5 cm^2. Frame elements of the central and the right block have the same dimensions as those of the left block. Floors are made of precast RC joists, oriented in the Y

direction, having a depth of 20.5 cm and an interaxle spacing of 25 cm, completed with clay bricks and a cast-in-place concrete slab 3 cm thick.

According to [4], the two lateral blocks of the building are irregular both in plan and along the height. The irregularity in plan is due the fact that the floors cannot be considered infinitely stiff in their plane, because they have an RC slab of only 3 cm, thinner than 4 cm, which is the minimum value required by [4]. The irregularity along the height is due to the stiffness decrease of about 40% between the first and the second floor in the X direction, due to the reduction in the columns' section. Moreover, the two lateral blocks are not torsionally stiff, according to the definition given in §3.1.5.

Based on the acquired data, the concrete cylindrical characteristic compressive strength is assumed equal to 26.5 MPa, hence the average strength is 26.5+8 = 34.5 MPa. The reinforcing bars are of the type Aq50, hence they have a characteristic yield strength equal to 264.9 MPa [20], and their average strength can be calculated as 264.9×1.125 = 298 MPa.

As for the previous case study, no test was carried out on the building to define the mechanical characteristics of the material. However, as for building A, a level of knowledge LC2 is assumed [4] for the analysis and the verifications, with the confidence factor FC=1.2.

Consequently, as described in §2.7.2, the concrete design compressive strength to be used for ductile mechanism verifications is:

$$f_{cd} = \frac{f_{cm}}{FC} = \frac{34.5}{1.2} = 28.8 \, MPa \tag{28}$$

and that for brittle mechanism verifications is:

$$f_{cd} = \frac{f_{cm}}{FC \cdot \gamma_c} = \frac{34.5}{1.2 \cdot 1.5} = 19.2 \, MPa \tag{29}$$

The steel design yield strength for ductile mechanism verifications is:

$$f_{yd} = \frac{f_{ym}}{FC} = \frac{298}{1.2} = 248.3 \ MPa \tag{30}$$

and that for brittle mechanism verifications is:

$$f_{yd} = \frac{f_{ym}}{FC} = \frac{298}{1.2 \cdot 1.5} = 215.9 \ MPa \tag{31}$$

3.2.2 Building's model

In the same way of building A, using SAP2000, beams and columns are modelled through frame elements, while walls are modelled with thick shell elements to consider in-plane and out-of-plane behaviour (Fig. 55).
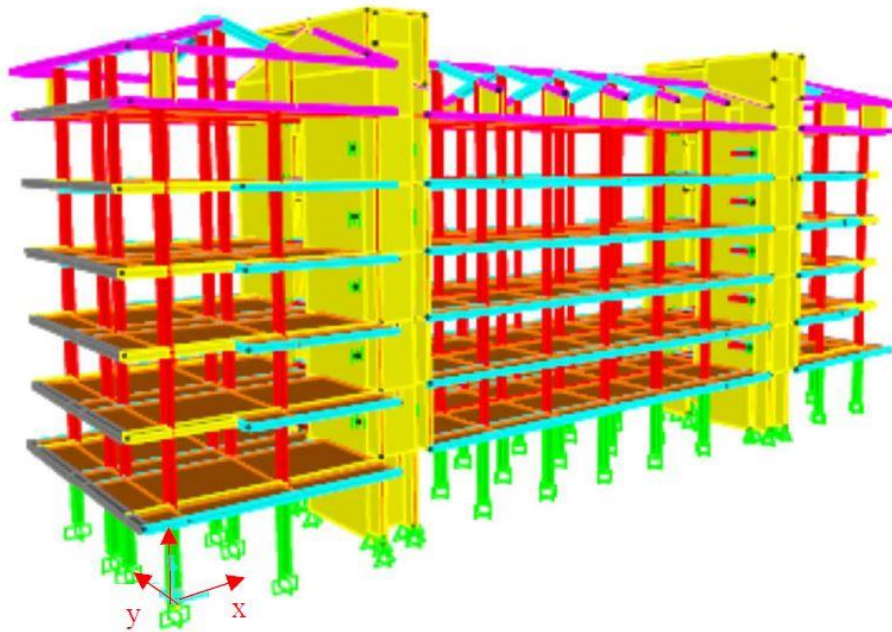
Fig. 55. Model of building B, without masonry.

As for building A, an FNA is carried out to analyse the lateral block of building B.

For the same reason set out in the §3.2.2 floors are not modelled as rigid diaphragms.

Gravity loads are represented by a dead load of 4 kN/m^2 on the story floors and 2.35 kN/m^2 on the under-roof floor. Infill walls are considered assuming a linearly distributed load of 7.15 kN/m acting on the beams below. Live loads are equal to 2 kN/m^2 on all the story floors, 4 kN/m^2 on balconies and staircases, 0.5 kN/m^2 on the under-roof floor, and 1.2 kN/m^2 on the horizontal projection of the roof due to the snow.

As for the first case the nominal design life, V_N, is assumed to be 50 years and the coefficient of use, C_U, is assumed equal to 1, The reference time period for seismic action, V_R, is obtained from $C_U \cdot V_N$, hence it is equal to 50 years. The topographic category is *T1* (flat surface), and the soil is B-type (coarse-grained soil).

Also in this case study the representability of the model was evaluated by comparing the stresses obtained from the model, due only to the vertical loads, with those reported in the structural report of the original project. Since the results obtained with the FE model were of the same order of value as those of the project, it was considered that the model had an acceptable level of reliability.

3.2.3 Results of the Model and FNA Analyses

As previously observed, the building can be divided into two lateral blocks and a central one, independent from each other, due to the presence of the seismic joints (Fig. 52). Analysis of the two lateral blocks showed that the left one had the more stressed members, especially the columns further away from the concrete wall. Hence, only the analysis of the left lateral block is presented in the following. Modal analyses are performed separately for the central block and the left lateral one, and the corresponding results are shown in Tab. 13 and Tab. 14, respectively, where the properties of the main modes are reported.

Tab. 13 Modal parameters of the central block of building B.

Vibration Mode	Period	Modal Participating Mass Ratios		
	(s)	Ux	Uy	Rz
1	1.13	0.79	0.0	0.0001
2	0.39	0.0	0.79	0.0
4	0.27	0.0	0.0	0.74

Tab. 14 Modal parameters of the lateral block of building B

Vibration Mode	Period	Modal Participating Mass Ratios		
	(s)	Ux	Uy	Rz
1	1.82	0.0	0.32	0.50
2	0.84	0.02	0.0	0.0
7	0.28	0.0	0.41	0.28

For the central block, Tab. 13 shows that the vibration modes 1 and 2 are purely translational along the X and Y directions, respectively. Mode 4 is purely rotational around the vertical axis Z. Hence, thanks to its symmetry in plan and along the height, the central block is not affected by irregular torsional behaviour.

For the left lateral block, Tab. 14 Modal parameters of the lateral block of building B

shows that mode 1 is rotational around the vertical axis Z and mixed translational along Y; mode 2 is translational along X, and mode 7 is translational along Y and mixed rotational around Z. These results highlight that the lateral block is affected by torsional components of response, which are due to the asymmetric distribution of the vertical structural elements in plan.

Since this research investigates the improvement of buildings' irregular behaviour obtained by the introduction of dissipative devices, only the left lateral block of the building is considered in the following. This is due to the fact that most of the checks for the central block are verified, and only local improvements are needed.

A preliminary hypothesis of mechanisms that could occur in the existing structure subjected to earthquake has been developed from the analysis of the

drawings of the building, technical reports and a site visit. The large spacing of transverse reinforcement (17.5 cm) at the ends of the columns could lead to shear brittle collapse. Moreover, at the base of the lateral blocks there are no infill walls, and this suggests the possibility of developing a soft story mechanism.

As define in §2.7.3, equation (12) is used for ductile mechanisms of beams and columns, and Equation (13) or (17) for brittle verification. Results are shown from Fig. 56 to Fig. 59, where the ratio between demand and capacity is reported in the vertical axis, and the names of the members shown in Fig. 52 are reported in the horizontal axis.

In the diagrams, for every structural member, six differently coloured columns are drawn. These columns indicate the position of the member with respect to the stories of the building, where the lightest coloured column corresponds to the lower level, while the gradually darker columns indicate higher and higher levels.
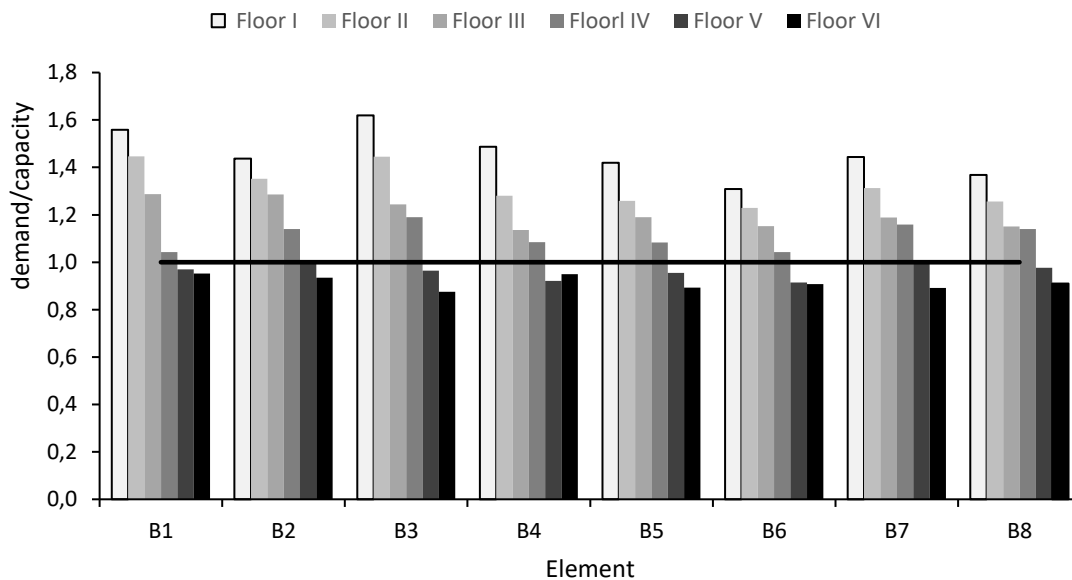
Fig. 56. Bending verifications of beams in as-built conditions.
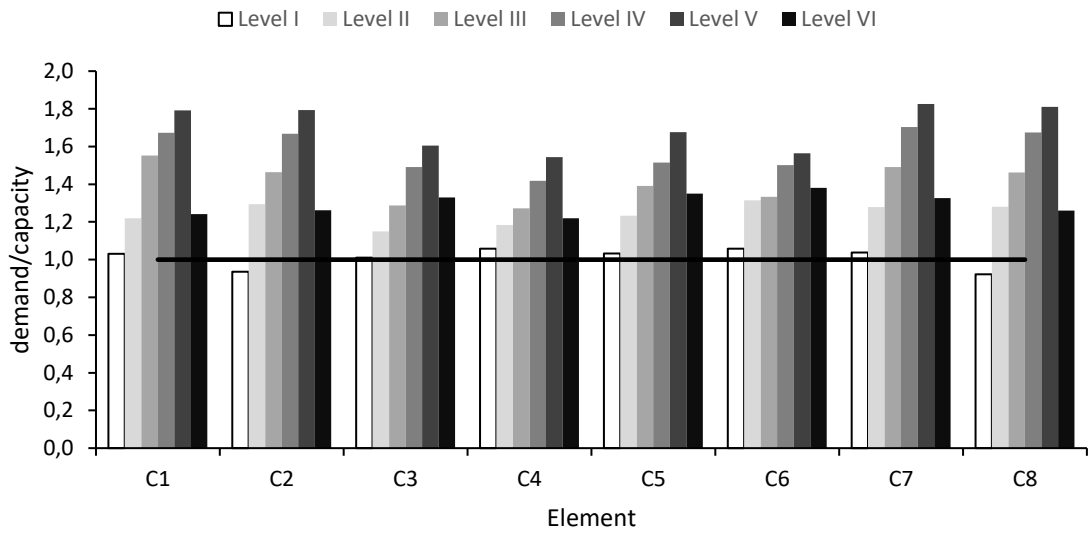
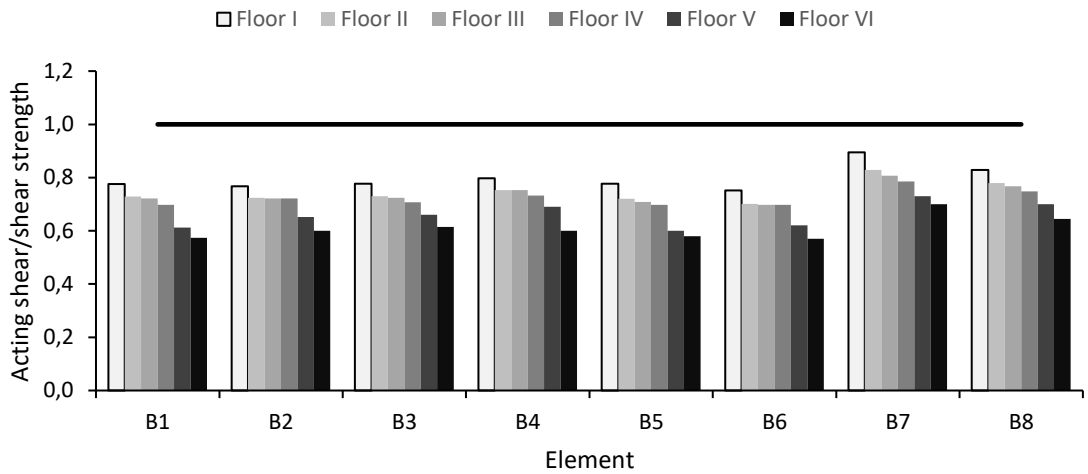**Fig. 57.** Combined bending and compression verifications of columns in as-built conditions.

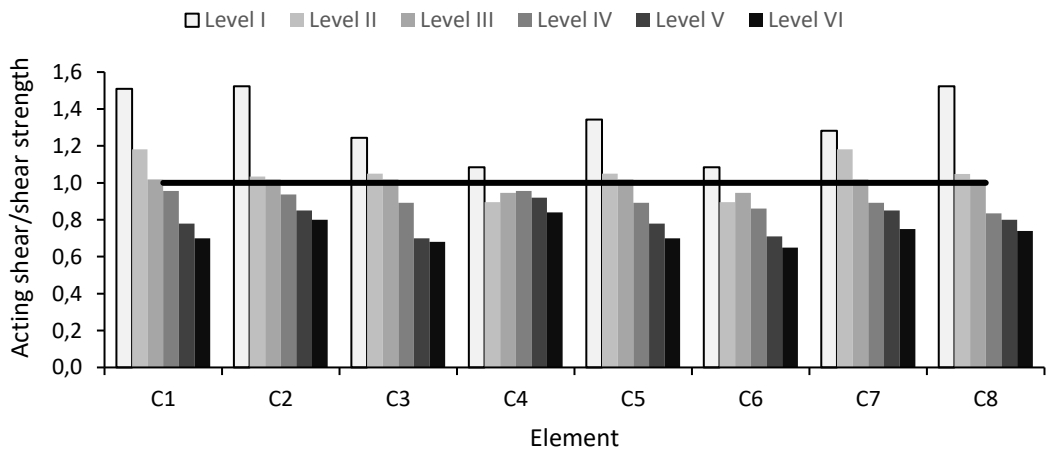**Fig. 58.** Shear verifications of beams in as-built conditions.

Fig. 59. Shear verifications of columns in as-built conditions.

107

From Fig. 56, Fig. 57, Fig. 58 and Fig. 59 it can be observed that all beams from the first to the fourth story are not verified for ductile mechanism and, in the worst case, the acting bending moment is more than 1.6 times the bending capacity. All beams of the fifth and sixth floors satisfy the ductile mechanism verification.

In Fig. 57, ductile verifications for columns of the lateral block are reported. It can be seen that the only elements that satisfy these verifications are columns C2 and C8 at the base, which have the sections with the greatest amount of reinforcing bars. For each column it is possible to observe that the ratio between demand and capacity increases with the height, because the resisting moment of the columns decreases. From Fig. 58, it is possible to observe that all beams of the lateral block satisfy shear verifications.

From Fig. 59 it can be observed that none of the first-level columns satisfy the shear verification and, in the worst case, the acting shear is 1.52 times greater than the shear strength. This is due to the presence of a small amount of transverse reinforcement in the columns and a great shear force at the building base. On the second level only two columns are verified, and the more eccentric second-level columns, with respect to the center of mass of the plan (C1 and C7), exhibit the maximum value of the acting shear/shear strength ratio. At this level most columns do not satisfy the verification, because there is a reduction in the section from the ground floor to the first floor and a consequent strength reduction. On the upper levels, the columns are mostly verified.

In conclusion, the seismic analysis carried out on this case study shows that a lot of bearing elements do not satisfy the verifications required by the Italian Building Code [4] for existing buildings. This is due to the characteristics of structural members and also to the marked torsional behaviour of the structure.

3.2.4 Retrofit Intervention with Viscous Fluid Dampers and Effects

Viscous fluid dampers (Jarret type) are viscoelastic fluid passive energy dissipation devices, whose response is dependent upon frequency. They can be used for protection from both wind and earthquake loads, because they develop energy dissipation also for small deformations.

The device consists of a holeless piston that can move inside a cylinder filled with a viscoelastic fluid. The relative movement between the piston and the external cylinder causes the flowing of the fluid through the thin annular space found between the piston head and the internal casing [30]. In this way the fluid is opposed to the motion of the piston, dissipating energy. The damping properties depend strictly on this orifice effect [31].

The fluid used is a silicon-based elastomeric material that provides an additional stiffness in addition to the damping. This characteristic is useful when the intent is not only to dissipate the input energy, but also to stiffen the structure. The forces generated by these device in the structure are usually out-of-phase with the internal forces resulting during the earthquake. Therefore, the maximum forces generated by the dampers do not occur simultaneously with the maximum internal force.

Jarret as belong to the category of velocity-activated devices. In this type of device the energy is dissipate through the relative velocities that occur between the connected points.

As it can be seen in Fig. 52, building B has six floors, and is therefore higher than building A analysed previously. As building B is higher, the speeds reached by its highest floors are greater than those of highest floors of building A. Moreover, the use of this devices allows to study in deep the effects of a retrofit method different from the one used in the previous case study. For these reasons in the retrofit intervention of building B it is decide to use Jarret devices.

A finite element model of a Jarret damper is obtained using Kelvin-Void's scheme, i.e., using the parallel combination of a non-linear damper element and an elastic spring one. In SAP2000, these two elements can be implemented with the Nlinks "*damper-exponential*" and "*spring*", respectively. The spring takes account of the elastic component of device strains, while the damper-exponential models the non-linear viscous behaviour of the fluid, which is described by the following force–velocity relationship, Equation (32):

$$F = c \cdot sgn[\dot{x}(t)]|\dot{x}(t)|^{\alpha} \qquad (32)$$

where *F* is the force component due to the fluid non-linear viscosity, *sgn* is the signum of the function, $\dot{x}$ is the instantaneous velocity of the piston rod, *c* is the damping coefficient and α is the damping exponent. In the current study, α equal to 0.15 and *c* equal to 85 kN(s/m)$^{0.15}$ are used.

As shown in the previous section, the verifications required by [4] are not satisfied due to both the characteristics of the structural members and the torsional behaviour of the building lateral block. The goals of the design strategy consist in reducing the seismic vulnerability and increasing the torsional stiffness of the building. The use of viscous fluid devices allows to dissipate a great part of the seismic input energy, thus reducing the stresses in the structural members of the building. Moreover, adequate positioning of the devices in plan effectively allows to reduce the torsional behaviour of the building.

For these reasons viscous fluid dampers of Jarret type BC5A-105 are used as a retrofit solution. Jarret choice inside the structure have been arranged by a trial and error method.

Pairs of dissipative devices are mounted at the tops of concentric V-shaped steel braces. The braces are connected to the concrete frame by metal anchors. The disposition of Jarret dampers, shown in Fig. 60, is the result of a comprehensive

design process, whose goal is the best performance behaviour of the dissipative system. The Jarret are placed in the most eccentric possible position and in the perpendicular direction to that of the wall.
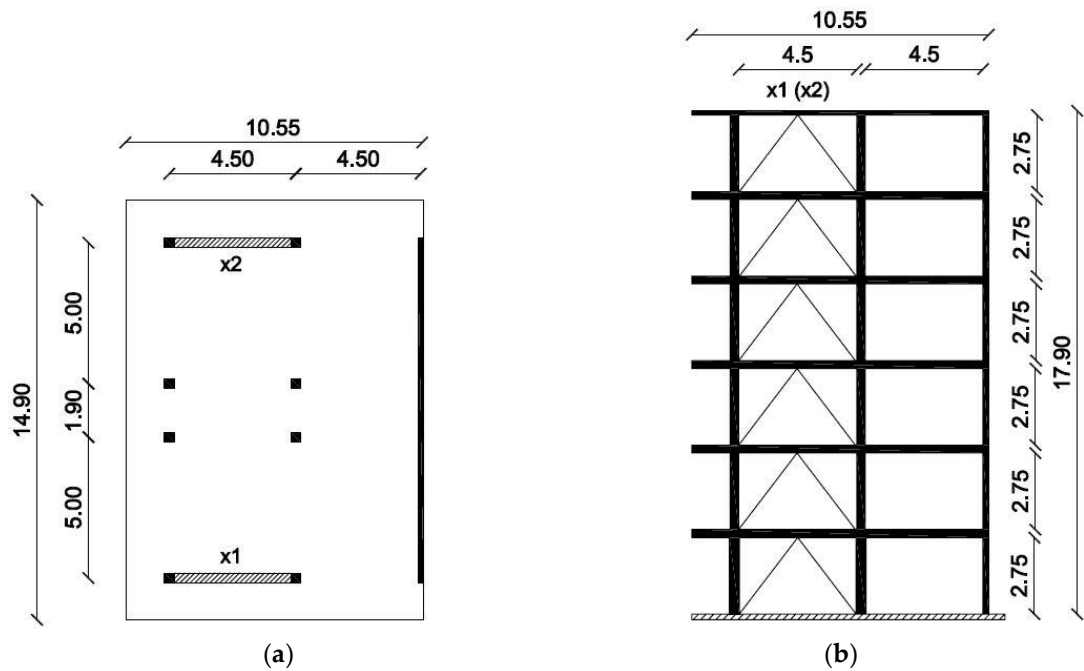

Fig. 60. Distribution of Jarret device in: (**a**) plan and (**b**) elevation.

Thus, the braces are inserted in the direction of least seismic resistance of the structure (x direction). They are positioned in the perimeter frames, to increase the torsional stiffness of the building. It is not possible to introduce a brace in the left external bay in y direction, because this bay is inside the housing unit. Although the building resistance in this direction is already mainly assured by the structural wall, to place a dissipative brace in this position would have served to re-align the center of rigidity with the center of mass.

As expected, the use of the viscous fluid dampers produces a reduction in the energy absorbed by the building (Fig. 61).
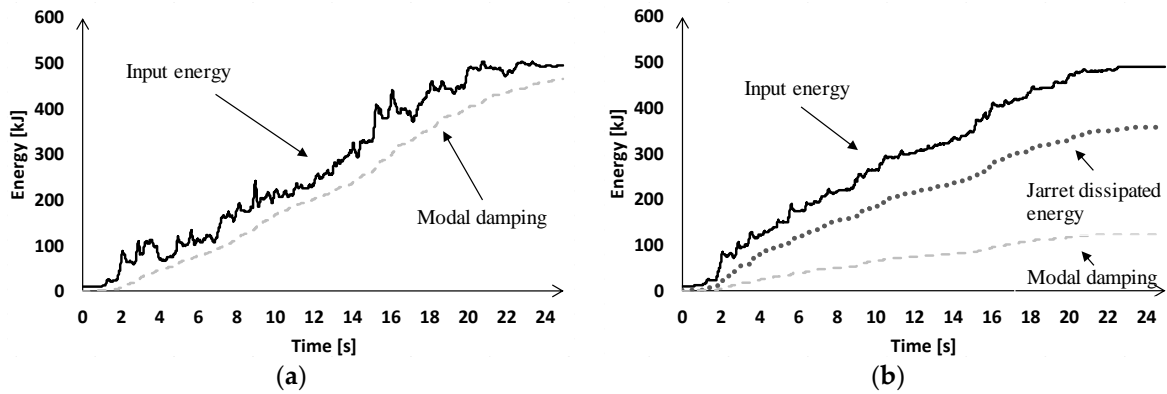
Fig. 61. Energy diagrams for building B in: (**a**) as-built configuration and (**b**) after retrofit.

In fact, as shown in Fig. 61 (b), 82% of the total input energy is absorbed by the 12 pairs of Jarret devices, while the remaining 18% is dissipated by the building through modal damping. In this way, the forces acting on the structural members result lower than in the as-built configuration.

As regards the devices' verification, the maximum displacement allowed by the dampers is 105 mm. In Fig. 62, the cyclic force–displacement responses obtained under the MCE for the most stressed devices are plotted.
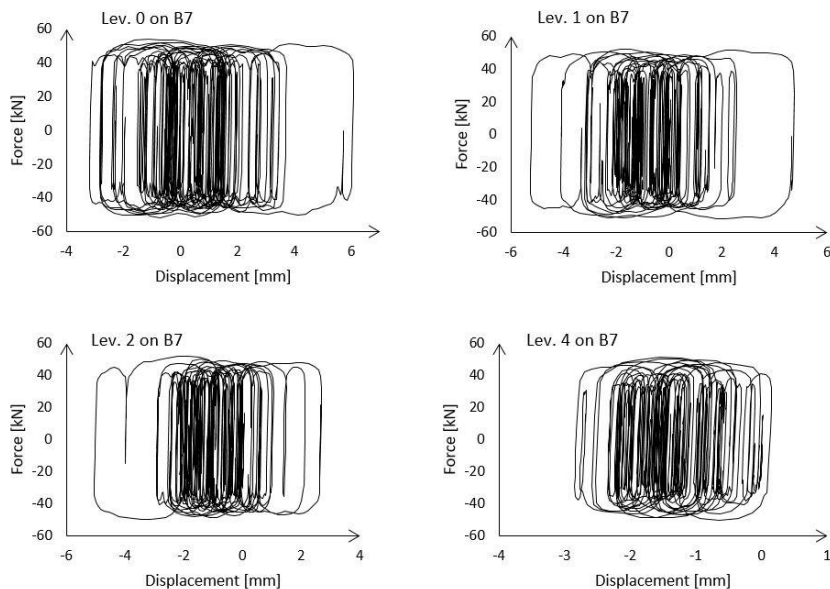
Fig. 62. Response cycles of the most stressed dampers under an accelerogram of the MCE.

The device peak displacement is obtained using the same procedure employed for building A. The highest peak displacement is 7.7 mm lower than the admitted

value. Hence, the verification is satisfied. Verifications of the building B structural members are performed similarly to the first case study, for the BDE.

Fig. 63 shows that, after the introduction of dissipative devices, all the beams satisfy the ductile verifications.
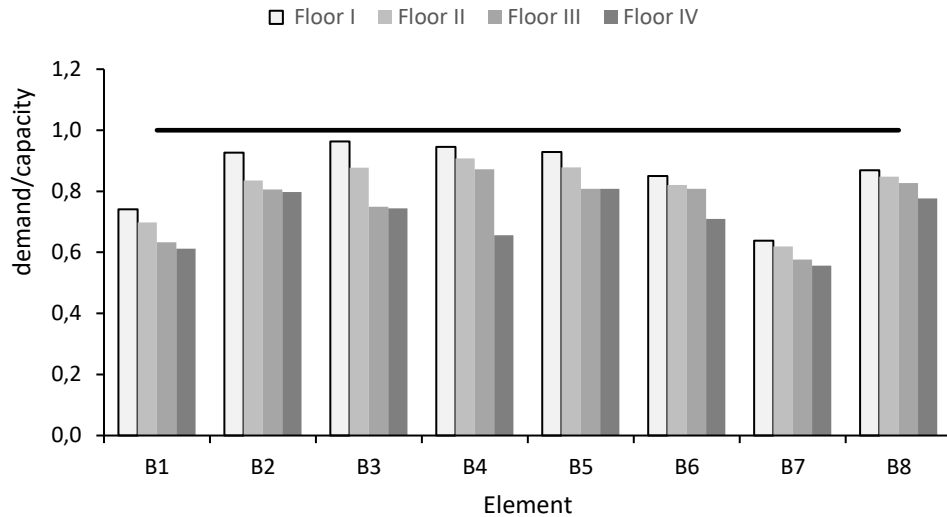

Fig. 63. Bending verifications of beams after retrofit.

The bending moment of the most stressed beam, which is B1 on the first floor, passes from a value of 162.8 kN·m to 77.4 kN·m, with a reduction of 53%. The ratio between demand and capacity, which in the as-built configuration is equal to 1.62, reduces to a value of 0.74, after the retrofit. On average, the reduction in the acting bending moment for beams is 43%.

In Fig. 64, it is possible to see that after retrofit, the columns also satisfy the ductile verifications.
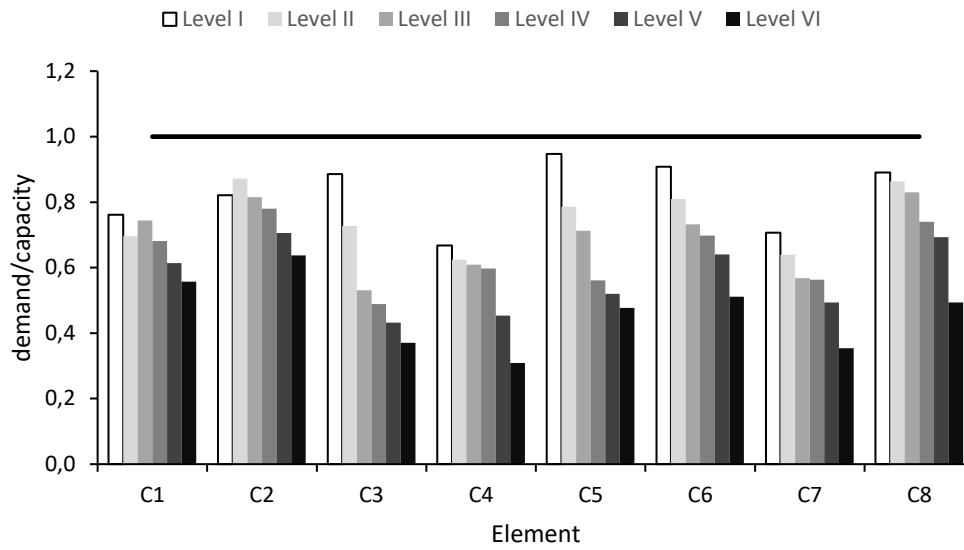
Fig. 64. Ductile verifications after retrofit of columns.

In the as-built configuration the most stressed column, C1, has a bending moment at the base equal to 321.4 kN·m, which reduces to 109.6 kN·m after retrofit. Shear verifications of beams were all already satisfied in the as-built configuration, as shown in Fig. 58.

Fig. 65 shows that shear verifications of all columns are satisfied after the introduction of the viscous fluid dampers. On average, the reduction in the acting shear of columns is 58%.
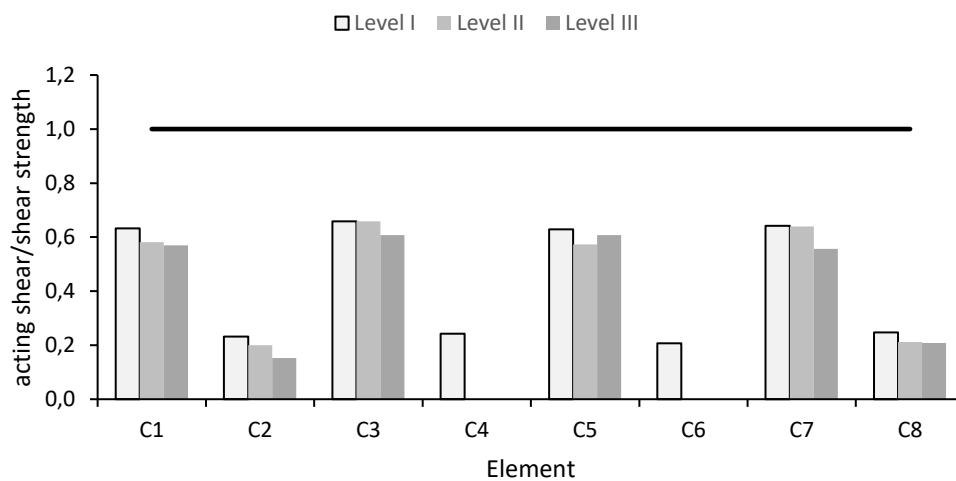

Fig. 65. Columns' shear verifications, after retrofit.

3.2.5 Building Torsional Stiffness

For building B, the torsional behaviour of the lateral blocks is one of the main issues to be faced in order to improve the building seismic behaviour. For this reason, the retrofit intervention by the introduction of steel braces with viscous fluid dampers is aimed not only at reducing the seismic energy dissipated by the building, but also at improving the torsional behaviour of the lateral block. To attain this goal, the braces are placed in the structure symmetrically along the perimeter (Fig. 60).

As was done for the first case study, the torsional stiffness, k_{tor}, of all floors in the as-built condition and after retrofit is calculated (Tab. 15).

Tab. 15 Comparison of torsional stiffness and deformability of building B before and after retrofitting.

Level	Before Retrofitting				After Retrofitting				k_{tor} Variation	r_s^2/l_s^2 Variation
	k_{tor} (GN·m/rad)	k_f (GN/m)	r_s^2 (m²/rad)	r_s^2/l_s^2	k_{tor} (GN·m/rad)	k_f (GN/m)	r_s^2 (m²/rad)	r_s^2/l_s^2		
1	10.64	9.33	1.14	0.041	30.30	9.38	3.23	0.116	+ 184.8%	+ 183.3%
2	9.35	7.84	1.19	0.043	28.68	7.87	3.63	0.131	+ 206.7%	+ 205.0%
3	9.43	7.84	1.20	0.043	28.57	7.87	3.63	0.131	+ 203.0%	+ 202.5%
4	9.35	7.58	1.23	0.044	28.52	7.60	3.76	0.135	+ 205.0%	+ 205.7%
5	9.26	7.97	1.16	0.042	28.54	7.77	3.68	0.132	+208.2%	+ 217.2%

The values of k_{tor} reported in Tab. 15 show that, after retrofit, the torsional stiffness of the floors increases to values that range from about 185% to 208% of the as-built stiffness. In this way, the torsional behaviour of the lateral block exhibits great improvement after the retrofit.

For building B, $l_s^2 = 27.8$ m². The values of the ratio r_s^2/l_s^2 are calculated as explained in §3.1.5, and the obtained results are shown in Tab. 15. In the as-built configuration, the r_s^2/l_s^2 ratio is about 0.04 for all floors. This is a value lower than 1.0, hence the building is considered torsionally deformable according to [4]. After retrofit, the ratio increases to the value of 0.12 for the first floor and 0.13 for the others, with variations ranging from about +183% to about +217%, respectively. The

final values of the ratio are not sufficient to consider the building not torsionally deformable. Nevertheless, the increase is substantial and demonstrates an improvement in the building torsional behaviour. Thus, it is possible to say that the use of dissipative devices is beneficial not only to absorb part of the input energy and reduce the force acting on bearing structures, but also to improve the building behaviour by reducing negative effects due to its irregularities.

4   Shape Memory Alloys (SMAs)

The improvement of seismic behaviour of buildings can be pursued through the use of innovative seismic retrofit technologies, as shown in the previous chapter, but also through the use of new smart materials, as for example Shape Memory Alloys (SMAs), whose mechanical and performance characteristics will be analysed in this chapter.

The Italian code [4] through the rules and prescriptions for the construction of new buildings, set as a goal the ensure of life safety and the prevention of the collapse of the buildings in the presence of seismic events, even of rare intensity. This goal is achieved by requiring that some parts of the structure perform plastic behaviour with the formation of plastic hinges which, however at the end of the seismic action, involve permanent deformation of the structural elements.

For this reasons researchers have increased interest in materials that could make a building capable to repair its own damage, restore its conditions after an earthquake. In this way, also to improve seismic behaviour of existing buildings, smart and innovative materials or device and reinforcement methods, which guarantee excellent performance and a significantly reduction in maintenance or repairing costs are being studied in the construction world.

Smart systems for civil structures are described as systems that can automatically change structural characteristics in response to external disturbance and/or unexpected severe loading toward structural safety, extension of the structure's life time, and serviceability [32]. To reach this goal one important step is the development and implementation of smart materials that can be integrated into the structure and supply functions such as self-centering.

Shape memory alloys (SMAs) can certainly be considered among the materials that arouse great study interest for their application in the construction industry. These materials have the capacity to undergo large deformation and go back to the initial shape when heated above their transformation temperature (shape memory effect) or through stress removal (superelasticity). This particular feature allows to considered SMAs into the category of advanced and smart materials.

Arde Ölander was the first researcher to discover shape memory alloy in 1932 [33]. William Buehler and Frederick Wang noticed the Shape Memory Effect (SME) in a nickel-titanium (NiTi) alloy working for the US Naval Ordinance Laboratory in 1962 ([34] and [35]). Since this date, the use of SMAs has spread to many industrial fields, such as medical [36], automotive [37], aerospace [38] and electronics.

In view of this, the use of SMAs in the world of civil engineering is of considerable interest. In fact the possibility of recovering their initial shape after having undergone great deformation is of great interest for their use as reinforcement in RC buildings. The use of pieces of SMA reinforcing bars in the areas where the formation of plastic hinges is expected would allow to dissipate part of the input seismic energy and, at the same time, at the end of earthquake, ensure that the RC elements recover their initial shape. Crushed concrete may be present, but it can be replaced and it is not necessary to demolish and reconstruct the building. For this reason they have the potential to be used in building smart structures [39].

In this chapter the characteristics of some SMAs will be analysed, their application will be presented on a case study and finally a model will be proposed to represent the behaviour of an existing beam-column joint with SMAs as reinforcement in the area where the formation of the plastic hinge is expected.

4.1   General behaviour and typology of SMAs

SMAs are obtained by the composition of different metal elements and in a different percentage. Nickel-Titanium alloys (NiTi), iron based alloy, such as Fe-Mn, and copper based alloys, as Cu-Zn, are studied and each one has its own characteristics and properties.

SMAs can be define as a polymorphic material, as they can have multiple crystal structures having the same chemical composition. The effect of shape memory is linked to the different configurations that the crystalline structure of the alloy can assume, which is therefore the first concept to be analysed. The phase in which the material is located depends on both temperature and external stress, but it also depends on the chemical composition and initial thermomechanical processing.

Shape memory alloys are characterized by two different crystal phases: the martensitic phase, stable at low temperature, and austenitic phase, stable at high temperature and their characteristics result from solid-solid transformation between these two phases. Taking in consideration the situation of the material at ambient temperature, Fig. 66 shows the phase transformation cycle as a function of temperature in a free-stress state: starting from the martensite phase that exists at low temperature, heating the material, there is a crystalline change that leads to the austenitic phase. It is possible to point out four distinct temperatures that identify the phase transformation: martensite start (M_s), martensite finish (M_f), austenite start (A_s) and austenite finish (A_f).

As is possible to see in Fig. 66, when the temperature (T) is lower than M_f, SMAs are in a fully martensitic phase. This phase is described as "twinned" state, in which one side of a microscopic material plane is a mirror image of the position of the atoms on the other side [41]. Heating the material to A_s it is possible to detect the starting point of a gradually change from martensitic to austenitic phase, that is

complete at A_f. During this transformation phase both martensite and austenite phase coexist. For temperature higher than A_f, shape memory alloys are in a fully austenitic phase. From this state, in which the material is 100% austenite, cooling the material to M_s a new transformation phase begin, from austenite to martensite phase, until temperature M_f is reached. In reason of that between M_s and M_f temperatures martensite and austenite phases coexist.
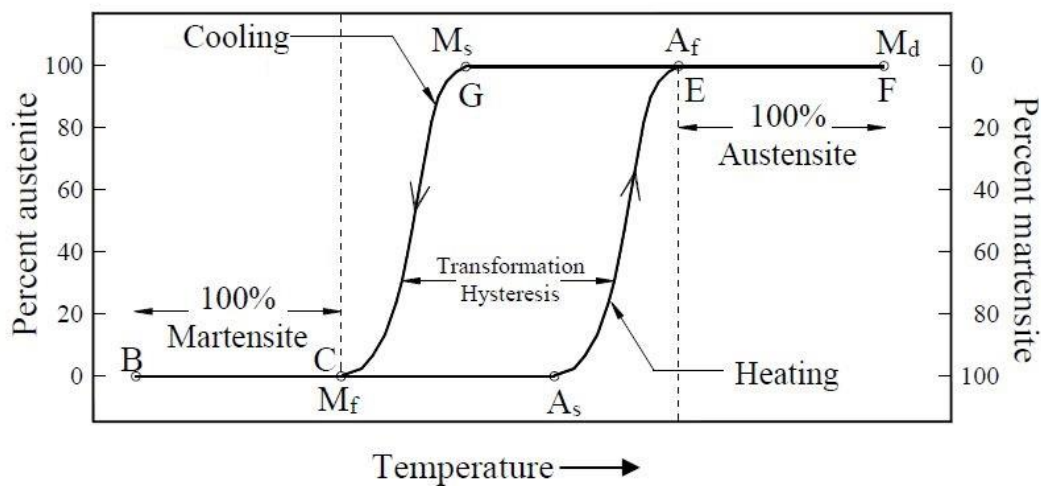

Fig. 66. Transformation phase for SMAs in a free-stress condition [40].

As shown in Fig. 66, the two transformation phase, from martensite to austenite and vice versa, take place at different temperature, which gives rise to the hysteretic cycle.

Summing up, therefore, SMAs are in a completely martensitic phase for temperature lower than M_s ($T<M_s$), in a completely austenitic phase for temperature higher than A_f ($T> A_f$), while, during the transformation phases from martensite to austenite and vice versa ($A_s<T< A_f$ and $M_s< T<M_f$), the two phases coexist.

By varying composition, elements concentration, treatment that the material undergoes during the production and microstructural details, it is possible to change the temperature of SMAs at which the crystallographic structure changes. These temperatures are therefore specific and unique to each individual alloy.

Another important temperature, also observable in Fig. 66 is M_d. In fact, if the temperature increases above this temperature (T>M_d), the superelasticity effect, which will be analysed in detail later, is lost.

In the case shape memory alloy is subjected to stress, its behaviour is related to the temperature of the material. Fig. 67 shows a graph that relates strain-stress characteristic curves, drawn in the vertical plane, with the temperature (axis perpendicular to σ-ε curves). In particular material's behaviour is represented within three different temperature ranges.
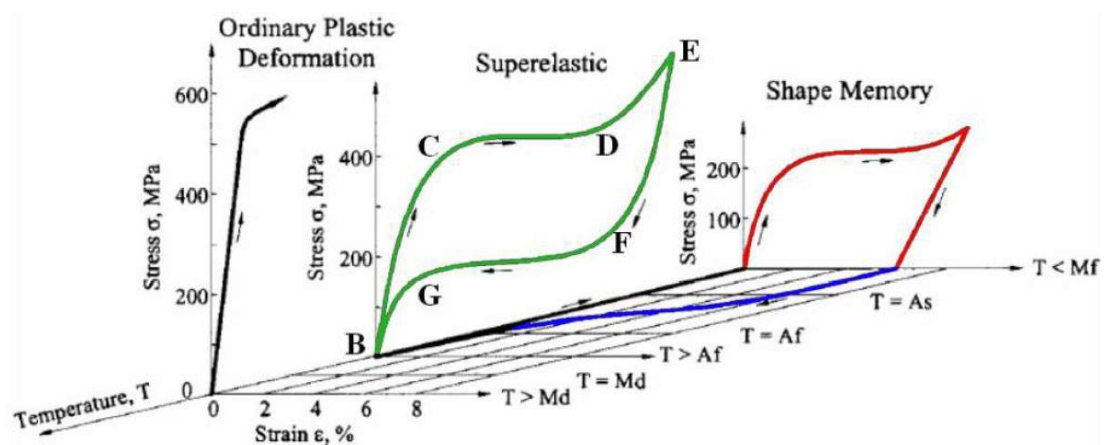
Fig. 67. SMAs subject to stress: strain-stress curves as a function of temperature.

The first effect analysed is the Shape Memory Effect (SME), represented with the red and the blue lines in Fig. 67. In this case, the material has a temperature lower than M_f, thus being in the martensitic phase. Applying a load and then removing it, i.e. following the red line of Fig. 67, at the end of the unloading phase, there will be a final residual strain. This is due to the internal reorientation of the atoms, that undergo a transformation from a "twinned" martensite to a "de-twined" martensite form, as shown in the upper part of Fig. 68. By heating the alloy above the temperature A_f, there is the transition from the martensitic to the austenitic phase. Thanks to the internal reorientation of the crystal structure occurring in this change phase, the complete recovery of the residual deformation and the return of the

material to its original shape after a loading and unloading cycle is possible, as shown by the blue line in Fig. 67.
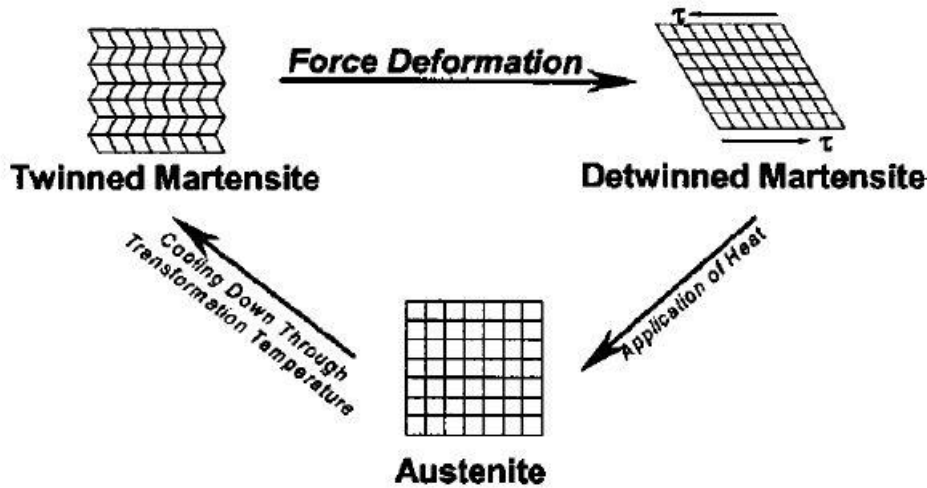

Fig. 68. Crystalline structure transformation during Shape Memory Effect [42]

The second effect analysed is the Superelastic Effect (SE), represented with the green line in Fig. 67. When the alloy is in the austenitic phase, so in the case its temperature is higher than A_f ($T > A_f$), and it is loaded and unloaded, referring to Fig. 67 is possible to identified six distinctive regions (BC, CD, DE, EF, FG and GB) in the strain-stress curve [41]. In Fig. 69 is shown the same strain-stress curve with the phasis transformations:

1. the initial part of the path, BC, is the elastic response of austenite at low strains (<1%);

2. part CD, with a long and constant plateau at intermediate and large strains (1-6%), represent the stress-induced transformation from austenite to martensite;

3. part DE, at large strains (ε >8%), represents the elastic response in the stress-induced martensite state, that, as shown in Fig. 69, is in the de-twinned martensite configuration;

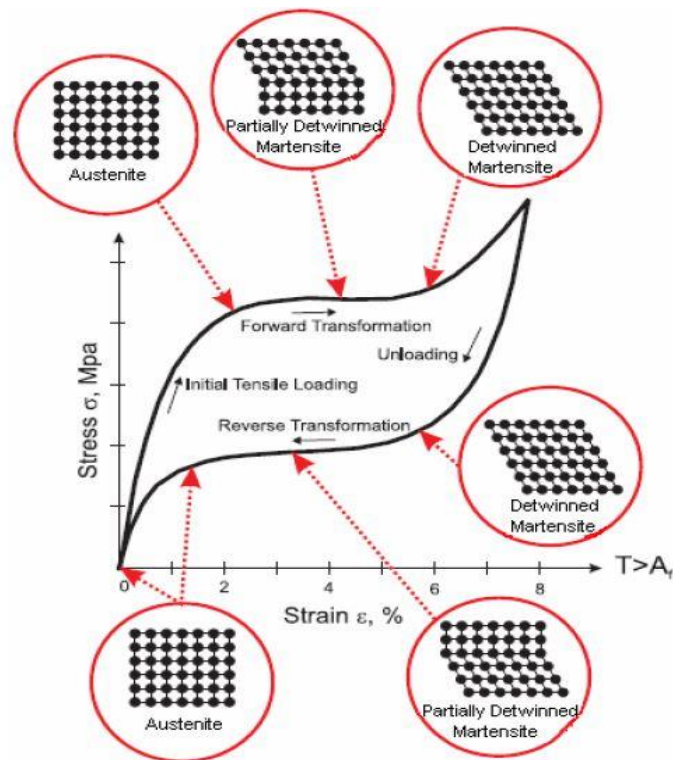4. part EF represent the elastic recovery of strain upon stress removal;

Fig. 69. Strain-stress curve for a superelastic SMAs with phase transformation [43].

5. part FG represents a recovery of strain at almost a constant stress path because of the reverse transformation, to austenite due to the instability of martensite at temperatures higher than A_f;

6. the last part, GB, represents the elastic recovery in the austenitic phase.

As said, transformation of the crystallographic structure is linked to many aspects. When the alloys is in the stress-induced de-twinned martensite phase and load is removed, reverse transformation occurs because martensite is unstable at high temperature. Once the applied stress is removed, the internal stress present in the material acts to drive the reverse transformation during unloading until the initial shape is recovered [41].

If the temperature is between A_s and A_f partial superelasticity occurs.

In both cases analysed, Shape Memory Effect and Superelastic Effect, hysteresis cycles are created, in which the energy is dissipated. Shape recovery is linked to

phase transformation, and the difference between the two effects is the way in which the transformation take place, thermally for Shape Memory Effect and mechanically for Superelasticity.

The last effect analysed is the Ordinary Plastic Deformation, identify by the black curve in Fig. 67. If temperature in the austenite phase increases above M_d, that is the maximum temperature at which martensite occurs, martensite cannot be stress-induce. In reason of this the superelastic effect is lost and does not occur. As a consequence alloy's behaviour is the same of that of an elastic-plastic material, with an initial linear elastic deformation followed by a plastic one.

4.1.1   Nickel and titanium (NiTi) SMAs

The use of shape memory alloys began to receive attention when, in 1962, the effects described in the previous section were discover in the Nickel-Titanium (NiTi) alloy, know also with the name Nitinol.

Nitinol is composed of approximately the same percentage of the two elements. However there is the possibility to add other elements to the alloy to modify both mechanical and thermal properties, that can change the transformation temperature of the system. Frequently used elements are iron and chromium (to lower the transformation temperature) and copper (to decrease the hysteresis and lower deformation stress of martensite) [44]. Other elements, as oxygen and carbon, worsen the mechanical characteristics of the alloy, and, therefore, it is necessary to pay attention, during the processing phases, that these elements do not contaminate the alloy.

The crystal structure of NiTi is body centered cubic (bcc) in the austenitic phase and face centered cubic (fcc) in the martensitic phase [45], as shown in Fig. 70.
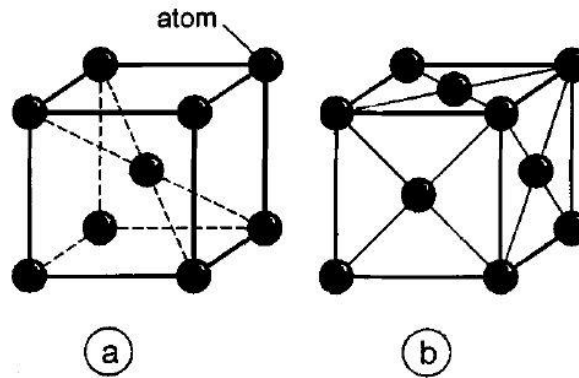
Fig. 70. Crystal structure: (a) body centered cubic and (b) face centered cubic [45].

For many applications NiTi alloy exhibits better characteristics that other SMAs, because of its greater strength, recover of large strains, high resistance to corrosion and fatigue.

Many works of different researchers examinate and describe the mechanical properties of NiTi.

Dolce and Cardone [46] made a series of loading-unloading tests on 200 mm long and 1.84 mm diameter austenitic wires, pre-tensioned (≈ 0.5%) at room temperature (≈ 20°C). Each test was characterised by four sequences of cycles, each made by two cycles, at maximum strains equal to 5%, 6%, 7.5% and 9%, with frequency of loading that was kept constant during each test and varied from 0.02 to 4 Hz. Results are shown in Fig. 71, where it is possible to observe that mechanical parameters as secant stiffness, energy loss per unit weigh, equivalent damping and stress-strain relationship depend on frequency and change significantly from pseudo-static (0.02 Hz) to dynamic condition (0.2-2 Hz). Increasing the frequency, the hysteresis loop of the stress-strain diagrams narrow and there is an increase in the stress level. From the graphs stress-strain on the right of Fig. 71, it is possible to see that, in the range 0.02-0.2 Hz, the secant stiffness increases by about 15%, the energy loss decreases by about 18% and the equivalent damping decreases by about 25% [46].
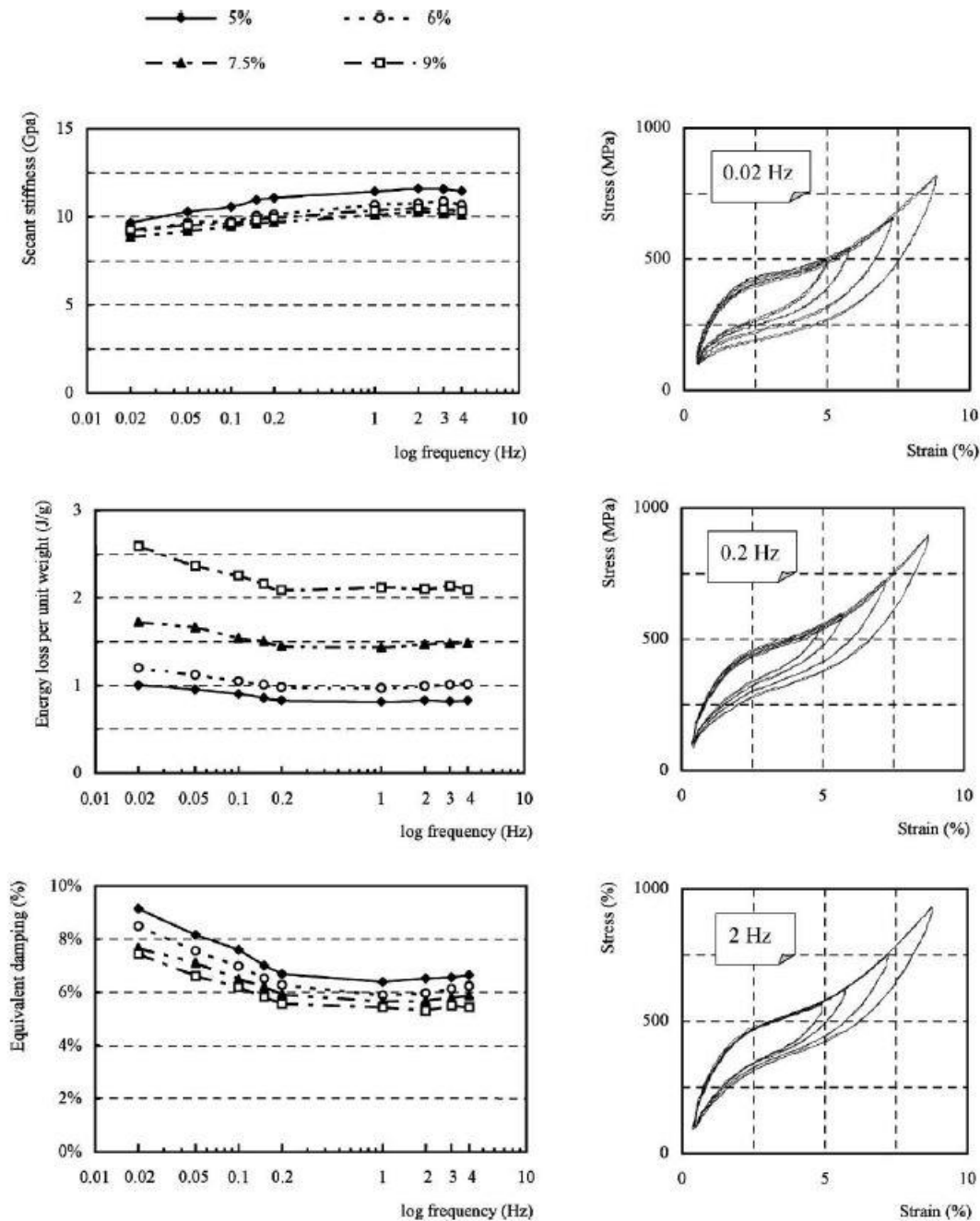
Fig. 71. Mechanical behaviour superelastic wires under tensile test as a function of frequency of loading and strain amplitude [46].

Plietsch and Ehrlich [47] carried out strain controlled tension and compression test on NiTi wires (diameter of 5.8 mm, nominal composition of 50.8 % Ni).

Considering that the approximate values for the transformation temperature are $M_s{\approx}268K$ (-5°C), $M_f{\approx}205K$ (-68°C), $A_s{\approx}249K$ (-14°C) and $A_f{\approx}293K$ (20°C). specimen were tested at three different temperature: (a) 384 K, in order to produce a

stable austenitic structure, which can no longer undergo a stress-induced martensitic transformation ($T>M_d$, referring to Fig. 67); (b) 293 K, to observe superelastic effect ($A_f <T<M_d$); and (c) 205 K, in the stable martensite state, where only a reorientation of the thermally induce martensite variants would occur upon loading ($T<M_f$). Results of the tests are shown in Fig. 72.
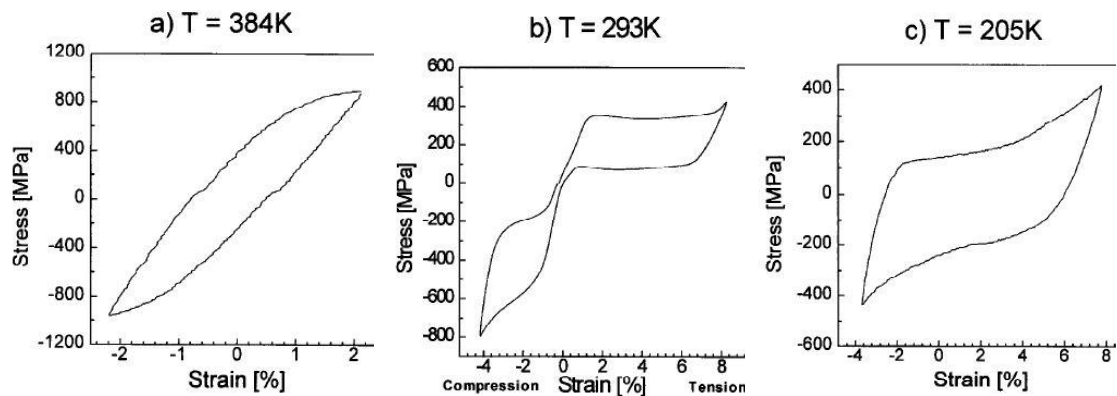

Fig. 72. Tension/compression test for (a) austenitic, (b) superelastic, (c) martensitic [47].

Sample (a) has a quite perfect symmetrical loading curve, while behaviour of the other two sample are different in tension and compression. Sample (b) has the most emphasized strength differential effect, in fact it is possible to observe that, in tension, a strain up to 8% is attained with a stress not exceeding 400 MPa, while, in compression, the same stress is reached at a strain less than 1%. The last sample (c) generates a back-stress (where change the slope of the curve) of approximately 200 MPa at a tension strain of 4% and 300 MPa at a compression strain of 1.6%.

Similar results of those in Fig. 72 were obtained by Van Humbeeck and Liu [48], that tested a NiTi bar in martensite state under tension and compression cyclic deformations (Fig. 73). For each strain level, 50 cycles were performed and the maximum attained strain was equal to 4% both in tension and compression.

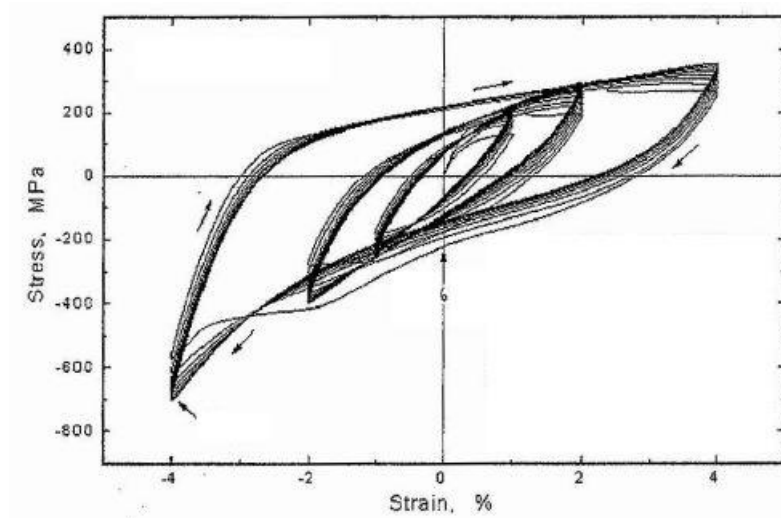The maximum force reached in compression phase was approximately twice the one reach in tension.

Fig. 73. NiTi bar in martensite state under tension and compression cycles [48].

Alam et al. [40] report that typical stress-strain diagram of austenite for a generic SMA under cyclic axial force are like those shown in Fig. 74, where it is possible to see that behaviour in tension and compression is quite similar.
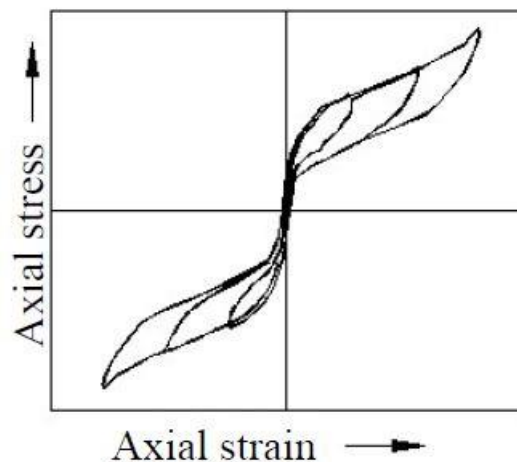

Fig. 74. SMAs behaviour under tension and compression cycles in austenite phase [40].

Flexural tests on bars in martensite phase are performed by Cardone et al. [49] and the results are shown in Fig. 75. From these tests NiTi bars show good energy dissipation capability, large residual strains after removing the load and good fatigue resistance.
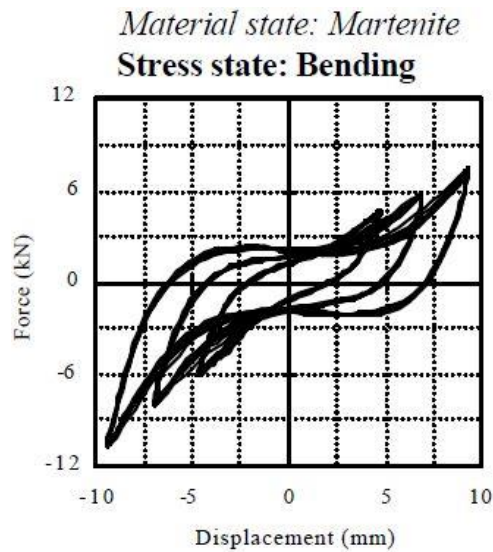
Fig. 75. Flexural behaviour of SMA bars [49].

Dolce and Cardone [50] conduct some tests also on martensite and austenite NiTi bars subjected to torsion. Fig. 76 shows the moment-rotation diagram of the test on big size bars in martensitic phase, in the left, and austenitic phase, on the right, as a function of strain rate (0.01, 0.5 and 1 Hz) and for strain amplitudes equal to 3%, 6%, 9% and 11%. For each strain amplitude 10 cycles were performed.

On the left in Fig. 76 it is possible to observed the diagram obtained for bars in martensite state. Results show a decrease of energy dissipation when increase frequency, while the equivalent damping keeps substantially constant (12-13%) for the material tested. These test also underline the great fatigue resistance, that are subject to more than 2300 cycles without failure. For the austinite phase an apparent residue at zero force characterised the shape of the hysteresis loops. This occurs because, for the temperature room, not all the stress-induced martensite change into austenite. However the residual rotation is one order less the maximum rotation ($\approx$ 0.18 rad). Contrary to what happen with martensite specimens, there is no appreciable decay and stabilisation of mechanical behaviour. Increasing the strain rate, the moment reached at a generic rotation increases and so does the secant stiffness. The energy loss per cycle remains practically the same.
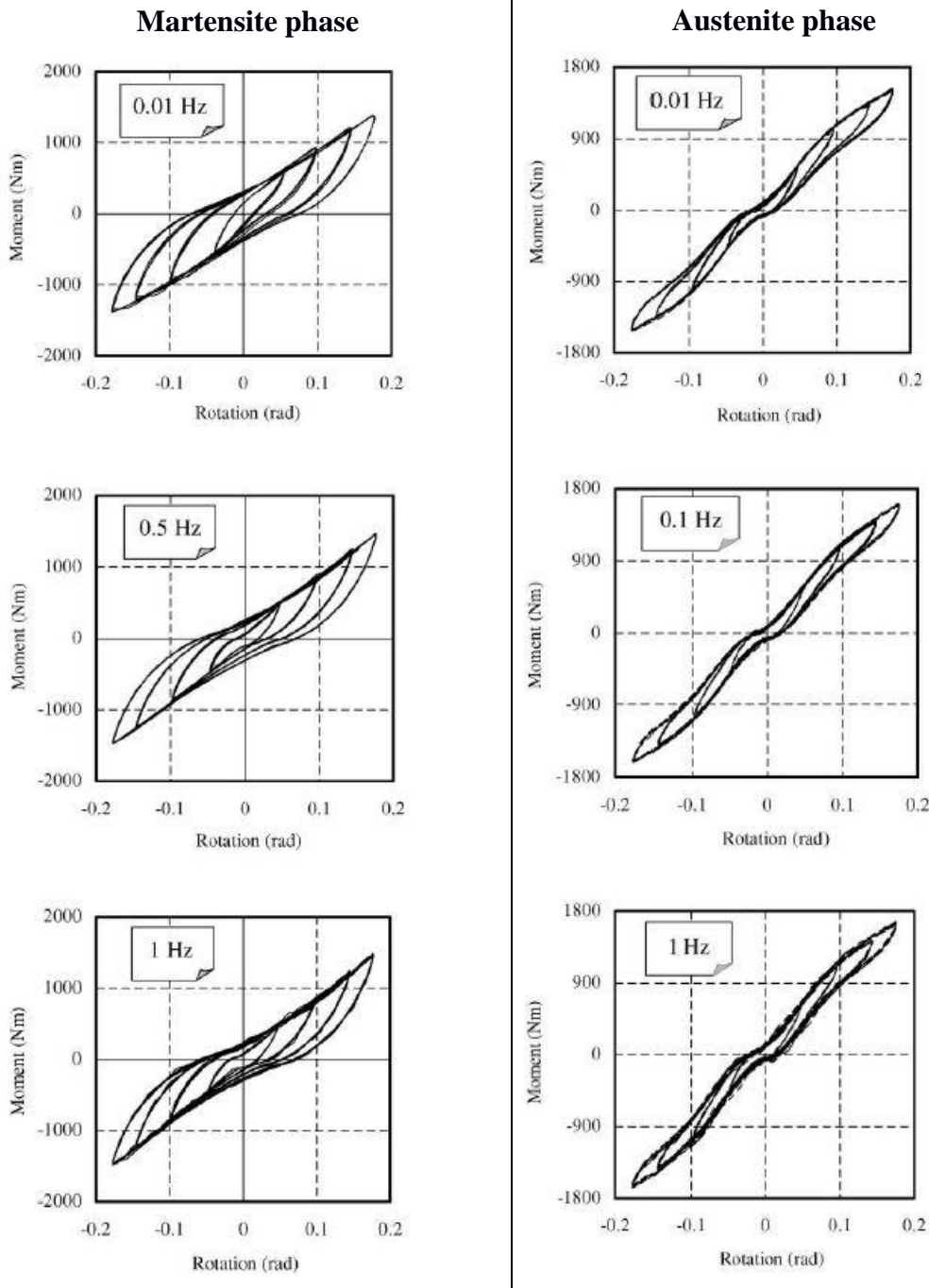
Martensite phase | **Austenite phase**

Fig. 76. Mechanical behaviour of big bars in different phase subject to torsion [50].

The rates which are most interesting for seismic application, for all the cases analysed, are the moderate ones (0.5-2 Hz).

The behaviour of NiTi elements under multiple load cycles is also investigated. Clarke et al. [51] examined a NiTi wire subjected to increasing cycling (tension only) load with a rate of 50% per minute up to a strain of 8%. Test's results showed that

increasing the number of cycles, the loop shifts downwards and there is a reduction of transformation yield stress, while shape of hysteresis loop remained constant for all the test. Similar results are obtained by Piedboeuf et al. [52] as shown in Fig. 77.
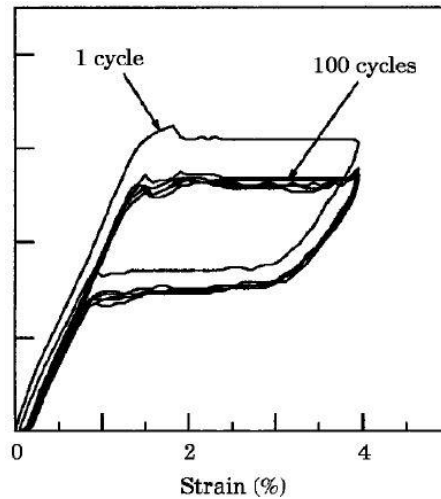

Fig. 77. NiTi wire subject to multiple cycles [52].

Dolce et al. [53] studied the behaviour of a 1mm diameter austenite wire (frequency 1 Hz, 3% pre-strain) as a function of temperature. During the test the temperature varied between 0 and 50° C, and some results are shown in Fig. 78. A linear dependence on temperature is detect, with increase of force of about 10% every 10° C, and decreases of equivalent damping of about 13% every 10° C.
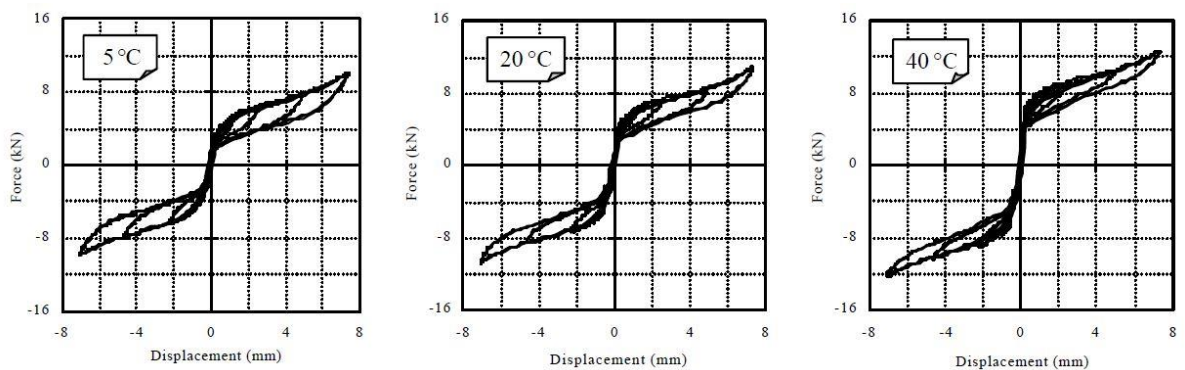

Fig. 78. NiTi wire in austenite phase: behaviour as a function of temperature [53].

Tab. 16 shows some indicative values of mechanical characteristics of NiTi alloys. The values are reported within an approximate range as they strongly depend on chemical composition and production process of the alloy itself.

Tab. 16 Indicative mechanical characteristics of NiTi alloys.

	Austenite	Martensite
Young's Modulus [GPa]	60 - 98	21 - 41
Yield strength [MPa]	130 - 700	50 - 300
Elongation at failure [%]	15 - 20	20 - 50
Ultimate tensile strength [MPa]	800 - 2000	
Recovery strain [%]	Up to 8 - 10	
Specific damping capacity [%]	15 - 20	

From Tab. 16 it is therefore possible to observe that the mechanical characteristics of NiTi alloys are suitable for their use as reinforcement bars, especially in the austenitic phase, which corresponds to a superelastic behaviour of the alloy. In fact, both for new buildings and the retrofit of existing ones, the use of SMAs characterized by a superelastic behaviour would allow to dissipate part of the input seismic energy and to completely recover deformations up to 8-10%.

In Tab. 17 it is possible to observe the transformation temperatures for NiTi alloys with different concentrations and fabrication processes. Also in this case, it emerges that the temperatures are strongly linked to these two aspects.

As it can be seen in Tab. 17, only the alloy [55] has characteristics that are acceptable, while the other analysed alloys analysed reach A_f for too high temperature. In fact the alloy [55] present a superelastic behaviour for temperature greater than 9°C, while between -3°C and 9°C the martensitic and austenitic phases coexist, and therefore a complete recovery of the deformation does not occur. At room temperature (assumed 20°C) the alloys [56] and [57] would have a partially

superelastic behaviour, having an A_s temperature of 9.2° C and 18° C respectively, and therefore being in a phase of coexistence of martensite and austenite.

Tab. 17 Transformation temperature of various NiTi SMAs.

Alloy	Composition Ni-Ti [%]	Fabrication Process	M_f [C]	M_s [C]	A_s [C]	A_f [C]
[54]	50.5 – 49.5	Hot-rolled and then cold-roled with intermediate annealing	4	33	44	62
[55]	50.8 – 49.2	Annealed followed by water quenching	- 46	- 21	- 3	9
[56]	55.7 – 44.3	Annealed	- 40	5	18	51
[57]	50.5 – 49.5	Vacuum annealed followed by water quenching	- 74.6	18.3	9.2	53.2

One of the major problems in the widespread use of NiTi SMAs in the civil engineering sector would be their high cost. Another important aspect to take into consideration, closely related to the previous one, is the large amount of material needed in civil engineering applications. The high cost of NiTi alloys is linked to the high cost of the materials, the production processes, which usually requires vacuum condition, and the thermal and mechanical treatments they undergo. Furthermore, the materials used in civil engineering must guarantee certain characteristics and sufficient performance, so specific elements concentration and processes are needed.

In the last decades there has been a significant reduction in prices of NiTi from more than 1000 USD to about 100 USD per kg. Certainly, in the future, the cost of this material will further reduce, but it is still too high for a wide use of NiTi SMAs in the world of civil engineering, considering the quantities of reinforcement required. For this reason SMAs made with cheaper materials and which guarantee performance equivalent or superior to NiTi are analysed in the following. Janke et al.

[58] in the comparison between NiTi and Fe-based SMAs highlight that the second one costs about 1/10 of NiTi.

4.1.2   Iron-based SMAs

As it emerge in the analysis of NiTi SMAs in the previous section, these alloys have good mechanical characteristics, elastic recovery of considerable deformation due to the superelastic effect and good fatigue resistance, but high cost of raw materials and consequent limited applications in civil structures. For these reasons alternative SMAs, as Fe-based SMAs are taken under consideration in the following.

Sato et al. [59] discovered the shape memory effect (SME) in a Fe-Mn-Si alloy in 1982 and since that date iron-based alloys have been studied and developed.

According to [60] it is possible to identify two different groups of iron-based SMAs.

In the first grove there are alloys as Fe-Pt, Fe-Pd and Fe-Ni-Co, which exhibit the typical characteristics of thermoelastic martensitic transformation similar to NiTi, with a narrow thermal hysteresis. However, at room temperature Fe-Pt and Fe-Pd have no pseudoeslastic effect. Study of Tanaka et al. [61] and Omori et al. [62] showed than some specific iron-based SMAs, adding concentration of Ni, Mn, Al or other elements, present recovery strain at room temperature between 5% and 13%, but this alloys still need to be studied and developed.

The second group consists of alloys such as Fe-Ni-C and Fe-Mn-Si, which have a larger thermal hysteresis in transformation but still exhibit the SME.

In Fe-Mn-Si alloys, manganese is necessary to stabilizes the austenite with a face cubic centered structured, while silicon is necessary to realize a recognizable shape memory effect, that would be very small with Fe-Mn only. According to [63] in the ternary Fe-Mn-Si system, optimum concentration range are 28~33 mass % for

Mn and 5~6 mass % for Si. Small amount of elements such as carbon, C, and nitrogen, N, are useful to stabilizes the austenite phase and reduce Mn concentration. Fe-Mn-Si based alloys is generally considered to be of non-thermoelastic type and do not show superelasticity. However, depending on composition, some of them show relatively large and non-linear spring-back on unloading that is addressed as a partial pseudo-elasticity.

Fe-based alloys, especially Fe-Mn-Si, show generally good corrosion resistance in different aggressive environments. A common factor of Fe-based alloys that has been found is that the higher the Cr content is, the higher the corrosion resistance, and that also the addition of Cu and Rare earth could improve the corrosion resistance [64].

This alloys present also good weldability, although other more in-depth studies will have to be conducted. Results of tests show that welding affects mechanical and shape memory properties: the material fractured in the welded zone and the degree of shape recovery decrease of 15% [65].

As for NiTi alloys, also the mechanical characteristics of Fe-based alloys are linked to the composition and fabrication process. In Tab. 18 indicative mechanical characteristics of Fe-based alloys are shown.

Tab. 18 Indicative mechanical characteristics of Fe-based alloys.

Young's Modulus [GPa]	140 - 170
Yield strength [MPa]	200
Elongation at failure [%]	Up to 35
Ultimate tensile strength [MPa]	650 - 1000
Recovery strain [%]	Up to 6

Fe-based SMAs presents a Young's Modulus about 20% lower than the one of steel use for reinforcing bars. In comparison to NiTi alloys, are characterised by a

lower recovery strain, but still enough to be thoughtful as an interesting material to make reinforcing bars.

4.1.3 Copper-based SMAs

Another category of SMAs that have received particular interest are copper-based SMAs. The most common copper-based SMAs are Cu-Al-Ni and Cu-Zn-Al.

Both of these alloys have the advantage of being made with relatively cheap materials and, as their fabrication mostly requires conventional metallurgical processes, have low production costs. Copper-based alloys can be readily hot worked in air. Alloys with higher aluminium content are not as easily cold workable, while Cu-Al-Ni are quite brittle at low temperature and can only be hot finished [44].

In some research works [66], [67], [68], the effects of adding a forth alloy element, such as Au, Cr, Fe, Co, Zn, Ag, to improve ductility, shape memory effect and superelastic effect are investigated.

Fig. 79 illustrates the trends of the of martensitic start transformation temperature as the percentage of fourth element added in the $Cu_{73}Al_{17}Mn_{10}$ alloy varies. As it can be seen, gold, Au, zinc, Zn, and silicon, Si, produce an increase the M_s temperature as their percentage in alloy increase [68]. The addition of iron increases this temperature for percentages higher than 0.5%.

As it can be seen from Fig. 79, the variation of the M_s temperature is strongly dependent on the element used and on its percentage. From the evaluation of this temperature, it is possible to understand when, in the cooling phase, the transformation from austenite to martensite start and therefore both phases begin to coexist in the material.
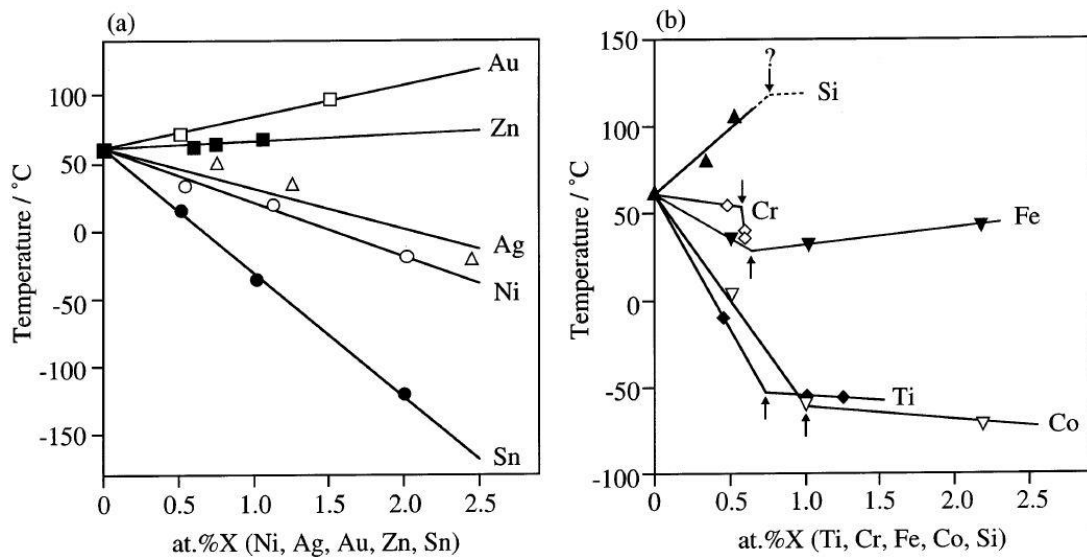
Fig. 79. Martensite start (M$_s$) trends transformation [68].

The influence on shape memory effect due to the addition of different fourth element is shown in Fig. 80. Recovery of ternary alloys was less than 95% and decrease when M_s increase, as is possible to observe from the position of circle symbols. The addition of Ni and Co allows to have almost perfect shape recovery. The addition of most alloying elements, except Ag, Si and Sn, at the same M_s temperature, improves the shape memory properties [68]. In fact it is possible to observe that the point enclosed in the darker area in Fig. 80 have better percentage shape recovery than the points related to the ternary alloy, enclosed in the lighter area.

Mallik et al. [67] add a fourth element in the Cu 12% - Al 5% - Mn alloy, keeping the ratio concentration of these three elements constant. Variation of transformation temperature related to the added fourth elements and their concentration are shown in Fig. 81. Zinc and nickel increase transformation temperatures: this result is in agreement with [68] regarding zinc, but a different trend is obtained for nickel.
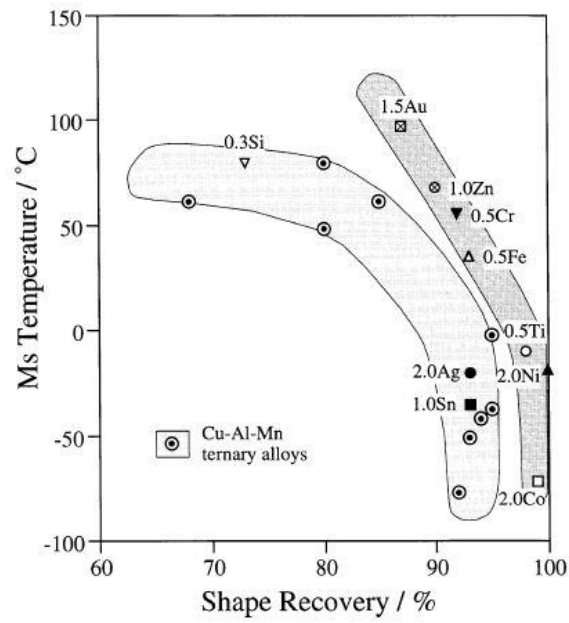
137

Fig. 80. Shape recovery comparison between quaternary and ternary alloys [68].
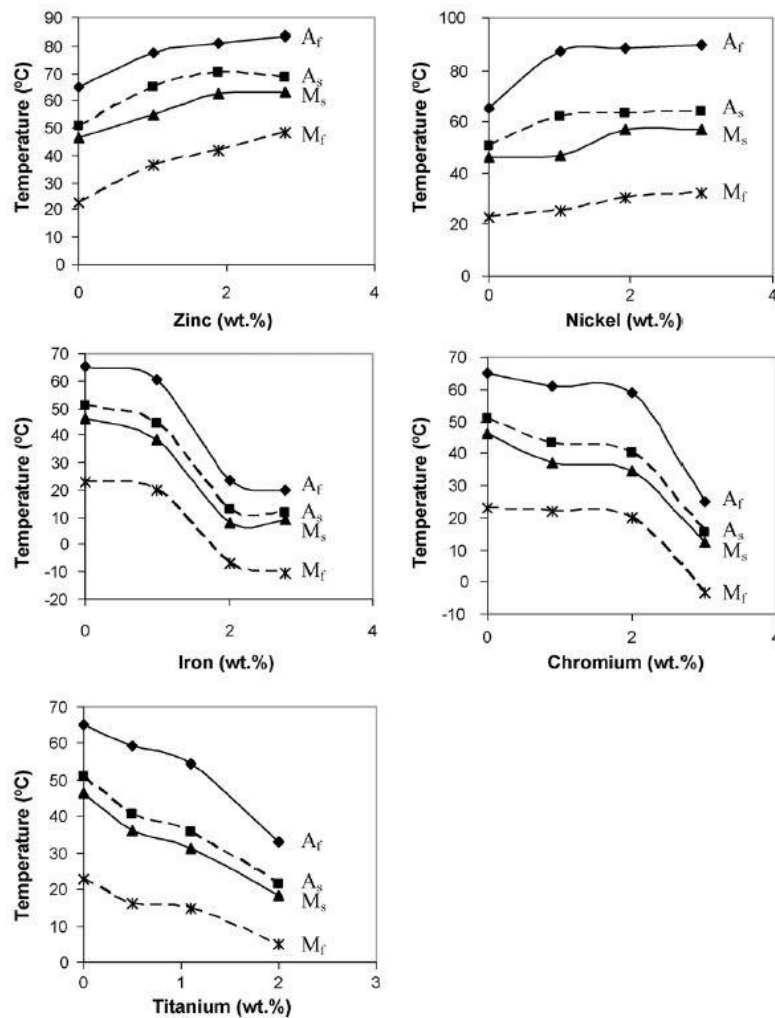

Fig. 81. Transformation temperature variation with fourth elements and their concentration [67].

As can be seen in the last diagram of Fig. 81, the addition of titanium leads to an almost linear reduction of the transformation temperature as its concentration increases. The addition of iron and chromium, on the other hand, causes a sudden change in the transformation temperatures for a concentration of between 1% and 2% for iron and between 2% and 3% for chromium. This allows to evaluate which element can be introduced into the ternary alloy and in what percentage to vary the temperature ranges, so that the alloys have a superelastic behaviour for temperatures suitable for their use in the civil engineering sector.

A strain recovery analysis is also conducted for SME in [67]. As it can be seen in Fig. 82, all the added elements improve the strain recovery capacity with the increase of their concentration in the alloy. Only iron produces a reduction for a concentration percentage between 1% and 2%. Alloys with Zn, Ni and Cr exhibit almost complete strain recovery by SME. Overall an increase of 4-8% in strain recovery by SME is observed in the alloys with the quaternary alloying additions.
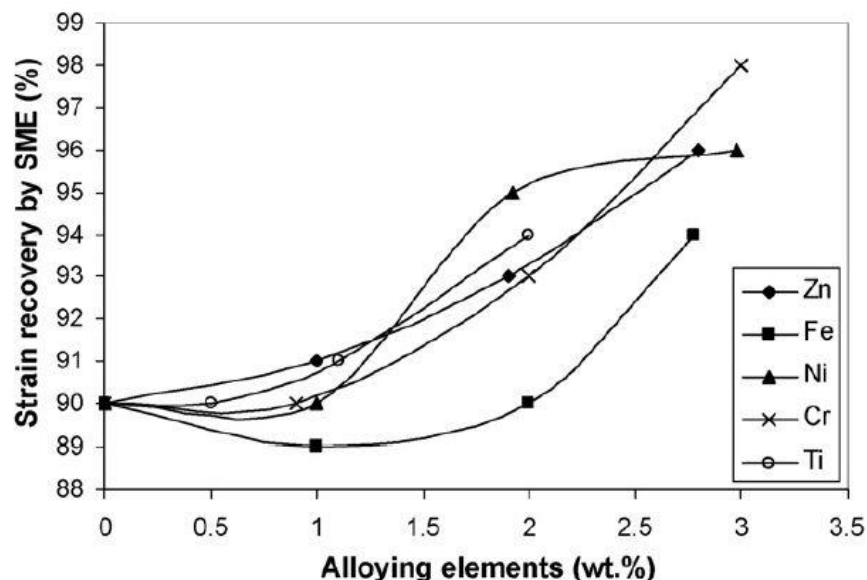

Fig. 82. Variation in strain recovery by SME with variation in fourth element addition [67].

Also tensile tests on specimens made by alloys in the austenitic phase with different fourth element added are carried out in [67]. Stress-strain results for

specimens with Magnesium (CAMMg 1) and nickel (CAMNi 3) are shown in Fig. 83. The superelastic strain is calculated as $\varepsilon_{SE} = \varepsilon_T - \varepsilon_e - \varepsilon_r$, where ε_T is the total strain, ε_e the elastic strain of the material and ε_r is the residual strain remaining in the material after complete unloading. CAMMg 1 show a strain recovery by SME of 75% and a superelasticity of 2.2%, while CAMNi 3 96% and 3.5% respectively. For all the specimens tested, the strain recovery by SME is between 75% and 98% and superelasticity between 2.2% and 4.5%.

The interesting aspect of these properties for a use of the material in the civil engineering sector is that after an earthquake, the recovery of deformations is possible by heating the alloy in case of shape memory effect and by the removal of the load in case of superelasticity.
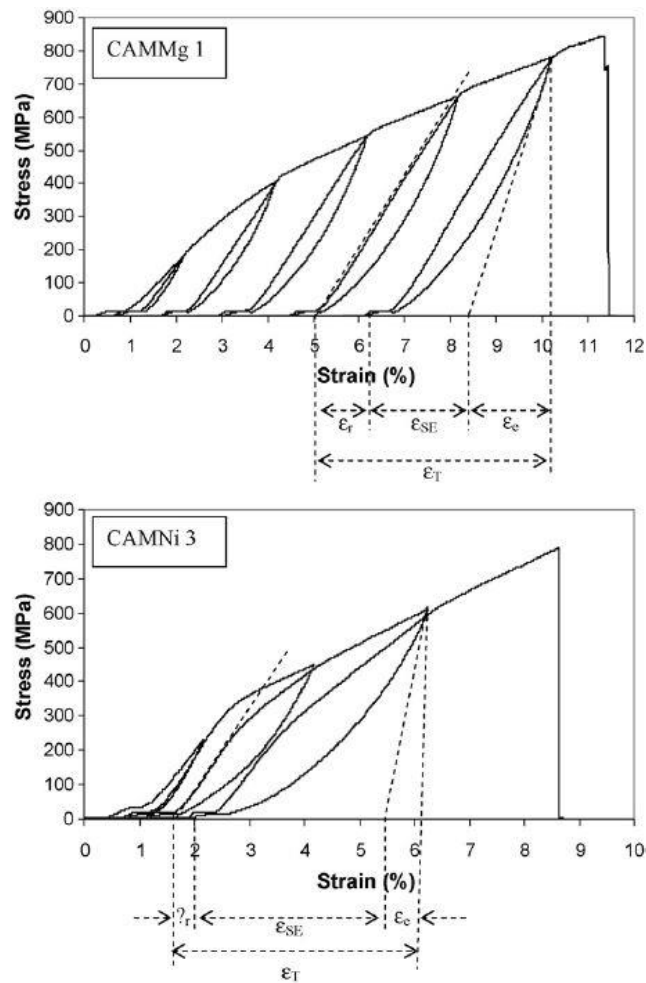

Fig. 83. Stress-strain curve for alloy with different fourth elements added [67].

As shown in Fig. 84 the addition of all fourth elements decreases the superelastic capacity, except in the case of adding small quantities of Fe, Cr and Ti (21%) which do not cause the variation of this characteristic. None of the tested elements improve at the same time the strain recovery by SME and superelasticity, indeed as it has emerged the addition of Fe in small concentration worsens the strain recovery.
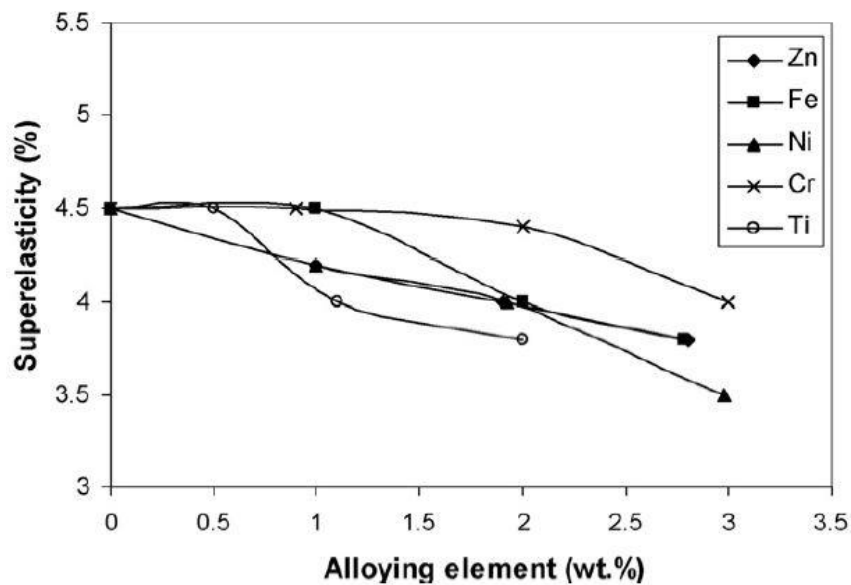

Fig. 84. Variation in superelasticity with variation in fourth element addition [67].

Liu et al. [69] performed cyclic tensile tests on samples having the following composition: Cu (17.8%)–Al (11.4%)–Mn, designed with special polycrystalline columnar-grained (CG) in different concentration (4%, 6%, 8%, 10%), in austenite phase. Samples were stretched to the strain amplitudes of 4%, 6%, 8% and 10%, and the results are shown in Fig. 85. No sample fractured up to 1000 cycles. Flag-shaped hysteretic loops with excellent superelasticity were observed at first cycles, and then the decays of transformation platform slope, recovery strain and transformation stress were observed. It can be seen that as the cycle number increases, the residual strain increases due to the accumulation of un-reversible martensite. For CG-4% sample (Fig. 85 (a)) up to about 2000 cycles, excellent strain recovery was observed, with a residual strain lower than 1%. For CG-6% (Fig. 85 (b)), CG-8% (Fig. 85 (c)) and

CG-10% (Fig. 85 (d)) this percentage of residual strain was reached at about 500, 150, 80 cycles. Then a rapid increase in residual strain was observed at more cycles. In any case the SMAs considered in [69] exhibited excellent superelastic fatigue properties at high strain amplitude.
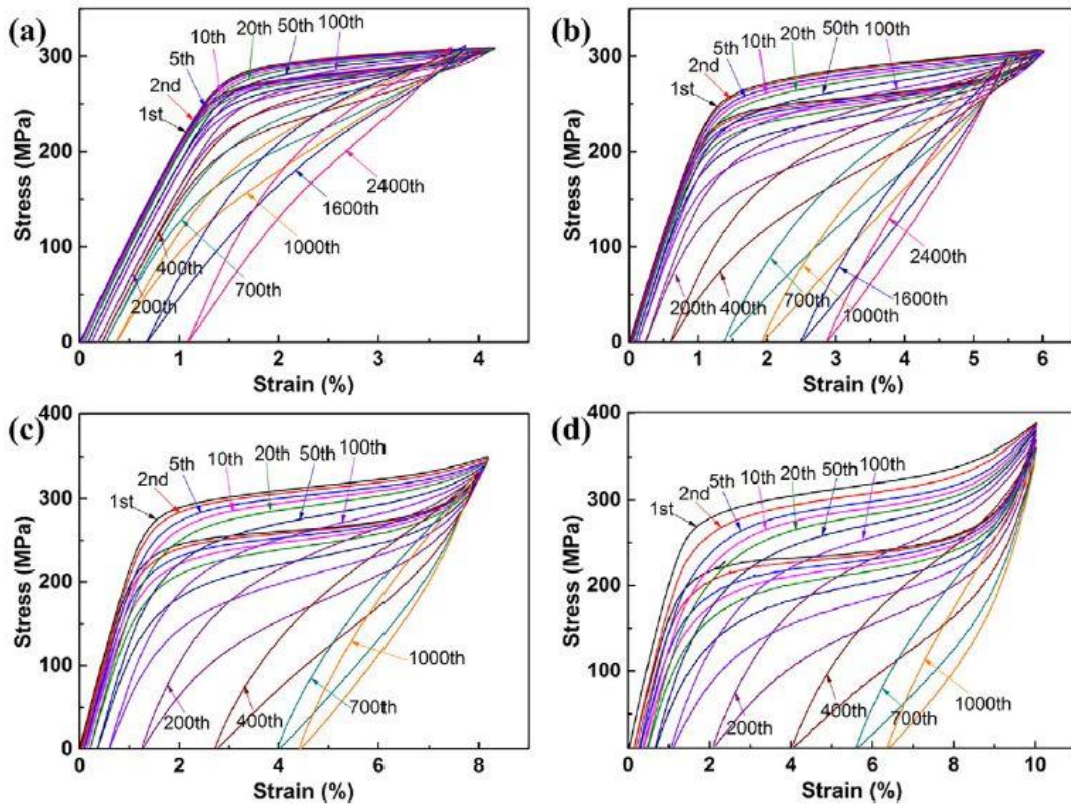

Fig. 85. Superelastic stress-strain curves under cyclic tension at different strain amplitudes [69].

Tests on the variation of transformation temperatures on specimens Cu-Al-Mn as the concentration of the three elements varied were carried out by Mallik et al. [70], and the relative results are reported in Tab. 19. From these results, it is evident that even a small variation in the concentration of the three elements leads to considerable variations in the transformation temperatures, which are therefore strongly linked to the chemical composition of the alloy. Diagrams in Fig. 86 show the variation of transformation temperatures as a function of different concentration of Mn and Al. From the diagrams on the left of Fig. 86 it is possible to see that, keeping the same Cu/Al ratio, an increase in the concentration of Mn leads to a

reduction in the transformation temperatures. From the diagrams on the right of Fig. 86, where the Cu/Mn ratio is kept constant, it can be seen that a variation in the Al content from 11% to 13% leads to a sudden reduction in the transformation temperatures.

Tab. 19 Chemical composition and transformation temperature of Cu-Al-Mn SMAs.

| Alloy ID	Composition (wt.%)			Cu/Al ratio	Cu/Mn ratio	Transformation temperatures (°C)			
	Cu	Al	Mn			M_f	M_s	A_s	A_f
CAM 1	82.54	10.49	6.97	7.8	11.8	35	56	58	80
CAM 2	83.2	10.8	6	7.7	13.8	49	72	69	94
CAM 3	85.35	11.65	3	7.3	28.4	63.4	88.1	96	114.2
CAM 4	85.04	11.89	3.07	7.1	27.7	62.5	78.2	83.3	105.2
CAM 5	84.26	11.87	3.87	7	21.7	52.3	70.8	72.3	94.8
CAM 6	80.5	11.5	8	7	10	6.5	21.8	30	48.2
CAM 7	83.85	11.99	4.16	6.9	20.1	45.4	62.3	65.8	88.6
CAM 8	82	12	6	6.8	13.6	21.2	44.4	47.8	68
CAM 9	80	12	8	6.6	10	−5.4	11.8	18.4	33.4
CAM 10	85.34	12.49	2.17	6.8	39.3	76.3	98	95	117
CAM 11	80.5	12.5	7	6.4	11.5	−3.8	10.8	16.2	34.5
CAM 12	79.5	12.5	8	6.3	9.9	−20.7	−6.8	8.9	22
CAM 13	81	13	6	6.2	13.5	1.8	20.4	25.8	43.1
CAM 14	80	13	7	6.1	11.4	−16.1	2.3	11.2	29.8
CAM 15	79	13	8	6	9.8	−28.2	−14.1	−8	13
CAM 16	84.97	13.33	1.7	6.3	49.9	48	66	70.1	93.8
CAM 17	80.26	13.36	6.38	6	12.5	−12	4	12	28.9
CAM 18	84.04	13.62	2.34	6.1	35.9	35	56	68	94
CAM 19	83.7	13.87	2.43	6	34.4	26.8	45.6	48	76
CAM 20	83.27	13.5	3.23	6.1	25.7	25	55	68	94
CAM 21	83.07	14.52	2.41	5.7	34.4	30	53.2	50.3	72.1
CAM 22	80.8	14.6	4.6	5.5	17.5	−44.1	−26.3	−29.7	−5.7
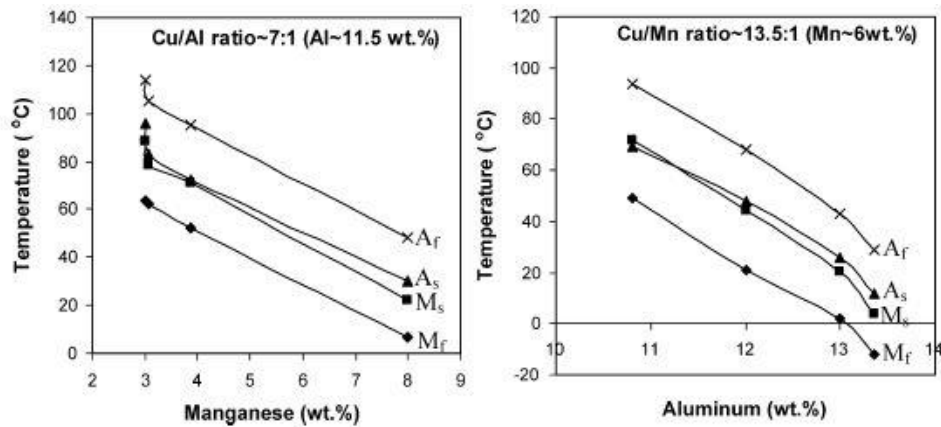
Fig. 86. Variation of transformation temperature of Cu-Al-Mn with Al and Mn variation [70].

In the same study [70] variation of damping properties with the change in concentration of Al and Mn was explored. Some results are shown in Fig. 87. From these test results it emerged that the damping capacity of Cu-Al-Mn alloy decreases by increasing the manganese content, while keeping constant the ratio Cu/Al, and it

increases as the percentage of aluminium increases, while keeping constant the ratio Cu/Mn.
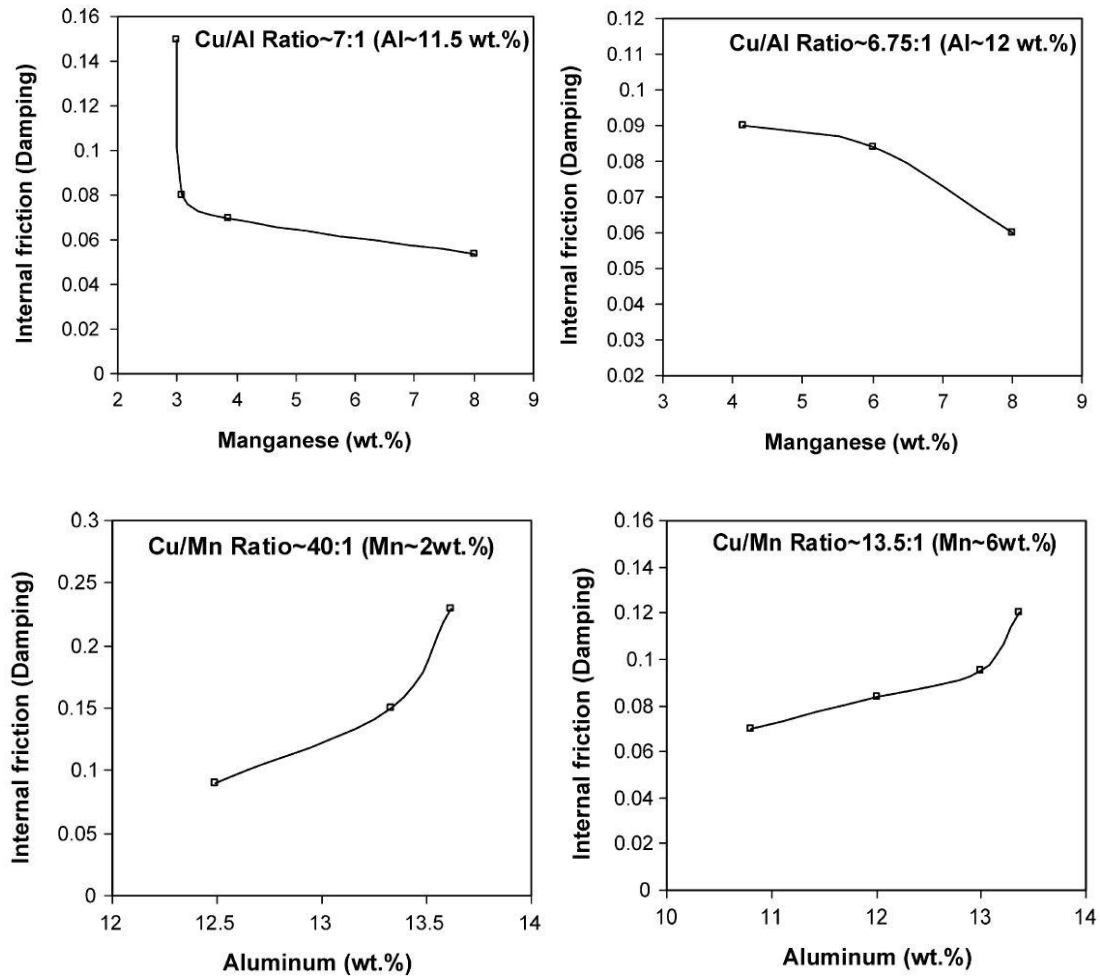

Fig. 87. Variation in damping capacity of Cu-Al-Mn with Al and Mn variation [70].

Work of other researchers [71]-[73] on Cu-based SMAs alloys, realized with different techniques and made by different constitutive elements, highlighted the transformation temperature presented in Tab. 20.

Tab. 20 Chemical composition and transformation temperature of some Cu-based SMAs.

Alloy	Composition Ni-Ti [%]	Fabrication Process	M_f [C]	M_s [C]	A_s [C]	A_f [C]
Cu-Zn-Al [71]	25.6-4.2-70.2	Annealed followed by aging in a quenching bath	15.5	19.7	20.5	25.6
Cu-Al-Ni [72]	82.0-14.0-4.0	Annealed followed by water quenching	- 21	- 27	1	12
Cu-Al-Be [73]	11.6-0.6-87.8	-	- 116	- 94	- 104	- 78

As seen for the previous shape memory alloys, mechanical characteristics depend on chemical composition and production process of the alloy itself. For these reasons Tab. 21 present values within an approximate for Cu-Zn-Al and Cu-Al-Ni alloys.

Tab. 21 Properties of some Cu-based alloys.

Property	Cu-Zn-Al		Cu-Al-Ni	
	Austenite	Martensite	Austenite	Martensite
Young's Modulus [GPa]	70 - 100	60 - 70	80 - 100	70 - 80
Yield strength [MPa]	150 - 350	80 - 300	150 - 300	150 - 300
Ultimate tensile strength [Mpa]	400 - 900	700 - 800	500 - 1200	1000 - 1200
Elongation at failure [%]	10 - 15		8 - 10	
Recovery strain [%]	3.5		2	

As it is possible to observed from Tab. 21, the Young's modulus for the two Cu-based SMAs is quite the same, and it is lower than the Young's modulus of steel. On the contrary Cu-based SMAs present ultimate tensile strengths greater than that of steel.

The cost of Cu-based SMAs is approximately 10%-20% of the cost of NiTi alloys.

4.2 Application of dissipative bracing in SMA – A case study

In this section the application of shape memory alloy as dissipative bracing on building A described in §3.1 will be analysed. Also for this case study the commercial software for structural analysis SAP2000 is used.

A shape memory alloy in the superelastic phase is considered, since, as seen above, it has the desired behaviour for the use in a building. The constitutive relationship for SMAs is not directly implemented in SAP2000, hence two different models are evaluated, in order to identify the one that best describes the special behaviour of SMAs and is easier to implement.

The improvement obtained by using SMAs as dissipative braces is evaluated and compared with that obtained by using BRADs.

4.2.1 Evaluation of two models to describe superelastic phase of SMAs

As anticipated in SAP2000 software there is no specific material that describes the flag constitutive law of SMAs in the austenitic phase. For this reason two different models to described this behaviour are analysed: the first is achieved by arranging two non-linear links in parallel, the second is made using the single *Damper-Friction spring* link present in the library of SAP2000.

To compare these two models it is decided to use the constitutive law of the shape memory alloy used by Hooshmand et al. [74] and illustrated in Fig. 88.

Considering the two-dimensional frame in Fig. 89 made with steel beams and columns, symmetrically loaded [75], the SMA braces are implemented using both the above mentioned models, in order to evaluate their ability to appropriately represent the SMA behaviour.
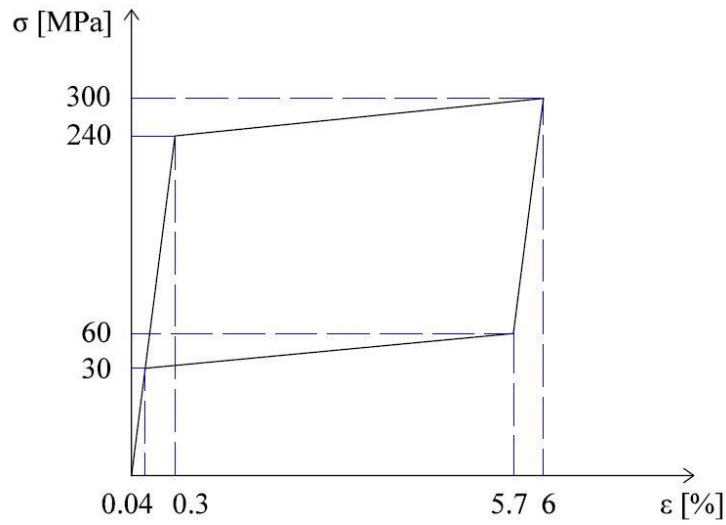
Fig. 88. Constitutive law [74] used to compare the two different superelastic models.

The frame has three floors, with an inter-storey height of 3.96 m. Columns have a W12x106 section, while beams have a W18x46 section. Both structural elements are made with steel having an elastic modulus equal to 200 GPa and a yield stress equal to 240 MPa.
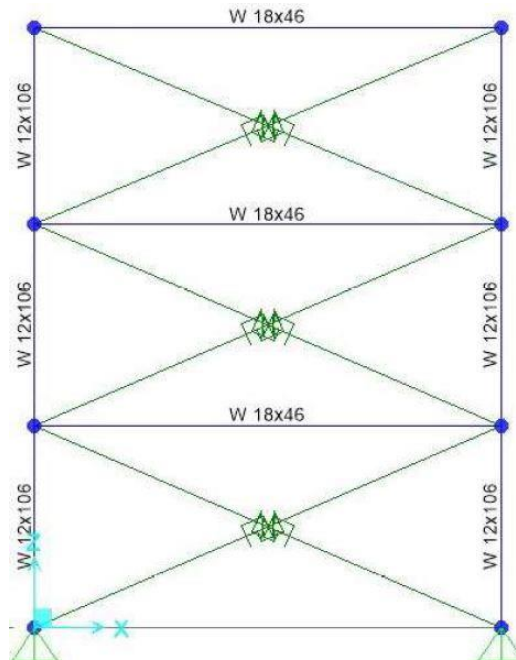

Fig. 89. Model of the frame described in with inserted links as braces [75].

Considering that the floors of the considered structures have a width of 9.14 m the calculated permanent structural load (G_1) is equal to 233 kN/m, the permanent

non-structural load (G_2) is equal to 241 kN/m and the variable load (Q_k) is equal to 66 kN/m. The seismic action is introduced in the structural model considering the accelerogram of the El Centro earthquake, that has a total duration of 53.74 s. To analyse the behaviour of the frame under this seismic load, a Fast Non-Linear Analysis is performed. Initially, through a ramp function, the structure is loaded until all the permanent loads are applied, and, then, only in a subsequent phase, the seismic action is applied. Being the structure made with steel, the modal damping parameter is set equal to 0.02.

4.2.1.1 First model: Two parallel link

As described by Andrawes et al. [76], it is possible to simulate the superelastic behaviour of a shape memory alloy using elements in parallel. The model described by Andrawes, illustrate in Fig. 90, is composed of two link elements, used to represent the initial branch with stiffness k_1 and the final branch with stiffness (k_2+k_3), respectively, and a truss element which represents the branch with stiffness k_2 and allows to take account of the dissipative behaviour.
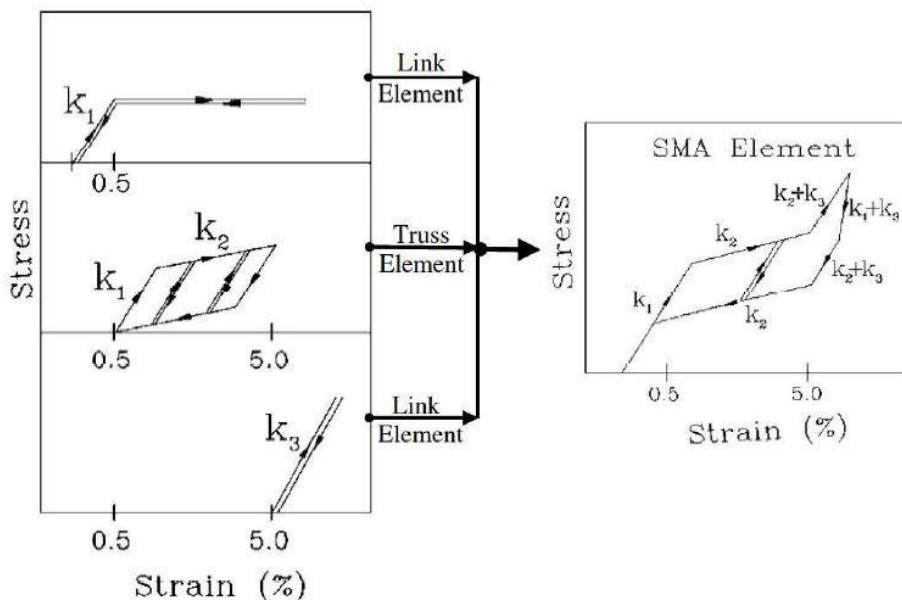

Fig. 90. Description of the model to represent SMA's superelastic behaviour [76].

148

In this case study, to represent the superelastic behaviour, it is decided to use a model similar to the one just described, but formed only by two links in parallel, neglecting the final stiffness increase. These two links are the *MultiLinear Elastic* and the *MultiLinear Plastic*.

The stress-strain diagram of Fig. 88 has been transformed into a force-displacement diagram, show in Fig. 91, since in SAP2000 the link elements are defined by the latter type of diagram, where *F* is the force and *δ* is the displacement. It is considered a braces with a part in SMA 2m long and the remaining part made with rigid steel profile.
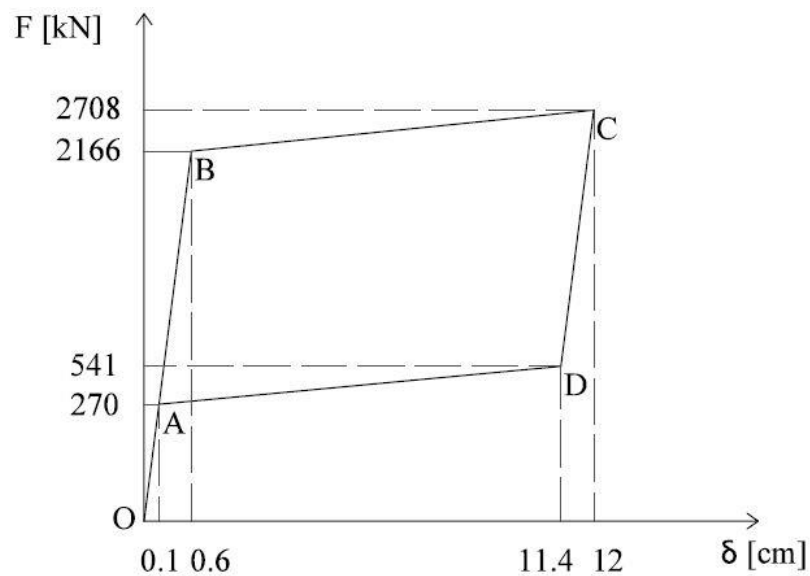

Fig. 91. Force-displacement diagram.

The *MultiLinear Elastic* link (Fig. 92) has the task of simulating the recovery of deformation after the application of stress. Since it is considered that braces work only axially, the behaviour of the link is defined only in the axial direction. The axial behaviour of the link is defined by inserting the values of the points O, A and D in Fig. 91, both in tension and in compression, i.e., as shown in Fig. 92, the following coordinates of displacement (in m) - force (in kN) values have been inserted: (-0.114;-541), (-0.001;-270), (0;0), (0.001;270), (0.114;541).
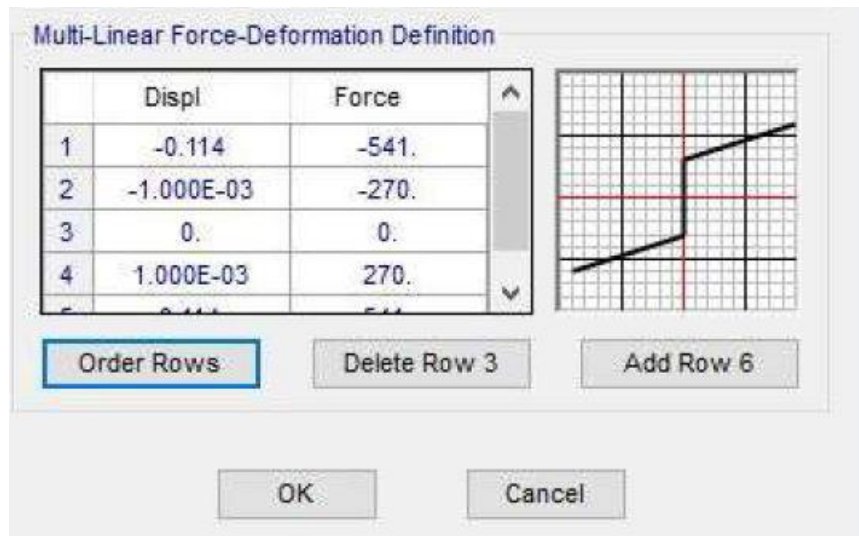
Fig. 92. Definition of Multilinear Elastic link.

The second link used is the *MultiLinear Plastic* one, already present in SAP2000 library, which has the task of simulating the dissipation of energy. In this case, the definition of the axial behaviour is more complex. First, the coordinate values of the points A, B and C in Fig. 91 have to be introduced in the link definition.

In order to consider the superposition of the effects of the two links, the values of the forces at the points A and B to be inserted in the *MultiLinear Plastic* link, are calculated as the difference between the ones in Fig. 91 and those included in the *MultiLinear Elastic* link. The y-coordinate of point C, that defined the force, is the same defined for point B, since the slope of B-C branch, as shown in Fig. 92, is already defined by the *MultiLinear Elastic* link. Therefore, to the point of the link which corresponds to point A in Fig. 91 a force $F_{p,A}=F_A-F_{el}=0$ kN is assigned, while to the point corresponding to point B in Fig. 91 a force $F_{p,B}=F_B-F_{el}=2166-270=1986$ kN is assigned. As for the previous case, behaviour in tension and in compression is defined, i.e. the following coordinates of displacement (in m) - force (in kN) values, as shown in Fig. 93, are inserted: (-0.12;-1896), (-0.006;-1896), (-0.001;0), (0;0), (0.001;0), (0.006;1896), (0.012;1896).

Fig. 93. Definition of Multilinear Plastic link.

For *MultiLinear Plastic* link it is also necessary to define the hysteresis type and the relative parameters, as shown in Fig. 92. For this case study *Pivot* hysteresis type is assumed, since, by defining the appropriate parameters, it is considered the most suitable for simulating the SMAs superelastic behaviour and define its hysteretic cycle. The definition of five parameters is requested (Fig. 94): α_1 and α_2 parameters position the Pivot point for unloading to zero respectively from positive and negative forces, β_1 and β_2 parameters position the Pivot point for the reverse load from zero towards respectively the positive force and the negative forces, η determines the amount of degradation of the elastic slopes after plastic deformation. In this case study the values α_1 and α_2 are set equal to 100 so as to have a slope of the discharge branch (C-D of Fig. 91) similar to the actual one, while the values of β_1, β_2 and η are set equal to 1.
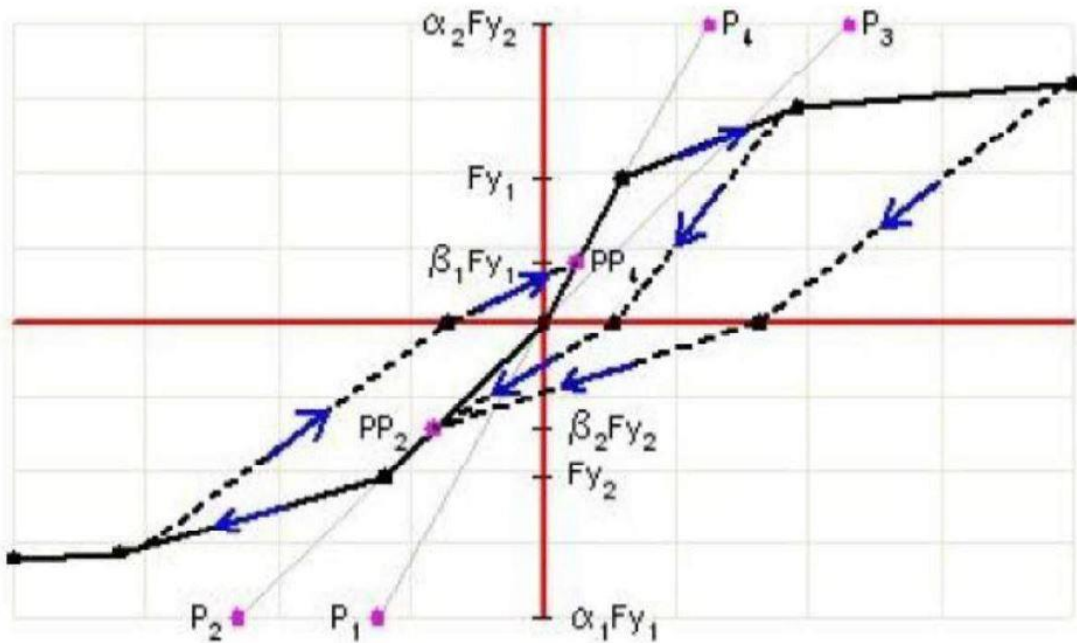
Fig. 94. Representation of the hysteresis parameter of Multilinear Plastic link.

4.2.1.2   Second model: Damper-Friction Spring link

The second model used to represent the behaviour of shape memory alloys in the superelastic phase is defined by using a single *Damper-Friction Spring* link. Unlike the two links used to define the previous model, the *Damper-Friction Spring* link is not defined through the points of the force-displacement link, but rather through the stiffness parameters of the various branches, as it can be seen in Fig. 95.

Also in this case, since it is considered that braces work only axially, the behaviour of the link is defined only in the axial direction. Continuing to refer to Fig. 91 and Fig. 95, the steps taken to calculate the parameters necessary for defining the axial behaviour of the *Damper-Friction Spring* link are shown below.
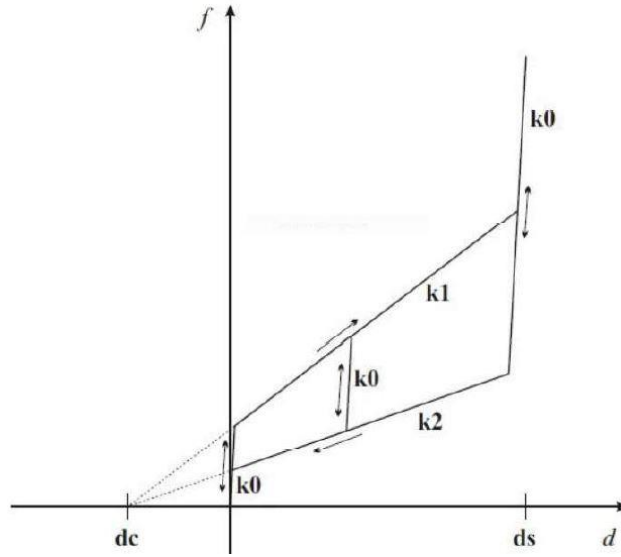
Fig. 95. Force-displacement diagram of *Damper-Friction Spring* link.

With reference to Fig. 91, the value of the initial stiffness k_0 of branch O-A-B is calculated with the following expression:

$$k_0 = \frac{F_B}{\delta_B} = \frac{2166}{0.006} = 361000 \; kN/m \tag{33}$$

The slope of branch B-C, identified by parameter k_1, is calculated as follows:

$$k_1 = \frac{F_C - F_B}{\delta_C - \delta_B} = \frac{2708 - 2166}{012 - 0.006} = 4754 \; kN/m \tag{34}$$

Branch B-C is extended toward left until it intersects the abscissa axis at point d_c (see Fig. 95), which is equal to 0.48 m. Since the extension of the branch A-D, by construction, must intersect the abscissa axis in d_c too (see Fig. 95), k_2 results equal to 563 kN/m. The value of d_s is set equal to 0.12 m, that is the maximum displacement reach by the SMA. In this way the diagram in Fig. 91 is univocally defined.

4.2.1.3 *Comparison between the results of the two models*

Once execute the FEM analysis with the two models above described the results shown in Fig. 96 are obtained. In this figure the results of the model with two parallel

link are represented with the blue line, while those of the model with the single link are represented with the orange line.
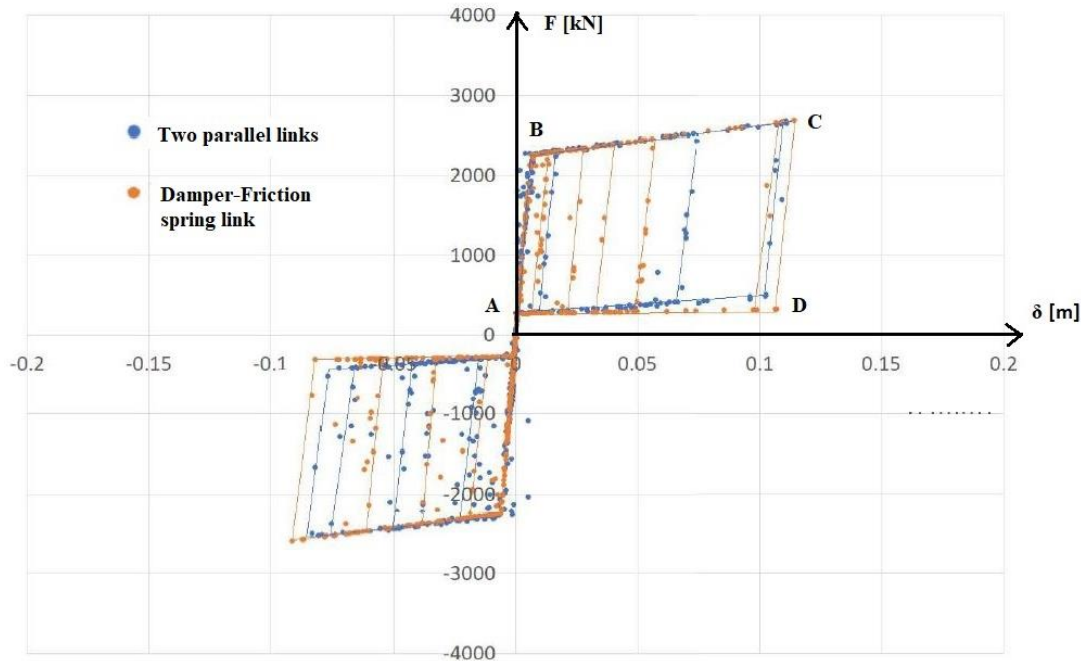

Fig. 96. Comparison between the results of the two models.

As it can be seen in Fig. 96 a similar behaviour is obtained through the two types of modelling. The elastic branch (A-B) and the branch of transformation (B-C) from austenite to martensite are practically undistinguishable, while small differences are found in the subsequent branches of recovery of the deformation (C-D and D-A). In the case of the use of two links in parallel, the slope of branch A-D is correct, while in the case of the representation with *Damper-Friction Spring* link the slope of this branch is near to zero. This is due to the fact that the branch, by construction, is bound to cross the branch of transformation from austenite to martensite at point d_c (Fig. 96).

Consequently, given that the two models showed almost identical behaviours, for the greater simplicity and speed of modelling, it is decided to use the model with single link in the case study illustrated in the following section.

4.2.2 Retrofit intervention with SMAs braces

Having defined the model to be used to represent the SMA behaviour with SAP2000 software, it is decide to apply the SMA bracing to the building described in §3.1, instead the BRADs used previously. This analysis is carried out for evaluating the effects in terms of stress reduction and residual displacements due to the use of SMAs, as well as comparing the energy dissipated by the two different retrofit methods.

Since the three two-unit blocks of which the building is made are equivalent to each other, also in this case study the analysis of only the block formed by units 5 and 6 is presented in the following. The geometry of units 5 and 6, as the mechanical and geometrical characteristics of the elements and the gravity loads applied are the same define in §3.1.

As made for building A, a Fast Non-Linear Analysis is used to analysed the structure. Firstly, only permanent and variable gravitational loads are applied to the building's model by means of a ramp function, and only in a second step, starting from the deformed state of the structure due to these loads, a seismic load is applied, by means of the same accelerograms used in §3.1. Three groups made by two artificial accelerograms, one in the X and one in the Y direction, are considered to represent the seismic action.

Therefore, starting from the model of the block consisting of unit 5 and 6 used in §3.1, it is proceeded to introduce the SMA braces inside the structural grid. The shape memory alloys used is the one illustrated by Sutou et al. [77] that is a copper-based alloy with the following chemical composition: $Cu_{73.5}Al_{17}Mn_{9.5}Ni_3$. The stress-strain diagram used for the definition of the SMA is illustrated in Fig. 97. Braces have a circular section, with an area that varies with the building level. As made for BRAD devices, starting from the first level of the building and going up braces with

gradually littler are used. In particular, braces with diameter of 40 mm $\phi 40$ are installed on the first story, $\phi 36$ mm on the second, $\phi 30$ mm on the third and, only in unit 5, which has a fourth story, $\phi 24$ mm on the last level.
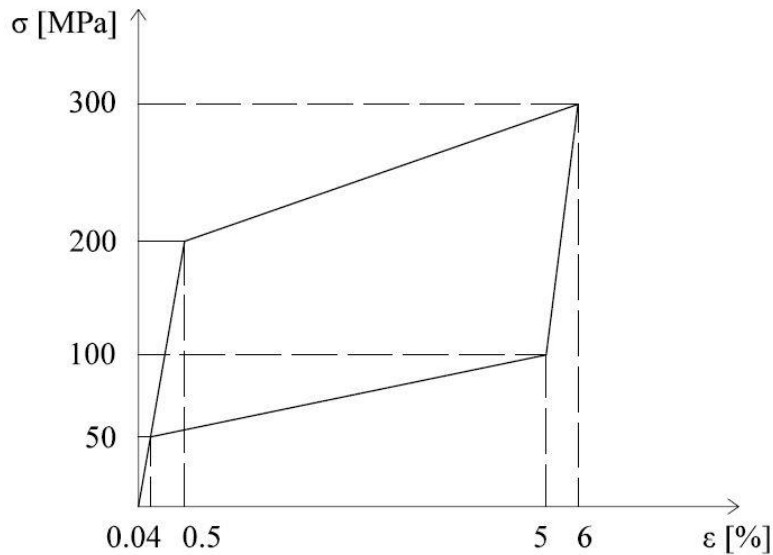

Fig. 97. Bond σ-ε of the alloy used in the modelling of braces.

As said the model with the single link *Damper-Friction Spring* is used to model the braces. Referring to Fig. 95, the parameters of each link used to model the braces inside the building are represented in Tab. 22.

<div align="center">Tab. 22 Links definition.</div>

	Link 1st level	Link 2nd level	Link 3rd level	Link 4th level
k_0 [kN/m]	100532	81432	56548	36192
k_1 [kN/m]	4569	3701	2571	1760
k_2 [kN/m]	1183	958	665	426
d_c [m]	- 0.053	- 0.053	- 0.053	- 0.053
d_s [m]	0.03	0.03	0.03	0.03

The position of the bracing is the same as that identified for the use of BRADs in the retrofitting proposal intervention illustrated in §3.1.4, so as to be able to directly compare the results obtained in the two different retrofit hypotheses, the one with

BRADs and the one using SMAs. Diameter of SMA braces have been arranged by a trial and error method. For this analysis, it is decided to make the links work only tensile action and, for this reason, differently from V-shaped braces used for BRADs, they are introduced with a cross configuration. The final configuration and the position of the braces are shown in Fig. 98 and Fig. 99.
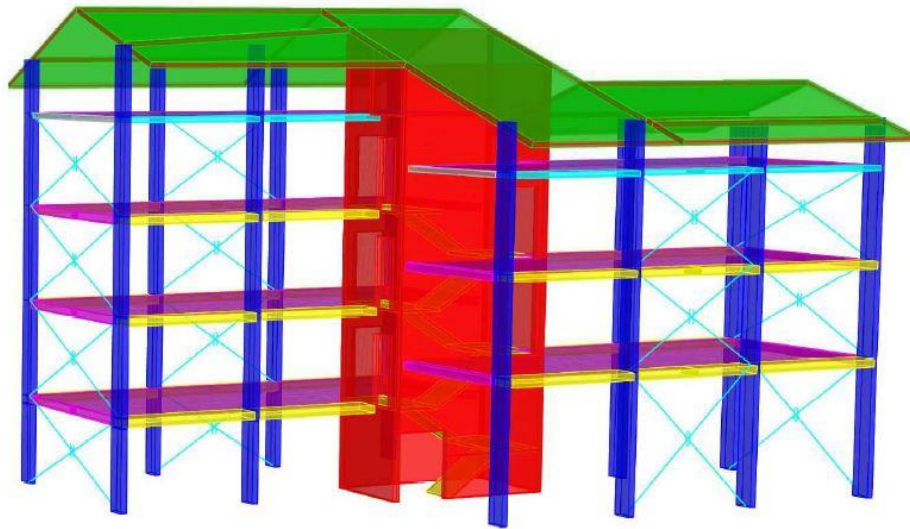
Fig. 98. Overview of the model in SAP2000.

As said to realize the building retrofit, SMA braces in a cross configuration are installed as show in Fig. 99.
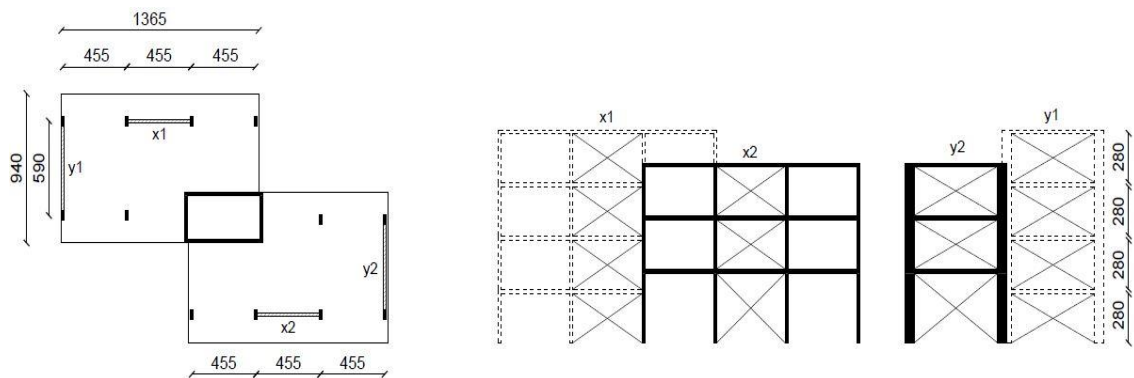

Fig. 99. Distribution of SMA braces in plan and elevation.

4.2.2.1 *Analysis results and results of the application of SMA braces*

After the introduction of the braces in the FE building model, the FNA is performed and the evaluation of the dissipated energy is carried out. In Fig. 100 (a),

(b) and (c) the graphs representing respectively the energy patterns of the as-built configuration, the configuration with BRADs and the configuration with SMA braces are plotted.
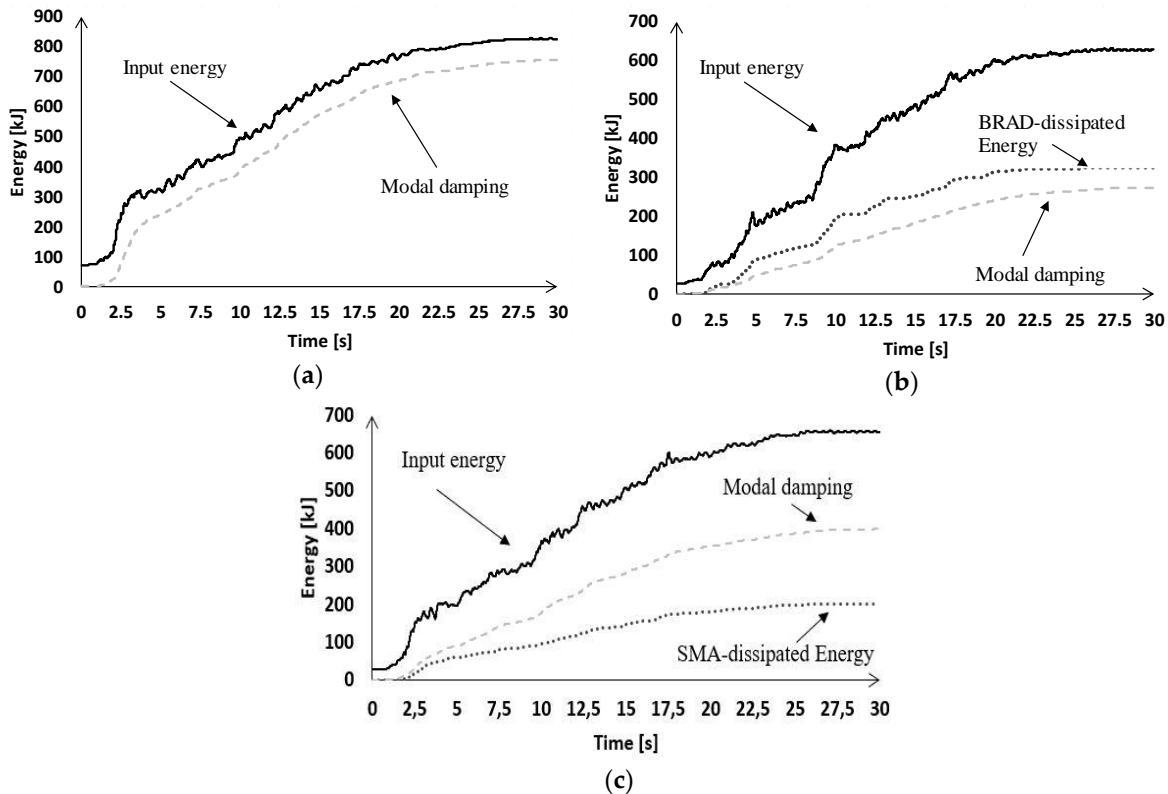
Fig. 100. Energy diagrams for building A in: (**a**) as-built configuration; (**b**) BRADs retrofit (c) SMA braces retrofit.

In Fig. 100 (a), it can be observed that the great part of input energy is dissipated by the building through modal damping, while Fig. 100 (b) shows that at the end of the seismic event, more than half of the input energy is dissipated by BRAD devices. Instead, as shown in Fig. 100 (c), the energy dissipated by SMA braces is almost one-third of the input energy. This difference in energy dissipated between BRAD and SMA braces is due to the fact that BRAD devices have larger hysteresis loops than SMA material.

Tab. 23 shows the values of the energy absorbed by the structure for the three groups of accelerograms in the three analysed configurations.

Tab. 23 Energy absorbed by the structure in the three analyzed configurations.

Group of accelerograms	As-built conf. [kJ]	BRADs retrofit [kJ]	SMA braces retrofit [kJ]
TH_BDE gr. 1	820	230	400
TH_BDE gr. 2	660	265	390
TH_BDE gr. 3	720	250	480

From Tab. 23 it can be seen that for all the three groups of accelerograms the energy absorbed by the structure in the case of retrofit with BRADs is always lower than that absorbed in the case of retrofit with SMA braces.

Fig. 101 shows the axial force-displacement cyclic response of four SMA braces, one for each level, under the BDE.
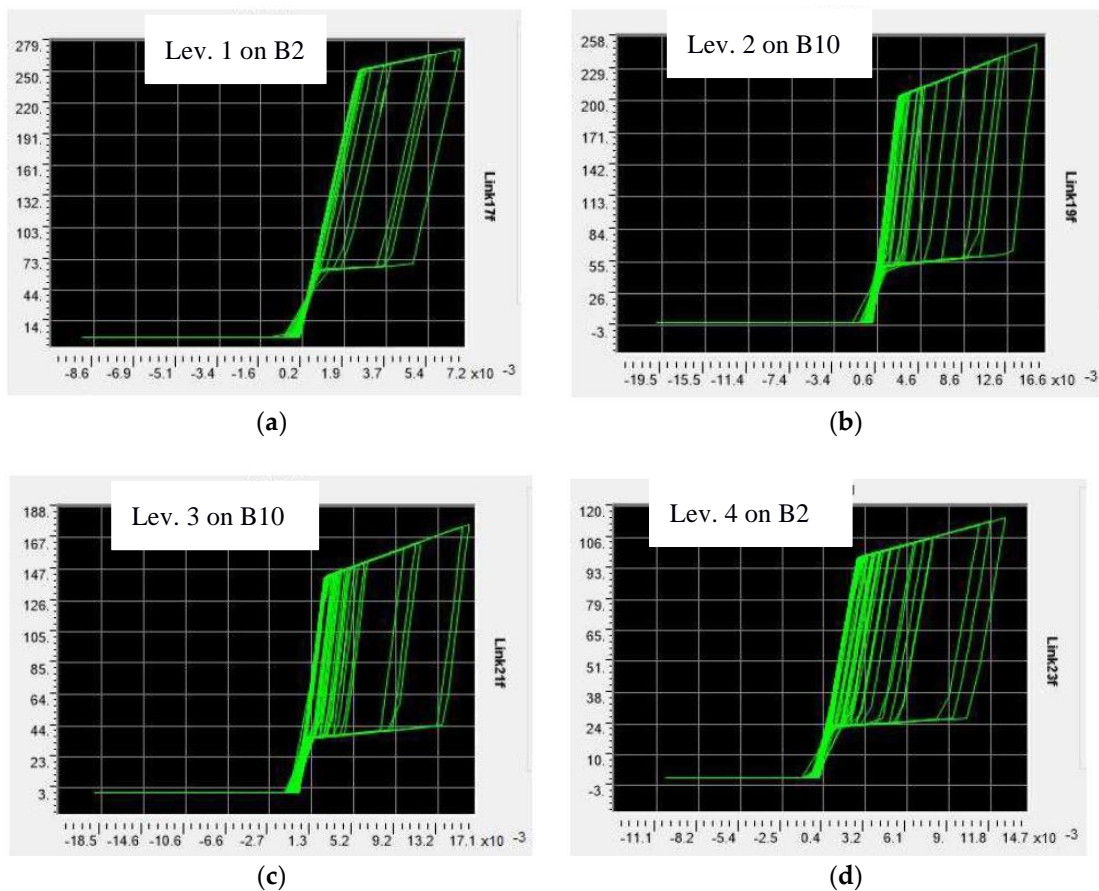

(a)

(b)

(c)

(d)

Fig. 101. Cyclic response of different SMA braces under an accelerogram of the Basic Design Earthquake (BDE): (**a**) 1st level; (**b**) 2nd level; (**c**) 3rd level; (**d**) 4th level.

From the diagrams in Fig. 101 it is possible to observed that, as defined in the model, SMA braces work in tension only. Moreover the cycles are large enough to dissipate a satisfactory amount of energy.

Subsequently, verifications of the structural members are performed. In the as-built configuration, secondary beams and some of the columns at the base do not satisfy ductile verifications. As made in the BRADs retrofit, the verifications of only these members of the retrofitted building with SMA braces are shown in Fig. 102.
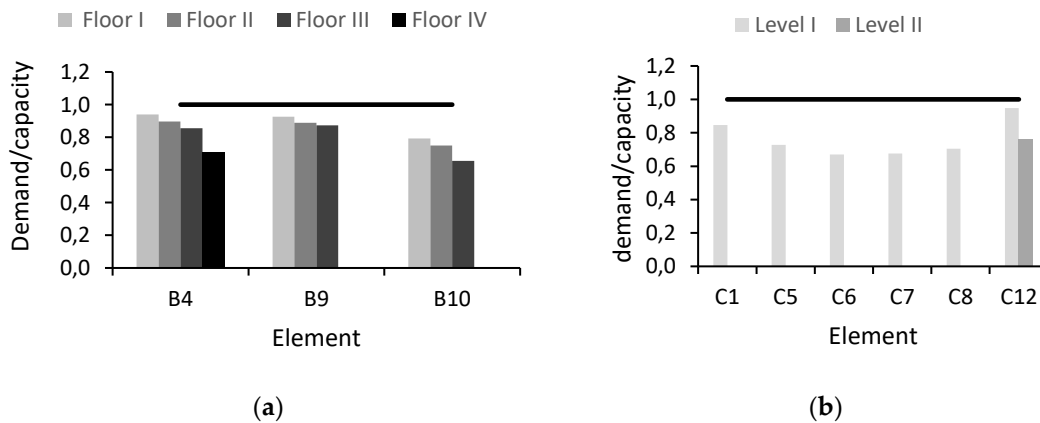
Fig. 102. Ductile verifications after SMA braces retrofit of: (**a**) beams and (**b**) columns.

The same nomenclature of the elements has been maintained, so the names of the members are reported in the horizontal axis, where beams are indicated with letter B and columns with C. From Fig. 102 it can be observed that, thanks to the retrofit intervention, the ratio demand/capacity is always lower than 1. In this case the reduction of acting moment is lower. For example, column C1, which does not satisfy the ductile verification in the as-built condition, after the BRAD retrofit intervention shows a reduction in the acting bending moment of about 66% (from 322.2 kN·m to 108.6 kN·m), while with the use of SMA braces the reduction of bending moment is about 44% (from 322.2 kN·m to 179.5 kN·m)

The results of brittle verifications only, for members not verified in the as-built configuration, are shown in Fig. 103.
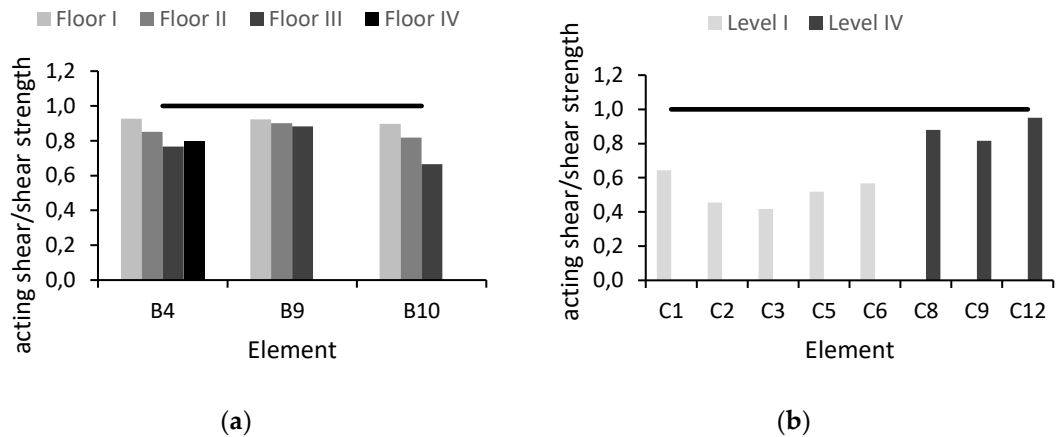
(**a**)   (**b**)

Fig. 103. Shear verifications after SMA braces retrofit of: (**a**) beams and (**b**) columns.

From Fig. 103 it can be observed that the demand/capacity ratio is slightly higher than the one obtained using BRADs. For example, beam B10, which did not satisfy the shear verification in the as-built condition, after the BRADs retrofit intervention shows a reduction in the acting shear of about 57% (from 23.4 kN to 10.1 kN), while with the use of SMA braces a reduction of about 42% (from 23.4 kN to 13.5 kN)

It can be concluded that the use of SMA braces has beneficial effects on the whole structure. As expected, the columns interacting with bracing undergo an increase in axial stress, which, on the ground floor, is about of 40%. For example, for column C12 at the first level, the axial force passes from 620 kN to 979 kN, from the as-built configuration to the one with SMA braces.

As described, one of the fundamental properties of shape memory alloys, which has increased the attention for its use in the world of civil engineering, is the almost elastic recovery of high deformations. This behaviour is also observed in this case study. As shown in Fig. 104, considering as control joints those at the intersection of column C12 with the three floors, a residual displacement equal to 0.4 mm at the 1st level (A), 0.7 mm at the 2nd level (B) and 1.1 mm at the 3rd level (C) is observed. Considering the same three control joints, in the case that BRADs are used, a

residual displacement equal to 0.5 mm at the 1st level (A), 1.2 mm at the 2nd level (B) and 3.1 mm at the 3rd level (C) is observed. The results show that there is a more considerable reduction in residual displacements in the higher floors.
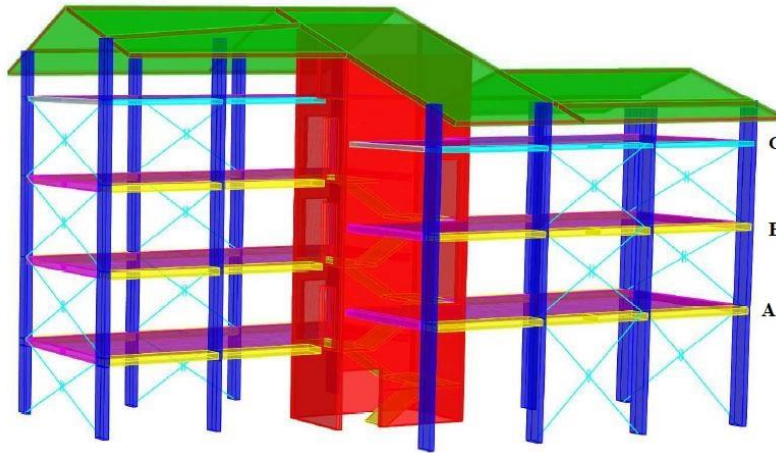

Fig. 104. Identification of the target joint for displacement in SAP2000 model.

4.3   Beam-column joint model

SMAs are material of great interest for use in structural applications, as shown above. In addition to the use of SMAs as dissipative braces, seen in the previous case study, these materials can also be used as reinforcement bars of concrete strctures, both in new and existing buildings.

The prescriptions of the Italian code [4] for new buildings are aimed at guaranteeing safety conditions and preventing the collapse of the buildings during seismic events. Following the performance-based design and the rule of strong column-weak beam, the formation of plastic hinges at the ends of the beams is desired, to dissipate the incoming seismic energy. In conventional RC structure this results in the yielding of the reinforcing bars and their plastic deformation, with consequent severe damage to the structures and high costs for their restoration. If plastic deformations are large and damage is serious and spread the building has even to be demolished. To reduce the restoration or reconstruction on costs and all the correlated problems, a new idea of using smart materials, with good deformation

capacity and able to reduce permanent deformation, such as self-centering materials, has received increasing interest.

These smart materials could be used also to improve seismic behaviour of existing buildings and reduce their restoration costs after an earthquake.

The use of SMAs in superelastic phase instead of steel as reinforcing bars allows both to dissipate a certain amount of input seismic energy, but especially to restore the RC element original shape after the seismic event, which is the most important feature. In this way SMA bars could undergo large strains and potentially recover the deformation when earthquake ends, reducing or, in the best cases, removing the problem of permanent deformation after an earthquake.

However, due to the high cost not all the reinforcement of a RC building can be made with SMA rebars. A possible solution, that could find application both in new and existing buildings, is the use of short pieces of SMA reinforcement. In new buildings SMA reinforcement replace the steel reinforcement in the building portions where the formation of the plastic hinges is expected, as was done in the beam-column joint that will be analysed below in this chapter [78]. For retrofitting of existing buildings, SMA bars could be installed externally to the RC beam-column joint in the regions where plastic hinges are expected, using external steel angles, as proposed in [79]. In this case, in the region where the SMA bars have to be positioned externally, inside the beam it is necessary to cut the existing steel bars, so that these bars non longer work and are completely replaced by the SMA bars.

In both cases, the goals of using SMAs in the plastic hinge region are the almost total recovery of the deformations following the earthquake and the dissipation of energy. In fact, the plasticization of steel bars due to the seismic event results in permanent deformations at the end of the event. In this case, there may be the need to demolish and re-build the structure, with consequent high cost. The use of SMA bars,

instead, thanks to their re-centering capacity, avoids great permanent deformations after the earthquake, so the structure does not need to be demolished, but it is only necessary to restore the damaged concrete in the plastic hinge regions.

In order to verify this solution and its applicability, two models that describe the behaviour of two beam-column joints, one reinforced with regular steel bars and the other reinforced with SMA at the plastic hinge region, is created using the Opensees software. The first step of the study in the model validation through the comparison between the analytical and experimental results. The joints used for this validation are those tested by Youssef et al. [78]. In a second phase, in order to compare the results that are obtained by the use of SMAs bars versus steel bars in a beam-column joint of an existing building, the implementation in this model of the two main failure mechanisms for existing beam-column joints are envisaged: failure by shear and loss of adhesion with consequent sliding of longitudinal bar.

The next paragraphs describe the experimental tests used for the validation, the details of how the model is created and the validation of the obtained results. An initial study to evaluate the effectiveness of the proposed technique is presented. Future development of this study may be the extension of this technique to all the beam-column joints of the entire building.

4.3.1 Test specimens and experimental program

Two beam-column joints (BCJ) were constructed in according to Canadian seismic standard (CSA A23.3-04) and tested at the Structures Laboratory of the University of Western Ontario by Youssef et al. [78]. One is reinforced with regular steel rebars (specimen BCJ-1), while the other is reinforced with SMA bars at the plastic hinge region of the beam along with regular steel in the remaining portion of the joint (specimen BCJ-2).

Design of the two BCJ is given in Fig. 105. Columns of the two BCJ specimens are equal as geometry and longitudinal and transverse reinforcement arrangements. Column's section is 250 mm by 400 mm with four longitudinal bars, one for each corner, that have 19.5 mm diameter. Transvers reinforcement consists in closed rectangular ties, with 11.3 diameter, spaced 80 mm in the joint region and 115 mm in remaining parts. The joint region is considered ± 640 mm from the face of the joint.

Also beams of the two BCJ are quite similar. Cross-section is 250 mm by 400 mm. There is a difference in the plastic region, calculated as 360 mm from the face of the column, between the two specimens: top and bottom longitudinal reinforcement for BCJ-1 are two steel rebars (19.5 diameter), while for BCJ-2 are 2-SE SMA20 (20.6 mm diameter) bars. As shown in Fig. 106, the total length of SMA rebars is 450 mm, while mechanical couplers are used to connect SMA rebars with steel ones.
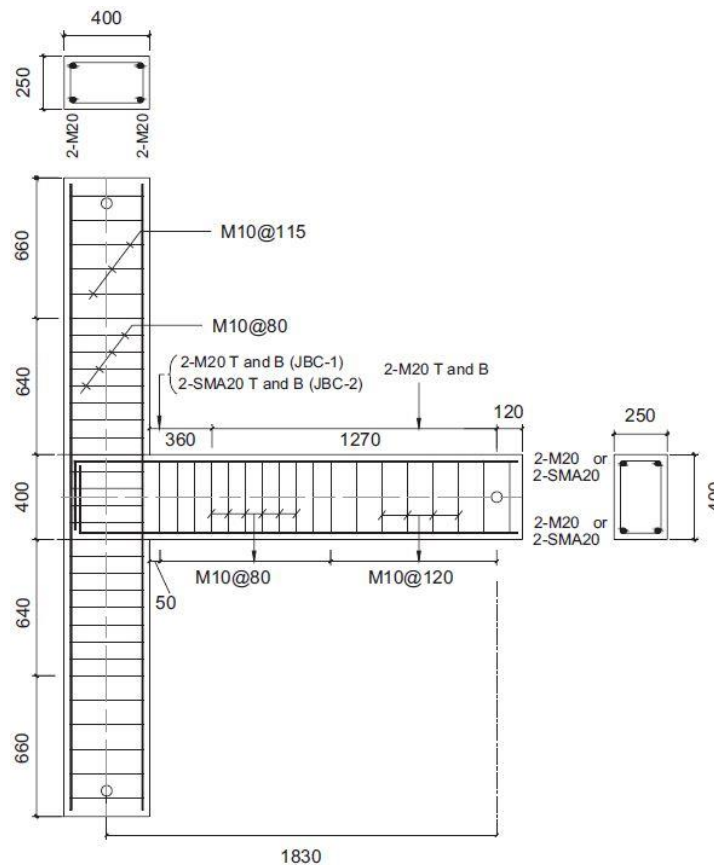

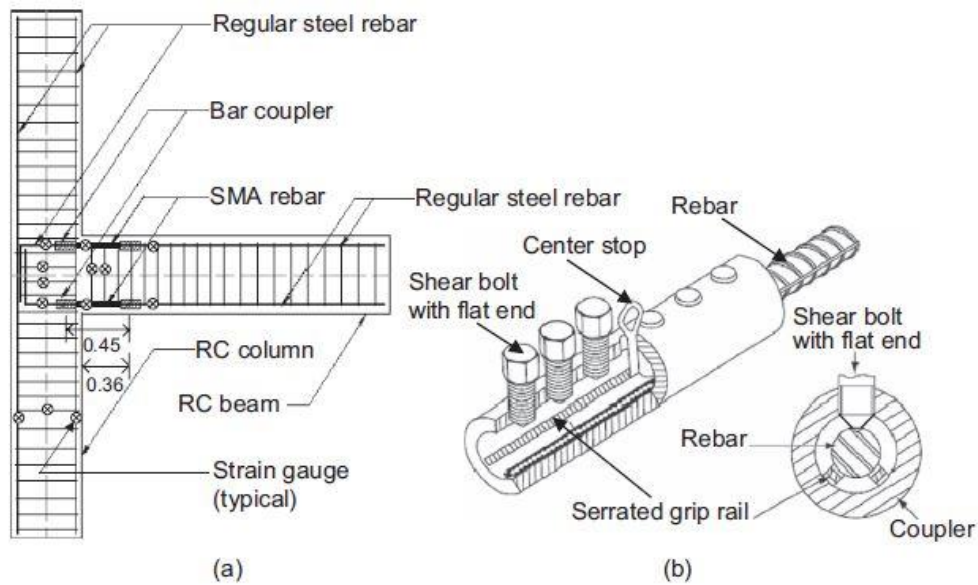**Fig. 105.** Details of BCJ-1 and BCJ-2, dimension in mm [78].

Fig. 106. (a) Details of BCJ-2 configuration and SMAs position (b) coupler [78]

As shown in Fig. 105, ties of the beam are spaced 80 mm for 800 mm length adjacent to the column and then 120 mm.

The differences between the two BCJ are in the materials mechanical characteristics. From laboratory tests, concrete compressive strength is 53.5 MPa for BCJ-1 and 53.7 MPa for BCJ-2. Longitudinal steel bar's yield strength, ultimate strength, and Young's modulus are 520 MPa, 630 MPa and 198 GPa for BCJ-1 and 450 MPa, 650MPa and 193 GPa for BCJ-2. Steel ties' yield strength and ultimate strength are 422 and 682 MPa respectively for both specimens in the parts with steel reinforcement.

Hot-rolled Ni-Ti alloy rebar, with a composition of 55% nickel and 45% titanium by weight, has been used as reinforcement in BCJ-2 specimen. The austenite finish temperature, A_f, at which all the martensite is transformed to austenite, ranges from -15°C to -10°C, and for higher temperature, the alloy is in the superelastic phase.

A constant axial load, equal to 350kN, at the top of the column and reversed quasi-static cyclic load at the beam tip are applied during both specimens' tests. Four

load control cycles are applied to define the loads causing flexural cracking in the beam and yielding of its longitudinal bars, recording the yield load, P_y and the yield displacement, Δ_y. After yielding, displacement-controlled loading is applied in the form of incremental multiplies of Δ_y up to a drift of 7.9%.

4.3.2 Models in OpenSees and validation of the results

A model using Opensees software is developed to represent the behaviour of the two BCJ tested by Youssef et al. [78].

OpenSees (Open System for Earthquake Engineering Simulation) [80] is an open source software framework. It is developed to simulate the performance of structural and geotechnical system subjected to earthquake. This software has no graphic interface for entering data, but input data have to written in an extended form of the Tcl programming language. There is no graphic interface also for output data, that have to be shown through the use of other programs as Matlab. In the last years some programs or interfaces, as OpenSees Navigator, have been developed to facilitate the use of OpenSees to users, but in the present work they have not been used.

In the following part, the code developed to model the behaviour of the beam column joint reinforced with regular steel rebars, the BCJ-1 in [78], is described. This is a two dimension model, with three degree of freedom per node.

In Fig. 107 is possible to see the graphical representation of the beam-column joint defined through the programming language code. First, using the code show in Fig. 108, the geometric configuration of the BCJ-1 is set, identifying the position of ten nodes in the space and defining the boundary condition at node 1, where a hinge constraint is define, and node 10, where a roller constraint is define.
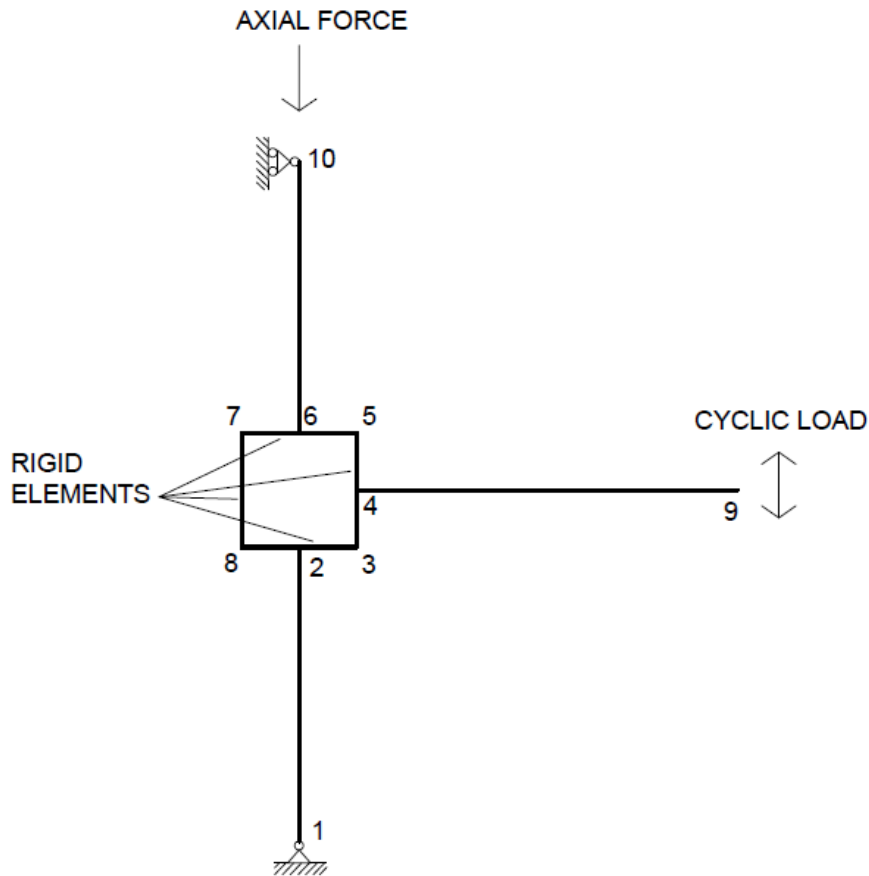
Fig. 107. Schematization of the beam-column joint BCJ-1 made in OpenSees.

Column and beam section geometry, as depth and width of the two elements are defined, as shown in Fig. 108. From these data, the code for the automatic calculation of the area and moment of inertia is then set. The thickness of the concrete cover, equal to 50 mm both for column and beam, the number of reinforcing bars and their area, the latter equal to 300 mm², are set for column and beam.

After having defined the geometry of the model, the materials are described. In order to describe the behaviour of the BCJ more accurately, it is decided to consider separately the behaviour of unconfined and confined concrete.

The mechanical characteristics of concrete are defined using the material *Concrete02*, characterized by the constitutive law shown in Fig. 109, which takes into account the tensile strength and the linear softening both in tension and compression, and, therefore, the degradation of the material. The meaning of the

parameters necessary to define the behaviour of material Concrete02 is illustrated in Fig. 110.

```
# Define GEOMETRY ------------------------------------------

# Nodal coordinates:
node 1    0        0;                    # node#, X Y
node 2    0        1300;
node 3    200      1300;
node 4    200      1500;
node 5    200      1700;
node 6    0        1700;
node 7    -200     1700;
node 8    -200     1300;
node 9    1950     1500;
node 10   0        3000;

set IDctrlNode 9;
set IDctrlDOF 2;
# Single point constraints -- Boundary Conditions
fix 1    1 1 0;              # node DX DY RZ # pinned constraint
fix 10   1 0 0;             # roller constraint

#Define column section geometry
set Hcol 400; #column depth
set Bcol 250; #column width
```

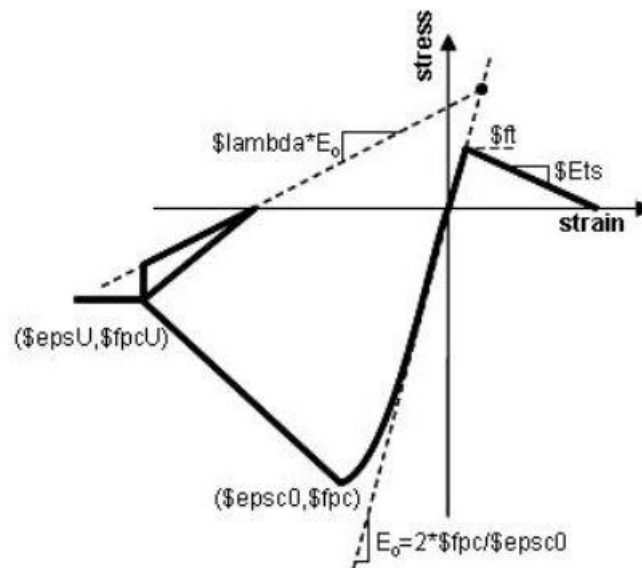**Fig. 108.** Part of the code that define node position and boundary condition.

Fig. 109. Constitutive law of the material Concrete02 [80].

uniaxialMaterial Concrete02 $matTag $fpc $epsc0 $fpcu $epsU $lambda $ft $Ets	
$matTag	integer tag identifying material
$fpc	concrete compressive strength at 28 days (compression is negative)*
$epsc0	concrete strain at maximum strength*
$fpcu	concrete crushing strength *
$epsU	concrete strain at crushing strength*
$lambda	ratio between unloading slope at $epscu and initial slope
$ft	tensile strength
$Ets	tension softening stiffness (absolute value) (slope of the linear tension softening branch)

Fig. 110. Definition of the parameter used [80].

Fig. 111 shows the mechanical characteristics for unconfined and confined concrete defined in the model. The instruction *UniaxialMaterial* represents uniaxial stress-strain relationship. In the instruction lines to define the materials, that for unconfined and confined concreate are the last two lines of Fig. 111, the first parameters, *$CoverConc* and *$CoreConc*, respectively, are necessary to recall the material in the code and assign it to the different sections of the elements.

Tension is defined with a positive number value, while compression with negative number. Concrete tensile strength is set equal to 3.5 MPa, from laboratory test. For unconfined concrete the compressive strength is equal to 53.5 MPa. Strain that corresponds to the maximum stress equal to 0.002 and ultimate strain equal to 0.0035 are set.

```
#Unconfined Concrete:
set fc -53.5; #compressive strenght of plain concrete [MPa] (+Tension, -Compression)
set epps -0.002; #strain that corrispond to fc' (max stress)
set epss -0.0035; #ultimate strain for unconfined concrete

#Confined Concrete:
#nominal concrete compressive strenght
set fc1 -72.2;                 # maximum stress
set eps1   -0.0055;            # strain at maximum strength of unconfined concrete
set fc2         [expr 0.2*$fc1]; # ultimate stress
set eps2   -0.028;            # strain at ultimate stress
set lambda 0.1;                # ratio between unloading slope at $eps2 and initial slope $

#tensile-strength properties
set ft 3.5; # tensil strenght [MPa]
set EtS [expr $ft/0.002]; #tension softening stiffness

uniaxialMaterial Concrete02 $CoreConc $fc1 $eps1 $fc2 $eps2 $lambda $ft $EtS;  # (CONFINED)
uniaxialMaterial Concrete02 $CoverConc $fc $epps 0.0 $epss $lambda $ft $EtS;   # (UNCONFINED)
```

Fig. 111. Mechanical characteristics of unconfined and confined concrete.

To define the mechanical characteristics of confined concrete, the calculated effective section area ratios of transverse reinforcement to core concrete in the two direction, ρ_x and ρ_y, result equal to 0.01 and 0.006, respectively. Using equations (35) and (36), the ratio between the effective confining stress that can be developed at yield of the transverse reinforcement (f_l') and the concrete compressive strength (f_c), are calculated in both directions:

$$f_{lx}' = K_e \cdot \rho_x \cdot \frac{f_y}{f_c} = 0.75 \cdot 0.01 \cdot \frac{520}{53.5} = 0.073 \tag{35}$$

$$f_{ly}' = K_e \cdot \rho_y \cdot \frac{f_y}{f_c} = 0.75 \cdot 0.006 \cdot \frac{520}{53.5} = 0.044 \tag{36}$$

where K_e is a confinement effectiveness coefficient that is equal to 0.75 for rectangular section. With this two value, entering in the graph of Fig. 112, a ratio between the compression strength of confined (f_{c1}) and unconfined (f_c) concrete equal to 1.35 is obtained.

The value of f_{c1} is thus calculated:

$$f_{c1} = f_c \cdot 1.35 = 72.2 \; MPa \tag{37}$$
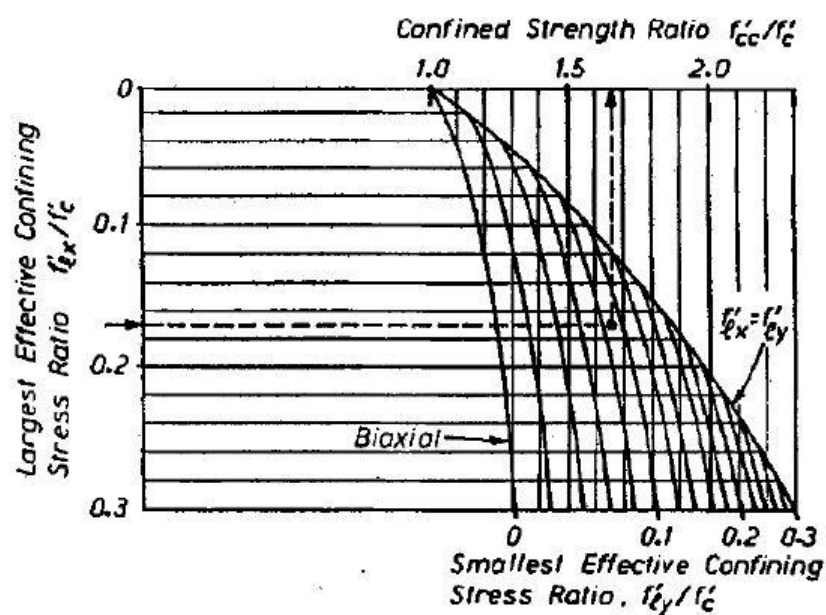

Fig. 112. Compression strength determination of confined concrete.

Strain at the maximum strength is obtained using equation (38):

$$\varepsilon_1 = 0.002[1 + 5 \cdot (f_{c1}/f_c - 1)] = 0.0055 \tag{38}$$

while the ultimate compression strain (ε_2) is obtained using equation (39) :

$$\varepsilon_2 = 0.004 + 1.4 \cdot \rho_s \cdot f_y \cdot \varepsilon_{sm}/f_{c1} = 0.028 \tag{39}$$

The behaviour of steel is define using the instruction material *Steel02*, which implements the constitutive law of Giuffre-Menegotto-Pinto, visible in Fig. 113, taking into account the isotropic strain hardening.
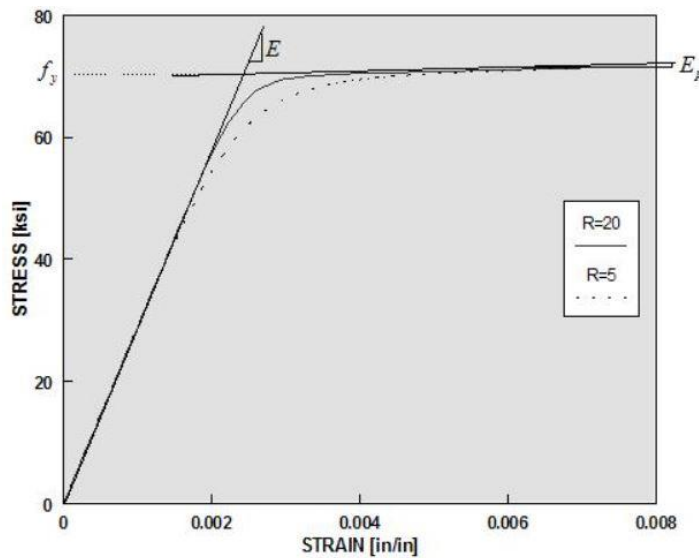
Fig. 113. Giuffre-Menegotto-Pinto model [80].

The meaning of the parameters necessary to define the behaviour of material *Steel02* is illustrated in Fig. 114.

Yield stress and elastic modulus are defined using the values obtained by the laboratory test on steel bars, longitudinal bars diameter is equal to 20 mm, and the three parameters R0, cR1 and cR2, that control the transition from elastic to plastic branches, are set equal to 15, 0.925 and 0.5 respectively. The parameters between the symbols < and > are not defined as they are not compulsorily necessary for the definition of the steel material.

uniaxialMaterial Steel02 $matTag $Fy $E $b $R0 $cR1 $cR2 <$a1 $a2 $a3 $a4 $sigInit>	
$matTag	integer tag identifying material
$Fy	yield strength
$E0	initial elastic tangent
$b	strain-hardening ratio (ratio between post-yield tangent and initial elastic tangent)
$R0 $CR1 $CR2	parameters to control the transition from elastic to plastic branches.
	Recommended values: **$R0**=between 10 and 20, **$cR1**=0.925, **$cR2**=0.15
$a1	isotropic hardening parameter, increase of compression yield envelope as proportion of yield strength after a plastic strain of $a2*($Fy/E0). (optional)
$a2	isotropic hardening parameter (see explanation under $a1). (optional default = 1.0).
$a3	isotropic hardening parameter, increase of tension yield envelope as proportion of yield strength after a plastic strain of $a4*($Fy/E0). (optional default = 0.0)
$a4	isotropic hardening parameter (see explanation under $a3). (optional default = 1.0)
$sigInit	Initial Stress Value (optional, default: 0.0) the strain is calculated from epsP=$sigInit/$E
	if (sigInit!= 0.0) { double epsInit = sigInit/E; eps = trialStrain+epsInit; } else eps = trialStrain;

Fig. 114. Definition of Steel02 parameters [80].

Using the code of *section fiberSec*, the sections of the column and the beam are then defined, as shown in Fig. 115. In the second line of Fig. 115, thorough the *patch quadr* command, the position of the four vertex of the rectangular shaped concrete core is defined. The material with the previously defined characteristics (*UniaxialMaterial Concrete02*) is assigned to the section through the first parameter CoreConc. In the same way it is defined the cover. To indicate the position of the reinforcement within the section, the *layer straight* command is used, through which the material, number and diameter of the reinforcing bars are recalled with the first three parameters of the sting code (*$SteelTag, $numBarsCol and $barAreacol*) while with the remaining parameters it is defined the position. Two line of the command *layer straight* are present, one to define the top layer reinforcement and the second to the bottom layer reinforcement.

```
section fiberSec $ColSetTag {   # Define the fiber section of the column
patch quadr $CoreConc $ncolfZ $ncolfY -$corecolY $corecolZ -$corecolY -$corecolZ $corecolY -$corecolZ $corecolY $corecolZ;
patch quadr $CoverConc $ncolfZ $ncolfY -$extcovercolY $extcovercolZ -$extcovercolY -$extcovercolZ $extcovercolY -$extcover
layer straight $SteelTag $numBarsCol $barAreaCol   $corecolY $corecolZ   $corecolY -$corecolZ; # top layer reinfocement
layer straight $SteelTag $numBarsCol $barAreaCol  -$corecolY $corecolZ  -$corecolY -$corecolZ;  # bottom layer reinforceme
```

Fig. 115. Definition of column's section.

In Fig. 116 the code lines used to define the beam, the two elements representing the column and the element representing the joint panel are presented. Referring to Fig. 107, column is divided in two elements, one from node 1 to 2, and the second

173

one from node 6 to 10, and to both elements the *ColSetTag* that recall geometry and material characteristics is assigned. For the beam only an element is used from node 4 to 9.

It is decided to represent the joint panel through a square polygon made up with seven rigid elements. To increase the stiffness of these elements it is decide to assign them an area equal to twice that of the beam. The square arrangement to the joint panel is due to the possibility to use extensional or rotational springs to describe the joint resisting mechanisms.

```
element nonlinearBeamColumn 1 1 2 5 $ColSetTag 1;          #element nonlinea
element nonlinearBeamColumn 2 6 10 5 $ColSetTag 1;
element nonlinearBeamColumn 3 4 9 5 $BeamSetTag 2;          #element nonlinea
element elasticBeamColumn 4 6 5  [expr 2*$Abeam] 35000 [expr $Izbeam*1] 1;
element elasticBeamColumn 5 6 7  [expr 2*$Abeam] 35000 [expr $Izbeam*1] 1;
element elasticBeamColumn 6 2 3  [expr 2*$Abeam] 35000 [expr $Izbeam*1] 1;
element elasticBeamColumn 7 2 8  [expr 2*$Abeam] 35000 [expr $Izbeam*1] 1;
element elasticBeamColumn 8 7 8  [expr 2*$Abeam] 35000 [expr $Izbeam*1] 1;
element elasticBeamColumn 9 3 4  [expr 2*$Abeam] 35000 [expr $Izbeam*1] 1;
element elasticBeamColumn 10 4 5 [expr 2*$Abeam] 35000 [expr $Izbeam*1] 1;
```

Fig. 116. Node connections.

The last step to complete the beam-column joint model is to assign the axial load, equal to 350kN, to the column, and to define the displacement-cycles peaks applied to the beam equal to (0.013; -0.013; 0.026; -0.026; 0.039; -0.039; 0.052; -0.052; 0.065; -0.065; 0.078; -0.078).

Completed the model, the analysis under the applied loads is performed.

A MatLab code is created to show the results of the analysis, and the comparison between the experimental results, in blue, and analytical results, in red, are presented in Fig. 117. From this figure it is possible to observed that the analytical model perfectly predicts the beam-tip load measured during the experiment, both for positive and negative storey drift. By comparing the initial stiffness, the red lines have a greater slope than the blue ones. The discharge branches have also a greater inclination than those obtained during experimental results. In general it is observed

that the experimental curves are narrower than the analytical ones. This difference is probably due to the presence of clearances in the experimental set up, proved by the presence of pseudo-horizontal segments in the diagram in Fig. 117. Moreover the difference between the experimental and FEM results may depend to the possible joint degradation related to shear behaviour and bond behaviour of the bars that have not been implemented in the model. Due to the observed differences the finite element model overestimates the dissipated energy.

However, as said, the analytical model gives good prediction of the peak force and is worth trying to improve it in the future including the effects of shear and bond degradation.
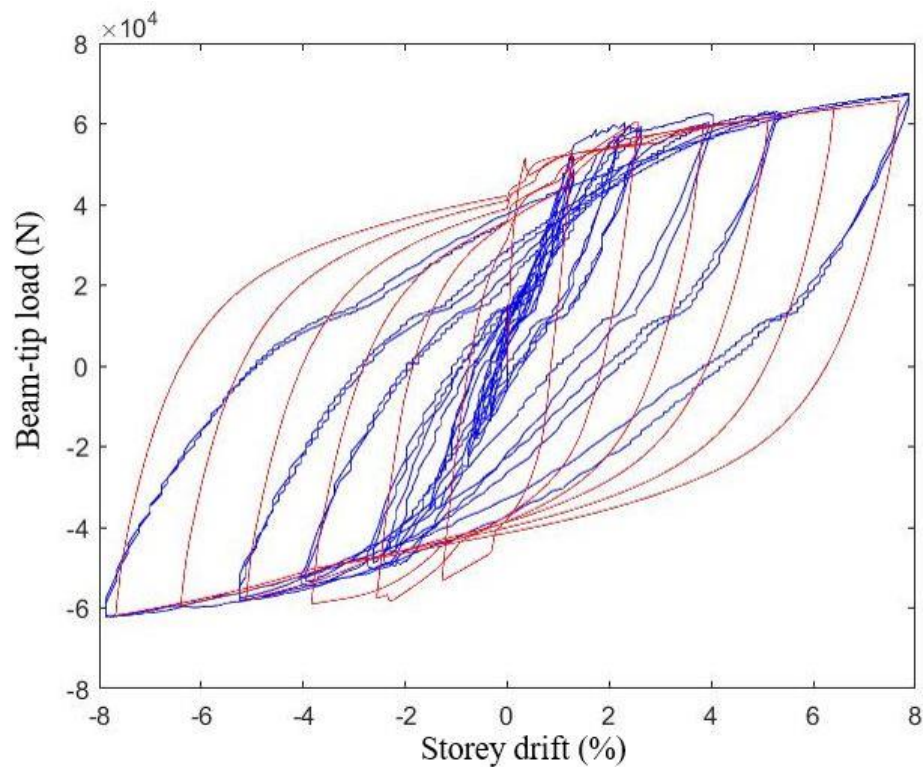

Fig. 117. Comparison between experimental (blue) and analytical (red) results for BCJ-1.

The model of the last one (BCJ-2) is developed similarly to the model of BCJ-1.

Boundary conditions are the same. Also the geometric configuration of the BCJ-2 is similar to the one of BCJ-1, but in this case, as shown in Fig. 118, a new node

between node 4 and node 9 is inserted. This new node, labelled as 11, it is necessary to define an element with the characteristics of the SMA between node 4 and node 11 itself.
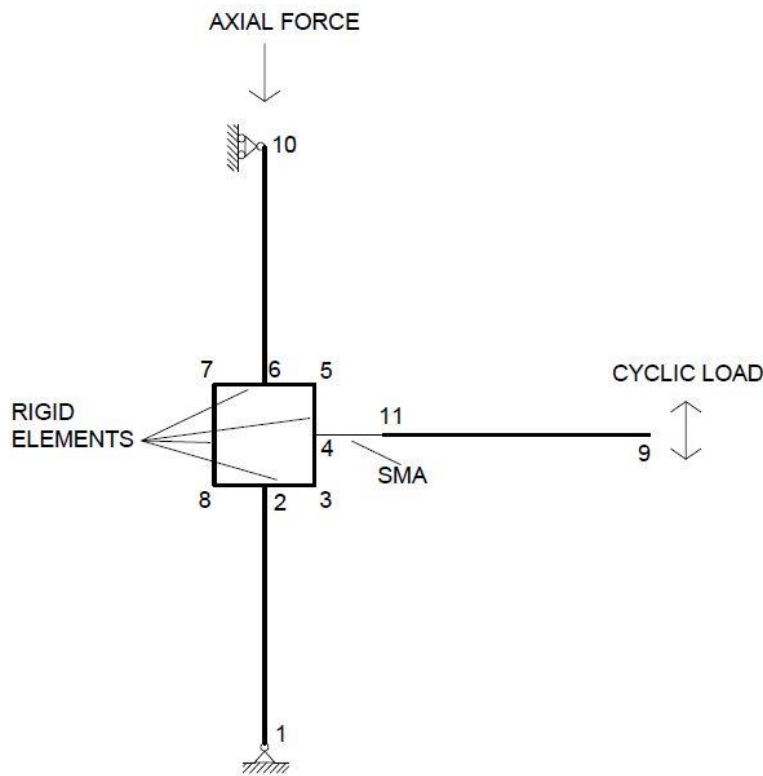
Fig. 118. Geometrical configuration of BCJ-2.

Section geometry of column and beam, defined through depth, width, area and moment of inertia, are the same of the previous model. Mechanical characteristic of unconfined and confined concrete, as the ones of steel, are set as shown for the first model, but considering the different concrete strength. To identify the mechanical characteristics of SMA, a new material is defined. To represent the behaviour of Shape Memory Alloy and its capacity to undergo great deformation and then go back to the initial shape, it is chosen to use the material defined in OpenSees as *uniaxialMaterial SelfCentering*, which is considered to be the most suitable to represent this mechanism thanks to its backbone hysteresis curve, show in Fig. 119.
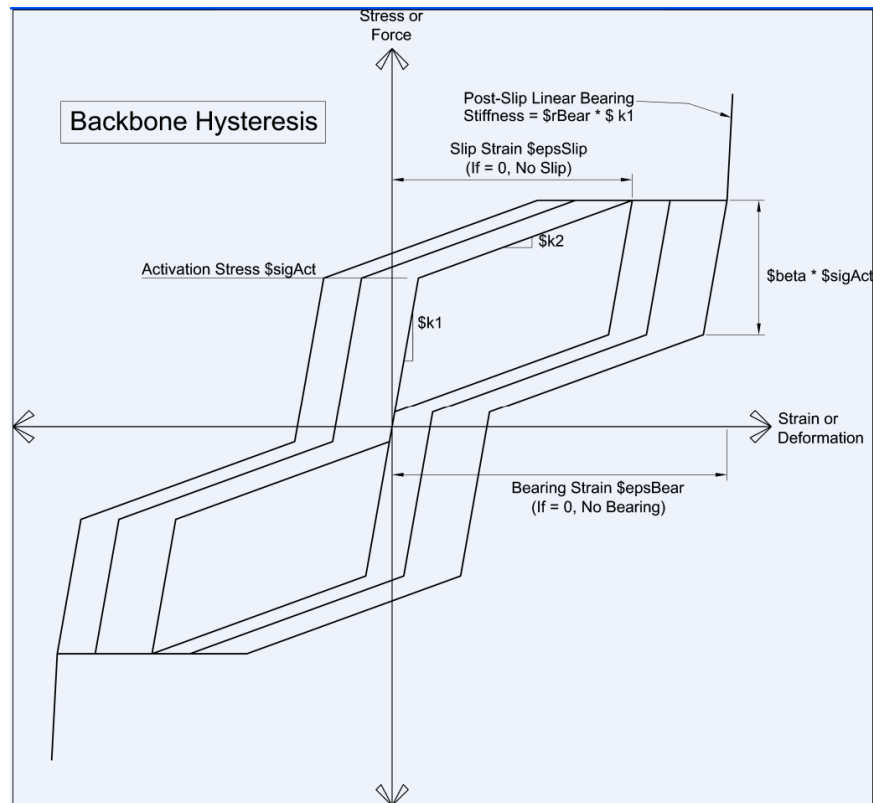
Fig. 119. Self centering material behaviour [80].

For the analysis it is necessary to define the initial stiffness, k_1, the post yield stiffness, k_2, the austenite yield stress, *sigAct*, and the ratio of forward to reverse activation force, β. From the results of the laboratory test on the SMA the following values are determined for the significative parameters: k_1 equal to 62500 MPa, k_2 equal to 2812 MPa, *sigAct* equal to 401 MPa and β equal to 0.65, as shown in Fig. 120.

```
set k1 62500;
set k2 2812;
set sigAct 401;
set beta 0.65;

uniaxialMaterial SelfCentering $SMA $k1 $k2 $sigAct $beta;
```

Fig. 120. Self centering material definition.

Defined the SMA material, as made for BCJ-1, the configuration of the columns and the beam sections is made. For BCJ-2, beam's section has two different configuration: one where the position of the steel bars is defined in the same way of

specimen BCJ-1, and one in which, in addition to the position of the bars, the previously defined SMA material has been assigned, as it is possible to observe in Fig. 121.

```
layer straight $SMA $numBarsCol $barSMAAreaBeam  -$coreY $coreZ  $coreY  $coreZ;
layer straight $SMA $numBarsCol $barSMAAreaBeam  -$coreY -$coreZ $coreY -$coreZ;
```

Fig. 121. Definition of the SMA material for the bars.

As can be seen in Fig. 118, since it has been inserted the new node 11, a new element, from node 4 to node 11 has been defined, to report the SMA reinforcement within the model and then consider their behaviour in the global analysis of BCJ-2. For this reason, in the case of the BCJ-2 specimen, the beam is divided into two elements (Fig. 118): the first portion in SMA material, which goes from node 4 to 11, is defined with the third line of the code in Fig. 122. The second portion, with steel reinforcement, which goes from node 11 to node 9, is defined in the last line.

The column elements and the elements of the joint panel are the same of specimen BCJ-1.

Axial load on the column and cyclic displacement on the beam remain the same.

```
element nonlinearBeamColumn 1 1 2 5 $ColSetTag 1;          #element nonlinea
element nonlinearBeamColumn 2 6 10 5 $ColSetTag 1;
element nonlinearBeamColumn 3 4 11 5 $BeamSMATag 2;        #element nonline
element elasticBeamColumn 4 6 5  [expr 2*$Abeam] 35000 [expr $Izbeam*1] 1;
element elasticBeamColumn 5 6 7  [expr 2*$Abeam] 35000 [expr $Izbeam*1] 1;
element elasticBeamColumn 6 2 3  [expr 2*$Abeam] 35000 [expr $Izbeam*1] 1;
element elasticBeamColumn 7 2 8  [expr 2*$Abeam] 35000 [expr $Izbeam*1] 1;
element elasticBeamColumn 8 7 8  [expr 2*$Abeam] 35000 [expr $Izbeam*1] 1;
element elasticBeamColumn 9 3 4  [expr 2*$Abeam] 35000 [expr $Izbeam*1] 1;
element elasticBeamColumn 10 4 5 [expr 2*$Abeam] 35000 [expr $Izbeam*1] 1;
element nonlinearBeamColumn 11 11 9 5 $BeamSetTag 2;
```

Fig. 122. Definition of elements for BCJ-2.

Also in this case, a MatLab code is created to show the results of the analysis, and the comparison between the experimental results, in blue, and analytical results, in red, for BCJ-2 are presented in Fig. 123. In this case, it is possible to see that, for the negative drifts, the analytical model perfectly predicts the beam-tip load

measured during the experiment, while, for positive storey drifts, the force of the model are a little bit lower than the experimental ones. The analytical red curve predicts the initial stiffness very well for negative drift, while it has a greater slope than the experimental curve for positive drift. This is due to the fact that, even the beam section is symmetrical, the laboratory test results are not perfectly symmetrical. In fact, it can be noted that the slope of the starting branch for negative drift is greater than that obtained for positive drift. Unfortunately the reason of this asymmetric behaviour is not explained in the considered paper [78].

Comparing the shape of the curves in Fig. 123, it is observed that the analytical red curves have a perfect flag shape, typical of shape memory alloys, while the experimental blue curves have a flatter shape. Furthermore, while in the red curves a complete recovery of the deformation is observed, in the blue ones at the end of the cycles small residual deformation are present. These differences may be due to having neglected shear and bond degradation in the f.e. model.
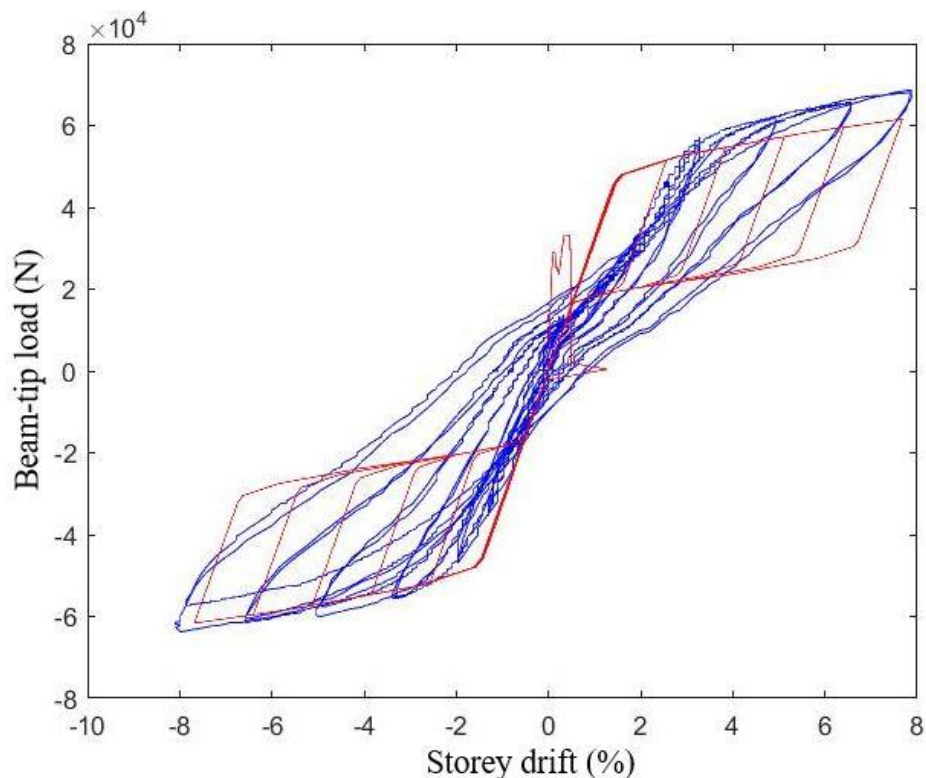

Fig. 123. Comparison between experimental (blue) and analytical (red) results for BCJ-2.

Also this comparison confirms that it would be worth to introduce these types of degradation in the FE model.

In Fig. 124 the comparison between the experimental results obtained from the BCJ-1, in black, and the experimental results obtained from BCJ-2, in red, is presented.

The sum of the areas enclosed within each cycle represents the dissipated energy. By comparing the two curves it is possible to observed that the energy dissipation is greater for specimen BCJ-1, reinforced with regular steel rebars, compared to specimen BCJ-2, reinforced with SMA bars at the plastic hinge region. This difference is due to the fact that the hysteresis loops obtained for BCJ-1 are wider and the area enclosed within each cycle is greater than those obtained for BCJ-2. In fact, last specimen is characterized by cycles with the classic flag shape of SMAs materials, which are narrower and flattened. This is evident by the different shapes of the individual hysteric loops of the load-displacement curves.

Comparing the amount of energy dissipated by both specimens, it is found that the energy dissipated by BCJ-2 at a storey drift of 5.4% is equivalent to the one dissipated by BCJ-1 at 4% storey drift. For a storey drift of 8%, the energy dissipated by BCJ-1 is equal to 26.5 kN·m, while the one dissipated by BCJ-2 is equal to 16.7 kN·m. At the end of the test, the energy dissipated by the BCJ-1 is 59% greater than that dissipated by the BCJ-2.

Considering again Fig. 124, with reference to the last cycle performed by the specimens, it can be observed that the ductility is equal to 3.5 for BCJ-1, while it is equal to 2.1 for BCJ-2. This result is due to the fact that the displacement for which yielding occurs in BCJ-2 is greater than that for BCJ-1. However, the result is also linked to the fact that the tests were performed under displacement control. By imagining the specimens subjected to the same seismic accelerogram, it is possible

that specimen BCJ-2 would attain displacements greater than specimen BCJ-1, to dissipate the same energy amount.

Finally, analysing Fig. 124 and comparing the last two cycles of BCJ-1 with the last two cycles of BCJ-2, it can be observed the high ability of SMAs to recover deformation suffered. In fact, the residual displacements in the penultimate and last cycle of BCJ-1 are about three and five times greater than that of BCJ-2, respectively.
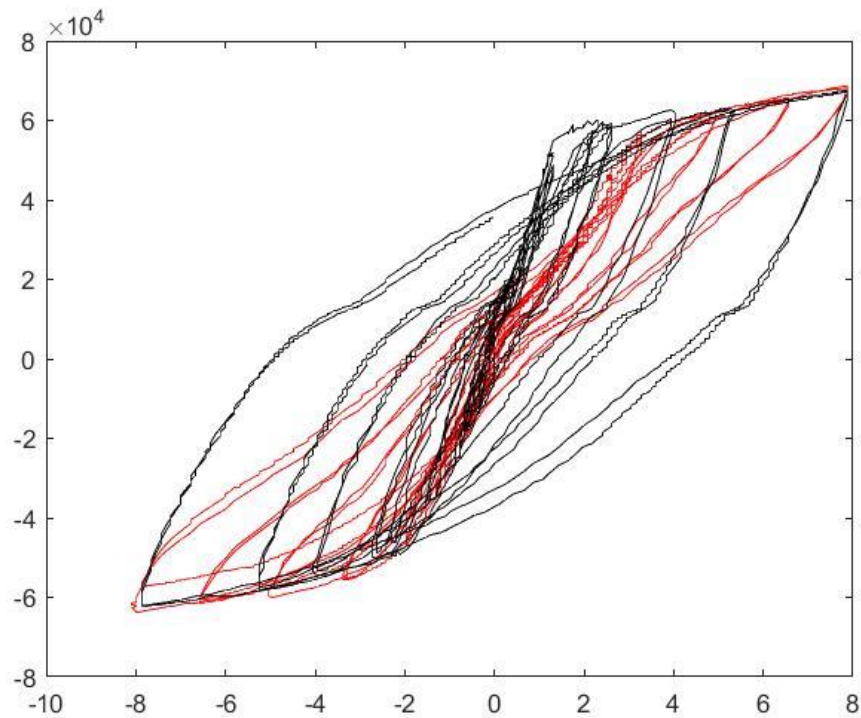

Fig. 124. Comparison between experimental results for BCJ-1 (black) and experimental results for BCJ-2 (red).

5 Conclusions

The benefits coming from the use of innovative seismic protection systems for existing buildings have been analysed in this thesis, through applications to two case studies.

The importance of seismic retrofit interventions is due to the fact that the Italian territory, characterised by a medium-high seismic risk, has a very large existing building heritage, in some cases also of considerable historical-artistic importance, but mostly designed only for vertical loads.

The techniques of survey and mechanical characterization of materials, that can be used to reach an adequate level of knowledge of the building, have been analysed. Investigation and test costs have been calculated to reach LC2 and LC3 levels of knowledge following different combinations.

It has been found that, when the building documentation is available, to reach the same level of knowledge, the use of destructive tests only or of both destructive and non-destructive tests does not involve large differences in price. In the case of lack of documentation, an increase in the price of about 50% is detected in comparison with the case in which the documentation is available. Moreover, a variable cost increase between 40% and 65% is assessed to move from LC2 to LC3.

The method of modelling structures through Building Information Modelling (BIM) also for existing building, called in this case Heritage BIM model (HBIM), have been considered. The most used techniques for the acquisition of the building geometry are laser scanning or photogrammetry. Regarding the subsequent introduction in the considered Heritage BIM model, two main problems have been observed: the first is that the process arrangement of the elements is not completely automatic yet. The second is that the point clouds only represent the external shape

of the building, while the internal properties have to be acquired from documentation and CAD drawings.

The characteristics of Shape Memory Alloys (SMAs) have been analysed. These materials are characterised by the capacity to undergo large deformations and go back to the initial shape when heated above their transformation temperature (shape memory effect) or through stress removal (superelasticity). The behaviour of the alloys is strictly linked to their chemical composition and to the weight percentages of the elements that constitute them. In particular, attention is focused on Ni-Ti, iron-based and copper-based SMAs. Ni-Ti SMAs are characterised by good mechanical characteristics and an elastic recovery of deformation up to about 8%, but also by a high cost. For this reason, copper-based and iron-based types of SMAs have been investigated.

It has been found that copper-based alloy is the most interesting for applications in the civil engineering field, having adequate mechanical characteristic, deformation recoveries and a price of about 1/5 respect to the price of Ni-Ti SMAs.

Retrofit interventions on two public housing buildings, building A and building B, both irregular in plan and elevation and designed for gravity loads only, have been proposed. FNA analyses have been performed on the FE models of the buildings both in the as-built and retrofitted configurations. The verifications, performed according to the Italian Building Code prescriptions for existing buildings, are not satisfied for many structural members of the buildings in the as-built configuration, which were designed without anti-seismic criteria. This is mainly due to insufficient transverse reinforcement of the members and column deformations caused by the additional displacements that arise from the buildings' torsional behaviour.

To increase the torsional stiffness of the building, the steel braces where the dissipative devices are mounted should be placed, if at all possible, in the perimeter frames.

Regarding building A, three analysis have been performed: one in the as-built configuration and two in the retrofitted configurations, one using BRADs and another using SMA braces.

In the case of SMA braces, two different models have been evaluated to describe the specific behaviour of SMAs in SAP2000. The first model uses two parallel link elements and the second one uses only one link element. Since both models gave good results, it was decided to use the model with one link element, that is easier to implement.

Application of copper-based SMAs in the superelastic phase as dissipative braces on building A have been performed.

From the comparison between the as-built configuration and the retrofit intervention with BRADs it has been observed that the designed dissipative system is able to absorb more than 50% of the input energy, thus reducing the forces acting on the existing building structural members. For example, it has been found a reduction of 64% in the acting shear of the columns. Another important aspect that has been observed is that the disposition of BRADs in plan increase the torsional stiffness of building A, which already had a good initial value of this parameter, by about 7%.

By comparing the two different retrofit interventions, the one with BRADs and the one with SMA braces, it has been found that BRADs are able to dissipate about 18% more input energy than SMAs braces. As a consequence, actions on the structural elements in the presence of SMAs braces are greater of about 15% than actions in the presence of BRADs. However also in the configuration with SMAs the verifications of all the building elements are satisfied.

Another important aspects that emerged from the comparison between the configuration with SMA braces and that with BRADs is related to the residual deformation of the two cases. It has been found that the use of SMA braces ensures an almost total recovery of the deformations, with residual displacements lower than those of BRADs.

Regarding building B, two analysis have been performed: in the as-built configuration and in the retrofitted configuration using Jarret viscous fluid dampers.

From the comparison between the as-built configuration and the retrofitted one, it has been found that the use of this type of device gives a good retrofit solution, since the obtained effects are the dissipation of a great amount of input energy and a reduction of the forces acting on the existing structural members. In particular, for building B it has been found that more that 80% of the input energy is absorbed by the Jarret dampers and there is a reduction of 65% in the acting shear of the columns. Moreover, the use of this dissipative system increases the building torsional stiffness by more than 200%, thus reducing the columns displacements, and consequently, their stresses.

Also the possible use of SMAs as reinforcing bars in RC building is investigated. The analyses of the experimental results available in the literature obtained from two test on beam-column joints, one reinforced with regular steel bars and the second one reinforced with SMA bars at the plastic region, have shown that the use of SMA reinforcing bars allows to obtain a ductile behaviour, even if the dissipated energy is lower. In particular, at the end of the test performed under displacement control it is observed that the energy dissipated by the beam-column joint reinforced with regular steel bars is 59% greater than that dissipated by the one with SMAs bars. On the contrary, the residual displacement of the last cycle for the

beam-column joint with SMAs is five times lower that the residual displacement of the one reinforced with regular steel.

Models of the two joints using Opensees software have also been realized.

Bibliography

[1] http://dati-censimentopopolazione.istat.it/Index.aspx?DataSetCode=DICA_EDIFICI1#

[2] Ministero dei Lavori Pubblici. Legge 2 Febbraio 1974, n.64. "Provvedimenti per le costruzioni con particolari prescrizioni per le zone sismiche". *Gazzetta Ufficiale*, 21th March 1974, n. 76. (In Italian).

[3] National Council of Engineers. Nota su rischio sismico in Italia: stima del numero di abitazioni interessate (e popolazione di riferimento) e costi per la loro messa in sicurezza; 2016

[4] Ministero delle Infrastrutture e dei trasporti. DM 17 gennaio 2018. Aggiornamento delle "Norme tecniche per le costruzioni". *Gazzetta Ufficiale*, 20th February 2018, n. 42. (In Italian)

[5] Ministero delle Infrastrutture e dei trasporti. 21 gennaio 2019, n. 7 C.S.LL.PP.— Istruzioni per l'applicazione dell'«Aggiornamento delle "Norme tecniche per le costruzioni"» di cui al decreto ministeriale 17 gennaio 2018. *Gazzetta Ufficiale*, 11 February 2019, n. 35. (In Italian)

[6] Maset E., slide del corso "Cartografia numerica e GIS", Università degli Studi di Udine, A.A. 2019/2020.

[7] Consiglio Superiore dei Lavori Pubblici, "Linee guida per la valutazione delle caratteristiche del calcestruzzo in opera", 2017.

[8] Vona M., Slide del corso "Riabilitazione strutturale", Università di Basilicata, A.A. 2018/2019.

[9] UNI EN 12504-4:2005. Prove sul calcestruzzo nelle strutture – Parte 4: Determinazione della velocità di propagazione degli impulsi ultrasonici. 1st January 2005 (in Italian).

[10] Dipartimento Protezione Civile, "Linee guida per modalità di indagine sulle strutture e sui terreni per i progetti di riparazione, miglioramento e ricostruzione di edifici inagibili".

[11] NDT 4 Recommendations for in situ concrete strength determination by combined non-destructuve methods. *Compendium of RILEM Technical Recommendations*, 1993 E&FN Spon, London.

[12] J. Gasparik, Prove non distruttive nell'edilizia. *Quaderno didattico AIPnD*, 1992, Brescia.

[13] Di Leo, Pascale G., Prove non distruttive sulle costruzioni in c.a. *Il giornale delle prove non distruttive n. 4*, 1994.

[14] Succar B. Building Information Modelling: conceptual constructs and performance improvement tools. PhD thesis, School of Architecture and Built

Environment Faculty of Engineering and Built Environment, University of Newcastle. December 2013.

[15] SCURT 2004. Collaboration, integrated information and the project lifecycle in the building design, construction and operation. Cincinnati, OH: The construction Users Roundtable.

[16] Murphy M., McGovern E, Pavia S. Historic building information modelling (HBIM). *Structural Survey*. 2009, 37, 311-327.

[17] Pepe M.. Domenica C., Alfio V.S. Scan to BIM for the digital management and representation in 3D GIS environment of cultural heritage site. *Journal of Cultural Heritage*. 2021, 1-10.

[18] Radanovic M., Khoshelham K., Fraser C. Geometric accuracy and semantic richness in heritage BIM: A review. *Digital Applications in archaeology and Cultural Heritage*. 2021, 1-10. 2019, 19, 1-12

[19] Regio Decreto – Legge 16 novembre 1939-XVIII n. 2229. *Gazzetta ufficiale*, 18th April 1940, n. 92 (in Italian).

[20] Verderame G.M., Ricci P., Esposito M., Sansiviero F.C. Le caratteristiche meccaniche degli acciai impiegati nelle strutture in c.a. realizzate dal 1950 al 1980. In Proceedings of the XXVI Convegno Nazionale AICAP. Padua, Italy, 19-21 May 2011. (in Italian).

[21] Samoilã D.M. Analytical Modelling of Masonry Infills. *Acta Tech. Napoc. Civil Eng. Arch.* 2012, *55*, 127–136.

[22] Moretti M.L. Seismic design of masonry and reinforced concrete infilled frames: A comprehensive overview. *Am. J. Eng. Appl. Sci.* 2015, *8*, 748–766.

[23] Syrmakesis C., Vratsanou, V. Influence of infill walls to RC frames response. In Proceedings of 8th European Conference on Earthquake Engineering, Istanbul, Turkey, 19-12 september 1986, pp 475–483.

[24] Schmidt T. An approach of modeling masonry infilled frames by the f.e. method and a modified equivalent strut method. Darmstadt Concrete. *Annu. J. Concr. Concr. Struct.* 1989, *4*, 171–180.

[25] Albayrak U., Ünlüoğl, E.; Doğab, M. An overview of the modelling of infill walls in framed structures. *Int. J. Struct. Civil Eng. Res.* 2017, *6*, 24–29.

[26] Tarque N., Candido L., Camata G., Spaccone E. Masonry infilled frame structures: State-of-art review of numerical modelling. *Earthq. Struct.* 2015, *8*, 225–251.

[27] Mainstone R.J. On the stiffness and strengths of infilled frames. *Proc. Inst. Civil Eng.* 1971, *49*, 57–90.

[28] Song T.T., Spender, B.F., Jr. Supplemental energy dissipation: State-of-the-art and state-of-the-practice. *Eng Struct*, 2002, *24*, 243–259.

[29] Steel Hysteretic Dampers. Available online: https://www.fipindustriale.it/index.php?area=106&menu=74&lingua=1 (accessed on 27.11.2020).

[30] Sorace S., Terenzi, G. Dissipative bracing-based seismic retrofit of R/C school buildings. *Open Constr. Build. Technol. J.* 2012, *6*, 334–345.

[31] Terenzi G. Dynamics of SDOF systems with nonlinear viscous damping. *J. Eng Mech.* 1999, *125*, 956–963.

[32] Otani S., Hiroishi H., Midorikawa M. Development of smart systems for building structures. *Proceedings of SPIE 2000*; 3988:2-9.

[33] Ölande A. An electrochemical investigation of solid cadmium-gold alloys. *Am Chem Soc.* 1932, *54*, 3819-33.

[34] Buehler W.J., Gilfrich J.V., Wiley R.C. Effect of low-temperature phase changes on the mechanical properties of alloys near composition TiNi. Appl Phys. 1963, 34, 1475-1477.

[35] Kauffman G., Mayo I. The story of Nitinol: the serendipitous discovery of the memory metal and its applications. *Chem Educator.* 1997, 2, 1-21.

[36] Duerig T., Pelton A., Stockel D. Superelastic nitinol for medical device. *Medical Plastics and Biomaterial Magazine.* March 1997.

[37] Butera F., Coda A., Vergani G. Shape memory actuators for automotive applications. *In Nanotec IT newsletter.* 207, 12-16.

[38] Bil C., Massey K., Abdullah E.J. Wing morphing control with shape memory alloys actuators. *J Intell Mater Syst Struct.* 2013, 221, 532-552.

[39] Hardwicke C.U. Recent Developments in Applying Smart Structural Materials. *JOM ABI/INFORM Trade&Industry.* 2003, 55, 15-16.

[40] Alam M.S., Youssef M.A., Nehdi M.L. Utilizing shape memory alloys to enhance the performance and safety of civil infrastructure: a review. *Canadian Journal of Civil Engineering.* 2007, 35, 1075-1086.

[41] Wilson J.C., Wesolowsky M. Shape Memory for Seismic Response Modification: A State-of-the-Art Review. *Earthquake Spectra.* 2015, 21, 569-601.

[42] Ocel J., DesRoches R., Leon R.T., Hess W., Krumme R., Hayes J.R., Sweeney S. Steel beam-column connections using shape memory alloys. *J. Struct. Eng.* 2004, 130, 732-740.

[43] McCormick J., DesRoches R. Characterization and optimization if shape memory alloy behavior for seismic vibration control – Application in building. The 14th World Conference on Earthquake Engineering. October 12-17, 2008, Beijing, China.

[44] Hodgon D.E. Shape Memory Alloys. *ASM Handbook.* 1990, 2, 897-902.

[45] Janke L., Czaderski C., Motavalli M, Ruth J. Applications of shape memory alloys in civil engineering structures – Overview, limits and new idea. *Material and Structures*. 2005, 38, 578-592.

[46] Dolce M., Cardone D. Mechanical behaviour of shape memory alloys for seismic applications – 2. Austenite NiTi wires subjected to tension. International *Journal of Mechanical Sciences*. 2001, 43, 2657-2677.

[47] Plietsch R., Ehrlich K. Strength differential effect in pseudoelastic NiTi shape memory alloys. *Acta Matter*. 1996, 45, 2417-2424.

[48] Van Humbeeck J., Liu Y. The high damping capacity of shape memory alloys. *Mater. Sci. Eng*. 1999, 46-60.

[49] Cardone D., Dolce M., Bixio A., Nigro D. Experimental Tests on SMA Elements. Proc. Final Workshop of the BRITE_MANSIDE project. Rome, 1999, 18pp.

[50] Dolce M., Cardone D. Mechanical behaviour of shape memory alloys for seismic applications – 1. Martensite and austenite NiTi bars subjected to torsion. *International Journal of Mechanical Sciences*. 2001, 43, 2631-2656.

[51] Clark P. W., Aiken I. D., Kelly J.M., Experimental and analytical studies of shape memory alloy damper for structural control. Proceeding of SPIE. *Smart Structure and Materials: Passive Damping*. 1995, 2445, 241-251.

[52] Piedboeuf M.C., Gauvin R., Thomas M. damping behavior of shape memory alloys: strain amplitude, frequency and temperature effects. *Journal of sound and Vibration*. 1998, 214, 885-901.

[53] Dolce M., Cardone D., Nigro D. Experimental tests on seismic device based on shape memory alloys. 12th WCEE 2000.

[54] Manach P.Y., Favier D. Shear and tensile thermomechanical behaviour of near equiatomic NiTi alloy. *Material Science & Engineering*. 1997, 222, 45-57.

[55] Delgadillo H.I, Kaack M., Yohannes T., Pelzl J., Khalil-Allafi J. Ultrasonic investigation of multistage martensitic transformations in aged Ni-rich Ni-Ti shape memory alloys. *Material Science & Engineering*. 2004, 378, 76-80.

[56] Hesse T., Gorashi M., Inman D.J. Shape memory alloy in tension and compression and its application as clamping-force actuator in a bolted joint: part I – experimentation. *Journal of Intelligent Material Systems and Structures*. 2004, 15, 577-587.

[57] Strnadel B., Ohashi S., Ishihara T., Ohtsuka H., Miyazaki S. Cyclic stress-strain characteristics of Ni-Ti and Ni-Ti-Cu shape memory alloys. *Material Science & Engineering*. 1995, 202, 148-156.

[58] Janke L., Czaderski C., Motavalli M., Ruth J. Application of shape-memory-alloys in civil engineering structures-overview, litrnadel B., Ohashi S., Ishihara T., Ohtsuka H., Miyazaki S. Cyclic stress-strain characteristics of Ni-Ti and Ni-

Ti-Cu shape memory alloys. *Material Science & Engineering*. 1995, 202, 148-156.

[59] Sato A., Chishima E., Soma K., Mori T., Shape memory effect in γ↔ε transformation in Fe-30Mn-1Si Alloy single crystals *Acta Metall*. 1982, 30, 1177-83.

[60] Maruyama T., Kubo H. Shape memory and superelastic alloys: technologies and application. *Woodhead Publishing Limited*. 2011, 12, 141-159.

[61] Tanaka Y., Himuro Y., Kainuma R., Sutou Y., Omori T., Ishida K. Ferrous polycrystalline shape-memory alloys showing huge superelasticity. *Science*. 2010, 327, 1488-490.

[62] Omori T., Ando K., Okano M., Xu X., Tanaka Y., Ohnum L. Superelastic effect in polycrystalline derrous alloys. *Science*. 2011, 333, 68-71.

[63] Takahiro S., Tadakatsu M., et al. Design concept and application of Fe-Mn-Si based alloys – from sshape memory to seismic response control. *Material transactions*. 2016, 57, 283-293.

[64] Lin H.C., Lin K.M., Lin C.S. The corrosion behaviour of Fe-based shape memory alloys. *Corros Sci*. 2002, 44, 2013-2016.

[65] Wu M., Johannesson B., Geiker M. A review: self-healing in cementitious materials and engineered cementitious composite as a self-healing material. *Constr Build Mater*. 2012, 28, 571-583.

[66] Dasgupta R., Jain A.K., Kumar P., Hussein S., Pandey A. Effect of alloy constituents on the martensitic phase formation in some Cu-based SMAs. *Journal of Material Research and Technology*. 2014.

[67] Mallik U.S., Sampath V. Influence of alluminium and manganese concentration on the shape memory characteristics of Cu-Al-Mn shape memory alloy. *Journal of Alloys and Compounds*. 2009.

[68] Sutou Y., Kainuma R., Ishida K. Effect of alloying elements on the shape memory properties of ductile Cu-Al-Mn alloys. *Material science and engineering*. 1999.

[69] Liu J., Huang H., Xie J., Xu S., Li F. Superelastic fatigue of columnar-grained Cu-Al-Mn shape memory alloy under cyclic tension at high strain. *Scripta Materialia*. 2017, 36, 106-110.

[70] Mallik U.S., Sampath V. Effect of composition and ageing on damping characteristics of Cu-AL-Mn shape memory alloys. *Material science & Engineering*. 2008, 478, 48-55.

[71] Vivet A., Orgeas L., Lexcellent C., Favier D., Bernardini J. Shear and tensile pseudoelastic behaviours of CuZnAl single crystals. *Scripta Materialia*. 2001, 45, 33-40

[72] Recarde V., Perez-Landazabal J.I et al. Thermodynamics of thermally induced martensitic transformation in Cu-Al-Ni shape-memory-alloys. *Acta Materialia*. 2004, 52, 3941-3948.

[73] Rejzner J., Lexcellent C., Raniecki B. Pseudoelastic behaviour of shape memory alloy beam under pure bending: Experiments and modelling. *Journal of Intelligent Material System and Structures*. 2001, 12, 671-680.

[74] Hooshmand M., Rafezy B., Khalil-Allafi J. Seismic retrofit in building structures using shape memory alloys. *KSCE Journal of Civil Engineering*. 2015, 19, 935-942.

[75] Sabelli R. Research on improving the design and analysis of earthquake resistant steel braced frame. *Professional Fellowship Report*. October 2009.

[76] Andrawes B., DeRoches R. Unseating prevention for multiple frame bridge using superelastic device. *Smart Materials and Structures*. 2005, 14, 60-67.

[77] Sutou Y., Omori T., Wang J.J. Kainuma R., Ishida K. Characteristics of Cu-Al-Mn based shape memory alloy and their applications. *Material science and Engineering*. 2004, 378, 278-282.

[78] Youssef M.A., Alam M.S., Nehdi M. Experimental Investigation on the Seismic Behaviour of Beam-Column Joints Reinforced with Superelastic Shape Memory Alloys. *Journal of Earthquake Engineering*. 2008, 12, 1205-1222.

[79] Elbahy Y.I., Youssef M.A., Meshaly M. Seismic performance of reinforced concrete frames retrofitted using external superelastic shape memory alloy bars. *Bulletin of Earthquake Engineering*. 2019, 17, 781-802.

[80] http://opensees.berkeley.edu

[81] Mckinsey Global Institute. Digital Europe: Realizing the continent's potential. Report, June 2016.